AD-A164 925 INTRUDER POLARIZATION(U) NORTHEASTERN UNIV BOSTON MA 1/2
H RAEMER ET AL. DEC 85 RADC-TR-85-234 F30602-81-C-0169

UNCLASSIFIED F/G 17/9 NL

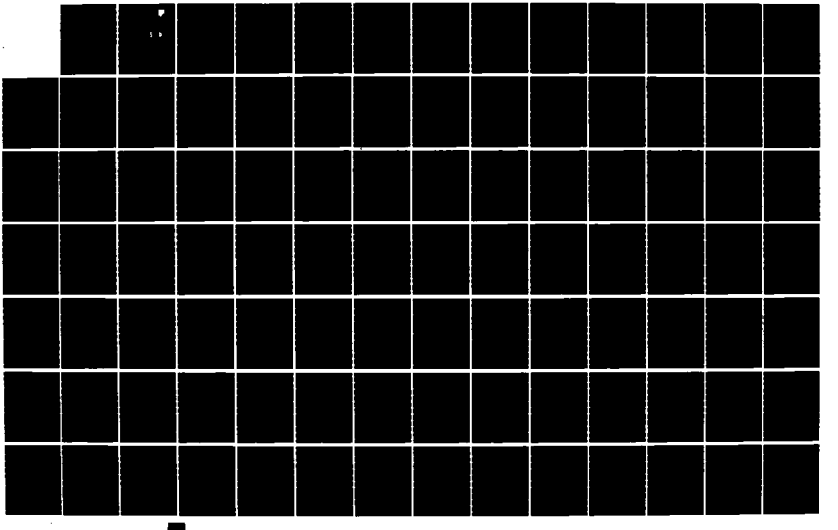

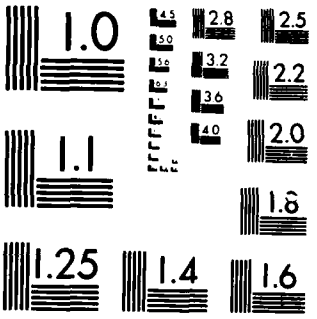

(12)

AD-A164 925

RADC-TR-85-234
Final Technical Report
December 1985

INTRUDER POLARIZATION

Northeastern University

Harold Raemer
Samuel Rosenthal

APPROVED FOR PUBLIC RELEASE; DISTRIBUTION UNLIMITED

This effort was funded totally by the Defense Nuclear Agency

ROME AIR DEVELOPMENT CENTER
Air Force Systems Command
Griffiss Air Force Base, NY 13441-5700

This report has been reviewed by the RADC Public Affairs Office (PA) and is releasable to the National Technical Information Service (NTIS). At NTIS it will be releasable to the general public, including foreign nations.

RADC-TR-85-234 has been reviewed and is approved for publication.

APPROVED: Nicholas V. Karas

NICHOLAS V. KARAS
Project Engineer

APPROVED: Allan C. Schell

ALLAN C. SCHELL
Chief, Electromagnetic Sciences Division

FOR THE COMMANDER: John A. Ritz

JOHN A. RITZ
Plans & Programs Division

If your address has changed or if you wish to be removed from the RADC mailing list, or if the addressee is no longer employed by your organization, please notify RADC (EECT) Hanscom AFB MA 01731. This will assist us in maintaining a current mailing list.

Do not return copies of this report unless contractual obligations or notices on a specific document requires that it be returned.

DISCLAIMER NOTICE

THIS DOCUMENT IS BEST QUALITY PRACTICABLE. THE COPY FURNISHED TO DTIC CONTAINED A SIGNIFICANT NUMBER OF PAGES WHICH DO NOT REPRODUCE LEGIBLY.

UNCLASSIFIED
SECURITY CLASSIFICATION OF THIS PAGE

AD-A164 925

REPORT DOCUMENTATION PAGE

1a REPORT SECURITY CLASSIFICATION: UNCLASSIFIED	1b RESTRICTIVE MARKINGS: N/A
2a SECURITY CLASSIFICATION AUTHORITY: N/A	3 DISTRIBUTION/AVAILABILITY OF REPORT: Approved for public release; distribution unlimited.
2b DECLASSIFICATION/DOWNGRADING SCHEDULE: N/A	
4 PERFORMING ORGANIZATION REPORT NUMBER(S): N/A	5 MONITORING ORGANIZATION REPORT NUMBER(S): RADC-TR-85-234
6a NAME OF PERFORMING ORGANIZATION: Northeastern University; 6b OFFICE SYMBOL (If applicable)	7a NAME OF MONITORING ORGANIZATION: Rome Air Development Center (EECT)
6c ADDRESS (City, State, and ZIP Code): Boston MA 02115	7b ADDRESS (City, State, and ZIP Code): Hanscom AFB MA 01731
8a NAME OF FUNDING/SPONSORING ORGANIZATION: Defense Nuclear Agency; 8b OFFICE SYMBOL (If applicable)	9 PROCUREMENT INSTRUMENT IDENTIFICATION NUMBER: F30602-81-C-0169
8c ADDRESS (City, State, and ZIP Code): Nuclear Security Division, Wash DC 20305	10 SOURCE OF FUNDING NUMBERS: PROGRAM ELEMENT NO 62715H; PROJECT NO DNAR; TASK NO 02; WORK UNIT ACCESSION NO 39

11 TITLE (Include Security Classification): INTRUDER POLARIZATION

12 PERSONAL AUTHOR(S): Harold Raemer, Samuel Rosenthal

13a TYPE OF REPORT	13b TIME COVERED	14 DATE OF REPORT (Year, Month, Day)	15 PAGE COUNT
Final	FROM Mar 84 TO Nov 84	December 1985	150

16 SUPPLEMENTARY NOTATION: This effort was funded totally by the Defense Nuclear Agency.

17 COSATI CODES			18 SUBJECT TERMS (Continue on reverse if necessary and identify by block number)
FIELD	GROUP	SUB-GROUP	Intrusion Sensor; Ported Coax Microwave; Polarization; Detection
17	09		

19 ABSTRACT (Continue on reverse if necessary and identify by block number)

In a previous project a class of RF intrusion sensor systems was analyzed and numerical results were obtained for various intrusion situations. The system consisted of a ported coaxial cable laid circularly around an area to be protected and an antenna near the center of the circle. The presence of an intruder (electromagnetic scatterer) near the cable perturbs the field and thereby changes the signal at the antenna. The analysis was based on the plane-wave spectral representation of fields and the assumed scatterer was a uniform spheroid with constitutive parameters designed to simulate those of a human frame. Emphasis was on polarization effects.

Although the previous analysis constituted an attempt to model this system quite accurately, the price for this accuracy was extremely large computer time. In order to reduce computer time, approximations were made along the way that reduced the overall accuracy. The present report discusses a follow-on to the above mentioned project whose objective was to produce

20 DISTRIBUTION/AVAILABILITY OF ABSTRACT	21 ABSTRACT SECURITY CLASSIFICATION
☐ UNCLASSIFIED/UNLIMITED ☒ SAME AS RPT ☐ DTIC USERS	UNCLASSIFIED
22a NAME OF RESPONSIBLE INDIVIDUAL: Nicholas V. Karas	22b TELEPHONE (Include Area Code): (617) 861-3193; 22c OFFICE SYMBOL: RADC (EECT)

DD FORM 1473, 84 MAR — 83 APR edition may be used until exhausted. All other editions are obsolete.

SECURITY CLASSIFICATION OF THIS PAGE
UNCLASSIFIED

a simpler, less computer-time-intensive model and associated software that can be readily used to study the effects of parameter changes on system performance. Steps were taken toward that objective, as follows:

(1) The software was thoroughly checked and redesigned for greater efficiency when that step was warranted.

(2) The model for the cable-generated fields was simplified.

(3) While many of the features of the plane-wave spectral representation of fields were retained, that approach was compromised by approximating the cable-generated fields, within the scatterer volume, as those of a single plane wave propagating in the direction of power flow of the true cable generated fields.

The result of these modifications is a new computer program with much-reduced running time which produces numerical results that are much more consistent and interpretable than those produced in the previous project.

Table of Contents

1. Introduction

The work described in this report is a continuation of research done on RADC Postdoctoral Contract F30602-78-C-0102, completed on November 1, 1981. The Final Report on that contract, entitled "Analysis of the Polarization Dependence of the Interaction Between Human Frame Targets and Radio Frequency Sensor Fields," is designated as Reference 1 in the present report.[1-13]

The previous project, referred to above, involved analysis of a particular type of RF intrusion sensor system. The system consists of a ported coaxial cable[14-28] laid circularly on the ground surface and a vertical receiving antenna at or near the center of the circle tuned to the frequency of the wave propagating in the cable. (See Figure 1.1). An intruder stepping or crawling across the cable in order to enter the circle scatters some of the electromagnetic energy impinging on him or her from the cable into the direction of the antenna,[29-65] changing the signal received by the antenna and thereby detecting the presence of the intruder.

Although the concept of this device is very simple, the electromagnetic theory problems encountered in attempting to model its operation analytically are extremely complicated. In the original project, as reported in Reference 1, the scheme upon which the analysis was based was the plane-wave spectrum representation of an electromagnetic wave. The electric and magnetic fields from the cable were calculated based on an analysis of the propagation along the cable and the use of the "Stratton-Chu"[66] (or "Kirchoff Huyghens") integral formula which gives the field components in space based on a knowledge of the fields at the cable slots. This was done as if the cable were in free space. Then the plane-wave spectral representations of each of the field components was calculated. Each "plane wave" was then taken through the ground-reflection process.

Figure 1.1

Intrusion Sensor System Configuration

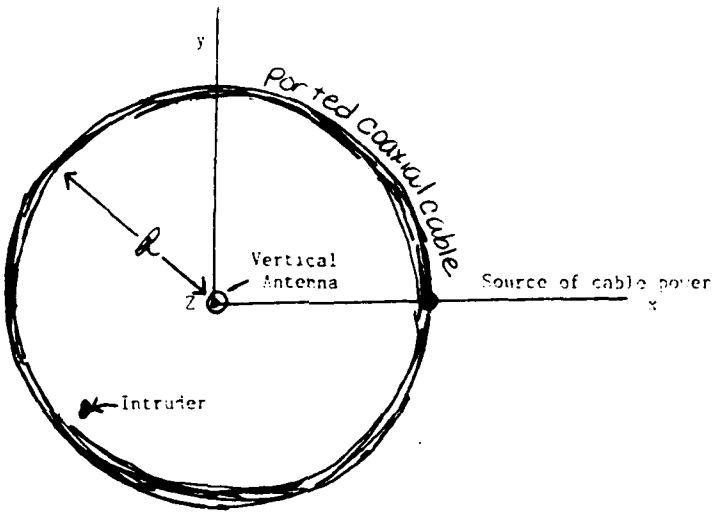

The total (direct-plus-ground-reflected) spectral field in the absence of an intruder was calculated. The intruder was modelled as an electromagnetic scatterer. The total spectral field at the intruder's location was considered as the field of a plane wave incident on the scatterer, which was modelled as a uniform spheroid with constitutive parameters chosen from a composite of those of the various constituents of the human body. A program originally developed by Peter Barber[41,45-57,59,52,57,61,62] at the University of Utah was used to perform the scattering analysis. This program was inserted into our software as a subroutine.

The scattered wave fields propagating directly toward the antenna and those reflected from the ground and then propagating toward the antenna were computed.

The program developed for this problem computes the components of the plane wave spectrum of four contributions to the electric field. They are:

(a) the field from the cable in the absence of the ground (i.e., in infinite free space)

(b) the ground-reflected cable-generated field

(c) The field scattered by the intruding object directly into the antenna

(d) the ground-reflected scattered field in the direction of the antenna

Each of the constituents (a), (b), (c) and (d) is a function of the normalized wave propagation vector $\underline{\beta}$. The final step in the computation was the inverse Fourier transformation of the spectral electric field components in order to produce the field components at the antenna site as a function of the position of the antenna. The end result of the computations was: (1) a set of field components consisting of the superposition of contributions (a) and (b), i.e., the field components in the absence of the scatterer; (2) the superposition of contributions (c) and (d), i.e., the field components due to the scatterer; and (3) the superposition of contributions (a), (b), (c) and (d), i.e., the components of the <u>total</u> electric field seen at the antenna site.

The purpose of the follow-on project was to produce an improved analytical model and an improved computer program that would be more useful in studying system performance. The problems with the original analytical model and associated software were:

(1) The computations, involving large numbers of summations of complex quantities arising from complicated theoretical calculations, were extremely sensitive to small errors that are very difficult to detect. For example, an erroneous sign in adding two or more complex contributions of comparable magnitude can result in enormous errors (e.g., a quantity that should be zero can appear as a large number or conversely, a large number can appear to be nearly zero). On the original project, there was insufficient time to provide adequate checking of the software to ensure that such errors do not occur.

(2) There were portions of the computations that required enormous amounts of running time. For example, the Barber scattering program, although it was considered to be an excellent vehicle for study of scattering from a human frame target, is very computer-time intensive. The plane-wave spectrum approach to the problem, although it should be accurate if carried out rigorously, requires that the Barber program be run for each value of each of the two components of the wave propagation vector $\underline{k}$. This means that, if we want to perform the two-dimensional inverse Fourier transformation (to transform from $\underline{k}$-space into position space) accurately, the Barber program must be run as many as 50 to 100 times for each position of the scatterer. This is an absolutely prohibitive expenditure of running time if we want to study many variations of the parameters. To render this computation feasible, the stationary phase approximation was used for part of the inverse Fourier transform computation, thus reducing the number of runs of the Barber program for each scatterer position to somewhat less than 50, perhaps as few as 25. The running time was still very high, but at least within reason. However, in some parameter regimes, the validity of the stationary phase method

at least marginal and in some cases questionable. This compromises the accuracy of the computations.

(ii) To summarize the difficulties encountered on the original project, they were largely due to the attempt to put the analysis of this system on a solid theoretical foundation. We were very careful about the assumptions involved and tried to make the model as realistic as possible. However, we were forced into tradeoffs between the realism of the model and the limitations of computer time. Although the equations programmed for machine computation may have contained a great deal of realism, compromises to save running time (e.g., insufficient points in a numerical integration) might in some cases produce a result less accurate than would have been obtained with a less rigorous but accurately computable model.

The measures taken on the new project to improve the analysis and computations are discussed in the present report. In Section 2, the calculation of the fields from the cable slots as if the cable were in free space are described. In the earlier project, these calculations were made for arbitrary modes propagating along the cable, i.e., TE, TM or TEM modes (Ref. 1, Appendix IV). While that model was very general and hence would cover many possible cases, it was also cumbersome and required a large amount of software. It was decided to formulate the fields on the cable slots using a simpler model based on propagation of a TEM mode along the cable. This yields a simpler, more easily interpretable set of formulas, requires considerable less software, and is sufficiently realistic for the purposes of this analysis. Also, it could easily be generalized if necessary and if data were available to allow correct assignment of parameter values for TE and/or TM modes.

In Section 3, the remaining steps in calculation of the received signal at the antenna are described. In effect, Section 3 contains brief summaries of the sections in Reference 1. Section 3.1 briefly summarizes the coverage of the plane wave spectral representation of fields that was presented in great detail in Sections 3 and 4 and Appendices II and III of Ref. 1. The emphasis in Section 3.1 is on the major results that were derived in Reference 1. Some new investigations on the use of this approach are introduced in Section 3.1 and further detailed in Appendix II.

Section 3.2 contains a brief summary of the key points on the ground reflected wave that were covered in great detail in Section 5 of Ref. 1. No significant changes in the analysis or the programs were made on the present project.

Sections 3.3, 3.4 and 3.5 contain brief summaries of the material presented in detail in Sections 6, 7 and 8 respectively of Ref. 1. This material concerns the coordinate transformations to allow the superposition of direct and ground-reflected cable-generated fields to be modelled as the field incident on the scatterer (Section 3.3), the action of the scattering program itself (Section 3.4) and the transformation of the scattered fields from scatterer-centered coordinates to earth coordinates (Section 3.5). Section 3.6 is a summary of ground-reflections of the scattered fields, presented in detail in Section 9 of Ref. 1.

Section 3.7 is a summary of the process of summing all field contributions and taking the inverse Fourier transform in order to convert from the plane-wave spectrum of the field components to the actual field components as functions of space coordinates.

Section 4 contains a detailed analysis of the new approach that was finally adopted on the later project. This approach has replaced the plane-wave

spectrum approach but has retained most of its features.* It involves the approximation of the fields incident on the scatterer as those of a single plane wave (not a spectrum of plane waves) whose direction of propagation is that of the Poynting vector (direction of power flow) at the center of the scatterer. This approach circumvents the problem of performing the two-dimensional inverse Fourier transformation and hence saves an enormous amount of computer time, allowing many more parameter regimes to be studied within a given time. In view of the degree of approximation required to implement the computations for the plane-wave-wave spectrum approach (See Appendix II for detailed discussion of these problems) the new approach offers many advantages in addition to that of increased computational speed. If the relationships arising in the plane-wave spectrum approach could be computed accurately without a prohibitive expenditure of computer time, that would be a superior methodology. However, the required compromises in computational accuracy might negate the advantages of the theoretical model itself. The new approach involves an approximation at the initial formulation stage which is physically satisfying, i.e., the idea that the "incident plane wave" that approximates the actual wave in the scatterer region is a linearly polarized transverse electromagnetic wave traveling in the direction of the power flow of the actual fields emanating from the cable at the scatterer's center.

The new approach produces results that appear to be very reasonable and physically interpretable. Since computer time is not so critical with this approach, it is possible to study many variations of parameters within a reasonable expenditure of time. All of this is discussed in detail in Section 5 of this report.

* The normalized wave propagation vector $\hat{a}_k$, which was used extensively in the original approach, is still retained in the new approach. It is used in modelling of scattering and ground reflection. All stages of the analysis reported in Section 3 remain essentially intact, with only minor modifications required.

2. Calculation of Fields from Cable Slots in Free Space

The approach used in the previous project (Ref. 1, Sections 3 and 4, and Appendices III and IV) has been considerable simplified. In the revised approach, the components of the field from the slots is calculated directly in the spatial domain rather than in the spectral domain (Ref. 1, Appendices II and III) as in the previous work. Again, the Stratton-Chu[66] (or Kirchoff-Huyghens) integral formula for the electric field components is used (Ref. 1, Appendix I, Eq. (I-3a)) where again contributions from aperture edges are neglected and volume current and charge densities are assumed to be zero. The TEM mode is assumed to be propagating down the coaxial line, whose curvature is neglected, i.e., the propagation down the line is assumed equivalent to that along a straight coaxial cable (Ref. 1, Appendix IV, Pages IV-6 and IV-7).

In this section, the field components will be formulated as if the cable were in free-space. From Eq. (I-3-a, b) in Appendix I of Ref. 1, we have for the electric and magnetic fields $\underline{E}$ and $\underline{H}$ at the point $\underline{r}$ (characterized by cylindrical coordinates (ρ, ϕ, z)) due to the fields on a cable slot located at the point r', (characterized by cylindrical coordinates $(\mathcal{R}, \phi', b')$, where $\mathcal{R}$ is the cable radius and b' is the vertical coordinate of the center of a slot):

$$\underline{E}(\rho, \phi, z) = -\frac{1}{4\pi} \iint_{S''} dS'' \left[j\omega\mu_o (\hat{n}'' \times \underline{H}(\underline{r}'')) G + (\hat{n}'' \times \underline{E}(\underline{r}'')) \times \nabla' G + (\hat{n}'' \cdot \underline{E}(\underline{r}'')) \nabla' G \right] \qquad (2.1\text{-a})$$

2.2

$$\underline{H}(\rho, \phi, z) = +\frac{1}{4\pi} \iint_{\Delta S''} dS'' \left[j\omega\varepsilon_o (\hat{\underline{\rho}}'' \times \underline{E}(\underline{\xi}'')) G - (\hat{\underline{\xi}}'' \times \underline{H}(\underline{\xi}'')) \times \nabla' G - (\hat{\underline{\xi}}'' \underline{H}(\underline{\xi}'')) \nabla' G \right] \qquad (2.1\text{-b})$$

where time dependence $e^{-j\omega t}$ is assumed and where

$\Delta S''$ = Slot area

G = Green's function = $\frac{e^{jkR}}{R}$

$R = |\underline{\xi} - \underline{\xi}'| = \sqrt{\rho^2 + \rho'^2 - 2\rho\rho' \cos\Phi' + (z - z')^2}$

$\Phi' = \phi' - \phi$

$\hat{\underline{\rho}}''$ = Outward normal unit vector at slot

$\nabla' = -\nabla = -\left(\hat{\underline{x}} \frac{\partial}{\partial x} + \hat{\underline{y}} \frac{\partial}{\partial y} + \hat{\underline{z}} \frac{\partial}{\partial z}\right)$

where

$(\hat{\underline{x}}, \hat{\underline{y}}, \hat{\underline{z}})$ = unit basis vectors

ε_o = Permittivity of free space = $\frac{1}{36\pi} (10^{-9})$ farads/meter

μ_o = Magnetic permeability of free space = $4\pi (10^{-7})$ henries/meter

For the TEM mode

$$\underline{E}(\underline{\xi}') = \hat{\underline{\rho}}'' E(\underline{\xi}') \qquad (2.2\text{-a})$$

$$\underline{H}(\underline{\xi}') = \hat{\underline{\phi}}'' H(\underline{\xi}') \qquad (2.2\text{-b})$$

where $\hat{\underline{\phi}}''$ is the unit basis vector in the ϕ'' direction in the double-primed coordinate system in which the slot position is represented (See Ref. 1, Section 4)

$$H(\underline{\xi}') = Y_{ca} E(\underline{\xi}') \qquad (2.2\text{-c})$$

where Y_{ca} = wave admittance of cable material, given by

$$Y_{ca} = \sqrt{\frac{\varepsilon_{ca}}{\mu_o}} = Y_o \hat{k}'_{ca} \qquad (2.2\text{-d})$$

where

Y_o = wave admittance of free space $= \sqrt{\frac{\varepsilon_o}{\mu_o}}$

$\hat{k}'_{ca} = \sqrt{\frac{\varepsilon_{ca}}{\varepsilon_o}}$

$\varepsilon_{ca} = \varepsilon_a + \frac{j\sigma_a}{\omega}$ = complex permittivity of cable material

ε_a = permittivity of cable material

σ_a = conductivity of cable material

For the TEM mode on a straight coaxial cable (our approximation)

$$\underline{E}(\underline{r}') = \underline{E}_o e^{-j(\omega\sqrt{\mu_o\varepsilon_{ca}} + \alpha)\ell_{ab}'} \qquad (2.3)$$

where

$\underline{E}_o$ = electric field strength at the power source along the cable, located at $\ell' = 0$

$k = \omega\sqrt{\mu_o\varepsilon_o}$ = free-space wave number

$\hat{k}_{ca} = \sqrt{\frac{\varepsilon_a}{\varepsilon_o}}$ = same as $\hat{k}'_{ca}$ if $\sigma_a = 0$

α = attenuation along cable in nepers/meter

From (2.2-a, b), it follows that

$$\hat{\ell}'' \cdot \underline{E}(\underline{r}') = \underline{E}(\underline{r}') \qquad (2.4\text{-a})$$

$$\hat{\ell}'' \cdot \underline{H}(\underline{r}') = 0 \qquad (2.4\text{-b})$$

$$\hat{\ell}' \times \underline{E}(\underline{r}') = 0 \qquad (2.4\text{-c})$$

Combining the pair of (2.2-c, d)

$$\hat{\ell}'' \times \underline{H}(\underline{r}') = \hat{\ell}'' \times \underline{E}(\underline{r}') = \hat{\ell}'' Y_o \hat{k}_{ca} \underline{E}(\underline{r}') \qquad (2.4\text{-d})$$

where $\hat{\underline{z}}''$ is the unit vector along the cable.

Using (2.2-a, b, c) and (2.4-a, b, c) and noting that $\nabla' = -\nabla$ we can simplify (2.1-a, b) as follows:

$$\underline{H}(\rho, \phi, z) = -\frac{1}{4\pi} \iint_{\Delta S''} dS'' \underline{I}(\underline{r}') \left[\hat{\underline{z}}'' \times j\omega\mu_o Y_o \hat{\underline{k}}'_{ca} G - \nabla G\right] \qquad (2.3\text{-a})$$

$$\underline{E}(\rho, \phi, z) = +\frac{1}{4\pi} \iint_{\Delta S''} dS'' \underline{I}(\underline{r}') \left[Y_o \hat{\underline{k}}'_{ca} \times (\hat{\underline{z}}'' \times \nabla G)\right] \qquad (2.3\text{-b})$$

The following relationships will facilitate further simplification of (2.3-a, b).

From Ref. 1, Page 4.10, Eq. (4.19-c)

$$\hat{\underline{z}}'' = \hat{\underline{x}}(-\sin\phi') + \hat{\underline{y}}(\cos\phi') \qquad (2.4\text{-a})$$

$$\nabla G = -\nabla\left(\frac{e^{jkR}}{R}\right) = \frac{jke^{jkR}}{R}\left(1 - \frac{1}{jkR}\right)\nabla R$$

$$\frac{jke^{-jkR}}{R^2}\left(1 - \frac{1}{jkR}\right)\underline{R} \qquad (2.4\text{-b})$$

$$\underline{R} = \hat{\underline{x}}(\rho\cos\phi - a\cos\phi') + \hat{\underline{y}}(\rho\sin\phi - a\sin\phi') + \hat{\underline{z}}(z - b') \qquad (2.4\text{-c})$$

From (2.4-a, b, c)

$$\hat{\underline{z}}'' \times \nabla G = \left\{\hat{\underline{x}}[(z - b')\cos\phi'] + \hat{\underline{y}}[(z - b')\sin\phi'] + \hat{\underline{z}}[a - \rho\cos(\phi - \phi')]\right\} \frac{jke^{jkR}}{R^2}\left(1 - \frac{1}{jkR}\right) \qquad (2.4\text{-d})$$

and, with the aid of (2.2-d) and (2.3-b)

$$\hat{z}'' j\omega\mu_o \hat{k}'_{ca} Y_o G - 7G = \frac{jke^{j'kR}}{R}\left\{\hat{x}\left[\hat{k}'_{ca} \sin \phi' - \frac{1}{\rho}\left(1 - \frac{1}{jkR}\right)(\rho \cos \phi - \alpha \cos \phi')\right]\right.$$

$$+ \hat{y}\left[\hat{k}'_{ca} \cos \phi' - \frac{1}{\rho}\left(1 - \frac{1}{jkR}\right)(\rho \sin \phi - \alpha \sin \phi')\right]$$

$$\left. + \hat{z}\left[-\frac{(z - b')}{R}\left(1 - \frac{1}{jkR}\right)\right]\right\} \qquad (2.7\text{-}b)$$

2.1 Field Components from a Single Slot

From (2.7-a, b) substituted into (2.5-a, b) and with the aid of (2.3) we obtain the rectangular field components at a point $\underline{r} = (\rho, \phi, z)$ from a single slot at the point $\underline{r}' = (\ell, \phi', h')$ as follows:

$$E_x(\underline{r}, \underline{r}') = K\left\{-\hat{k}'_{ca} \sin\phi' - \frac{1}{R}\left(1 - \frac{1}{jkR}\right)(\rho\cos\phi - \ell\cos\phi')\right\} \tag{2.8-a}$$

$$E_y(\underline{r}, \underline{r}') = K\left\{\hat{k}'_{ca} \cos\phi' - \frac{1}{R}\left(1 - \frac{1}{jkR}\right)(\rho\sin\phi - \ell\sin\phi')\right\} \tag{2.8-b}$$

$$E_z(\underline{r}, \underline{r}') = K\left\{-\frac{(z - h')}{R}\left(1 - \frac{1}{jkR}\right)\right\} \tag{2.8-c}$$

$$H_x(\underline{r}, \underline{r}') = -K Y_o \hat{k}'_{ca} \frac{(z - h')}{R} \cos\phi' \left(1 - \frac{1}{jkR}\right) \tag{2.9-a}$$

$$H_y(\underline{r}, \underline{r}') = -K Y_o \hat{k}'_{ca} \frac{(z - h')}{R} \sin\phi' \left(1 - \frac{1}{jkR}\right) \tag{2.9-b}$$

$$H_z(\underline{r}, \underline{r}') = -K Y_o \hat{k}'_{ca} \left[\frac{\ell - \rho\cos\Theta'}{R}\right]\left(1 - \frac{1}{jkR}\right) \tag{2.9-c}$$

where

$$K = K(\underline{r}, \underline{r}') = -\frac{E_o}{4\pi} e^{-(jk\hat{k}_{ca} + \alpha)\ell\Theta'} \frac{jke^{jkR}}{R} L_s W_s$$

and where L_s and W_s are the length and width of the slot respectively. For the purpose of facilitating integration over the cable it is convenient to separate out the ϕ'-dependent factors in each term of (2.8-a, b, c) and (2.9-a, b, c). To this end, we note that $\phi' = \phi + \Theta'$ and express these equations in the forms

$$E_x(\underline{r}, \underline{r}') = C(\phi)\, e^{j\hat{\varphi}(\underline{r}, \underline{r}')} \left\{e^{j\Theta'}\left[-\frac{\hat{k}'_{ca}}{2jR} + \frac{\ell}{2R^2}\left(1 - \frac{1}{jkR}\right)\right] e^{j\rho} \right.$$

$$\left. + e^{-j\Theta'}\left[+\frac{\hat{k}'_{ca}}{2jR} + \frac{\ell}{2R^2}\left(1 - \frac{1}{jkR}\right)\right] e^{-j\rho} - \frac{\rho}{R^2}\left(1 - \frac{1}{jkR}\right)\cos\phi\right\} \tag{2.10-a}$$

$$E_y(\zeta, \zeta') = C(\phi)\, e^{j\Psi(\zeta, \zeta')} \left\{ e^{j\phi'} \left[\frac{\hat{k}'_{ca}}{2R} + \frac{\mathcal{R}}{2jR^2} \left(1 - \frac{1}{jkR}\right) \right] e^{j\phi} \right.$$

$$\left. + e^{-j\phi'} \left[\frac{\hat{k}'_{ca}}{2R} - \frac{\mathcal{R}}{2jR^2} \left(1 - \frac{1}{jkR}\right) \right] e^{-j\phi} - \frac{\rho}{R^2} \left(1 - \frac{1}{jkR}\right) \sin \phi \right\} \quad (2.10\text{-b})$$

$$E_z(\zeta, \zeta') = -C(\phi)\, e^{j\Psi(\zeta, \zeta')} \frac{(z - b')}{R^2} \left(1 - \frac{1}{jkR}\right) \quad (2.10\text{-c})$$

$$H_x(\zeta, \zeta') = -Y_o \hat{k}'_{ca} C(\phi)\, e^{j\Psi(\zeta, \zeta')} \left(1 - \frac{1}{jkR}\right) \left(\frac{z - b'}{2R^2}\right) \left\{ e^{j\phi'} e^{j\phi} + e^{-j\phi'} e^{-j\phi} \right\} \quad (2.11\text{-a})$$

$$H_y(\zeta, \zeta') = -Y_o \hat{k}'_{ca} C(\phi)\, e^{j\Psi(\zeta, \zeta')} \left(1 - \frac{1}{jkR}\right) \left(\frac{z - b'}{2R^2}\right) \left\{ e^{j\phi'} e^{j\phi} - e^{-j\phi'} e^{-j\phi} \right\} \quad (2.11\text{-b})$$

$$H_z(\zeta, \zeta') = -Y_o \hat{k}_{ca} C(\phi)\, e^{j\Psi(\zeta, \zeta')} \left(1 - \frac{1}{jkR}\right) \left\{ \frac{\mathcal{R}}{R^2} - \frac{\rho}{2R^2} e^{j\phi'} - \frac{\rho}{2R^2} e^{-j\phi'} \right\} \quad (2.11\text{-c})$$

where

$$C(\phi) = -\frac{\Gamma_o}{4\pi} e^{-(jk\hat{k}_{ca} + \mathcal{R})} jk\, l_s\, w_s$$

$$\Psi(\zeta, \zeta') = \beta - (jk\hat{k}_{ca} + \gamma)\mathcal{R}'$$

The forms (2.10-a, b, c) and (2.11-a, b, c) are particularly useful for purposes of integrating over all the slots on the cable, as will become apparent in Section 2.2. To study the fields from a single slot, the forms (2.8-a, b, c) and (2.9-a, b, c) are less cumbersome and therefore easier to use. Reverting to those forms, we can obtain the radial (ρ-directed) and azimuthal (ϕ-directed) components from (2.8-a, b) and (2.9-a, b). Note first that for any vector $\underline{v} = v_x \hat{\underline{x}} + v_y \hat{\underline{y}} = v_\rho \hat{\underline{\rho}} + v_\phi \hat{\underline{\phi}}$, where $\hat{\underline{\rho}}$ and $\hat{\underline{\phi}}$ are unit basis vectors in the ρ and ϕ directions respectively,

$$v_\rho = v_x \cos\phi + v_y \sin\phi \tag{2.12-a}$$

$$v_\phi = -v_x \sin\phi + v_y \cos\phi \tag{2.12-b}$$

Applying (2.12-a, b) to $\underline{E}$ and $\underline{H}$ in (2.8-a, b) and (2.9-a, b) respectively, we have

$$E_\rho = K\left\{-\hat{k}'_{ca} \sin\theta' - \frac{1}{R}\left(1 - \frac{1}{jkR}\right)(\rho - \ell\cos\theta')\right\} \tag{2.13-a}$$

$$E_\phi = K\left\{+\hat{k}'_{ca} + \frac{1}{R}\left(1 - \frac{1}{jkR}\right)\ell\sin\theta'\right\} \tag{2.13-b}$$

$$H_\rho = -K Y_o \hat{k}'_{ca} \frac{(z - b')}{R}\left(1 - \frac{1}{jkR}\right)\cos\theta' \tag{2.14-a}$$

$$H_\phi = -K Y_o \hat{k}'_{ca} \frac{(z - b')}{R}\left(1 - \frac{1}{jkR}\right)\sin\theta' \tag{2.14-b}$$

where (See (2.8-a, b, c) and (2.9-a, b, c))

$$K = -jk \frac{E_o L_s W_s e^{-(jk\hat{k}_{ca} + \cdots)\ell\phi}}{4\pi} \cdot \frac{e^{-(jk\hat{k}_{ca} + \cdots)\ell\theta' + jkR}}{R}$$

To complete the systems of equations (2.13-a, b) and (2.14-a, b), we repeat (2.8-c) and (2.9-c) here and assign new equation numbers:

$$E_z = K\left\{-\frac{(z - b')}{R}\left(1 - \frac{1}{jkR}\right)\right\} \tag{2.14-c}$$

$$H_z = -K Y_o \hat{k}'_{ca}\left[\frac{\ell - \rho\cos\theta'}{R}\right]\left[1 - \frac{1}{jkR}\right] \tag{2.14-c}$$

2.2 Integration Around Cable

To obtain the total field at a point (ρ, ϕ, z), we must integrate over all the slots along the cable, i.e., integrate the expressions in (2.10-a, b, c) and (2.11-a, b, c) on θ' from $\theta' = 0$ to $\theta' = 2\pi$. This step leads to two expressions

$$E_x(\underline{r}) = \frac{C(\phi)}{jk}\left\{-\frac{\hat{k}'_{ca}k}{2}\left[I_1^{(+)}e^{j\phi} - I_1^{(-)}e^{-j\phi}\right] - \rho\cos\phi\left[jk\,I_2^{(0)} - I_3^{(0)}\right]\right.$$
$$\left. + \frac{\rho}{2}\left[e^{j\phi}\left\{jk\,I_2^{(+)} - I_3^{(+)}\right\} + e^{-j\phi}\left\{jk\,I_2^{(-)} - I_3^{(-)}\right\}\right]\right\} \quad (2.15\text{-a})$$

$$E_y(\underline{r}) = \frac{C(\phi)}{jk}\left\{\frac{jk\hat{k}'_{ca}k}{2}\left[I_1^{(+)}e^{j\phi} + I_1^{(-)}e^{-j\phi}\right] - \rho\sin\phi\left[jk\,I_2^{(0)} - I_3^{(0)}\right]\right.$$
$$\left. + \frac{\rho}{2j}\left[e^{j\phi}\left\{jk\,I_2^{(+)} - I_3^{(+)}\right\} - e^{-j\phi}\left\{jk\,I_2^{(-)} - I_3^{(-)}\right\}\right]\right\} \quad (2.15\text{-b})$$

$$E_z(\underline{r}) = -\frac{C(\phi)(z - b')}{jk}\left[jk\,I_2^{(0)} - I_3^{(0)}\right] \quad (2.15\text{-c})$$

$$H_x(\underline{r}) = -\frac{Y_o\hat{k}'_{ca}C(\phi)(z - b')}{2jk}\left\{\left[jk\,I_2^{(+)} - I_3^{(+)}\right]e^{j\phi} + \left[jk\,I_2^{(-)} - I_3^{(-)}\right]\right.$$
$$\left. e^{-j\phi}\right\} \quad (2.16\text{-a})$$

$$H_y(\underline{r}) = +\frac{Y_o\hat{k}'_{ca}C(\phi)(z - b')}{2k}\left\{\left[jk\,I_2^{(+)} - I_3^{(+)}\right]e^{j\phi} - \left[jk\,I_2^{(-)} - I_3^{(-)}\right]\right.$$
$$\left. e^{-j\phi}\right\} \quad (2.16\text{-b})$$

$$H_z(\underline{r}) = -\frac{Y_o\hat{k}'_{ca}C(\phi)}{jk}\left\{\rho\left\{jk\,I_2^{(0)} - I_3^{(0)}\right\} - \frac{\rho}{2}\left\{jk\,I_2^{(+)} - I_3^{(+)} + jk\,I_2^{(-)}\right.\right.$$
$$\left.\left. - I_3^{(-)}\right\}\right\} \quad (2.16\text{-c})$$

where (for $n = 1, 2, 3$)

$$I_n^{(0)} = \int_0^{2\pi} d\theta' \frac{e^{-jkR - (jk\hat{k}_{ca} + \alpha)\rho\cos\theta'}}{R^n} \tag{2.17-a}$$

$$I_n^{(+)} = \int_0^{2\pi} d\theta' \frac{e^{-jkR - (jk\hat{k}_{ca} + 0)\rho\cos\theta' + j\theta'}}{R^n} \tag{2.17-b}$$

$$I_n^{(-)} = \int_0^{2\pi} d\theta' \frac{e^{-jkR - (jk\hat{k}_{ca} + \alpha)\rho\cos\theta' - j\theta'}}{R^n} \tag{2.17-c}$$

It was shown in Ref. 1 (Page 4.36, Eqs. (4.51)(4.53)) that

$$I_n^{(+)} \simeq I_n^{(-)} \simeq I_n^{(0)} = I_n \tag{2.18}$$

Using (2.18) in (2.15-a, b, c) and (2.16-a, b, c), we obtain the approximate field components

$$E_x(r) \simeq \frac{C(\phi)}{jk}\left\{-j\hat{k}'_{ca}k\, I_1 \sin\phi - (\rho - \alpha)\cos\phi\,(jk\, I_2 - I_3)\right\} \tag{2.19-a}$$

$$E_y(r) \simeq \frac{C(\phi)}{jk}\left\{j\hat{k}'_{ca}k\, I_1 \cos\phi - (\rho - \alpha)\sin\phi\,(jk\, I_2 - I_3)\right\} \tag{2.19-b}$$

$$E_z(r) \simeq -\frac{C(\phi)}{jk}(z - b')(jk\, I_2 - I_3) \tag{2.19-c}$$

$$H_x(r) \simeq -\frac{Y_o\,\hat{k}'_{ca}\,C(\phi)(z - b')}{jk}\cos\phi\,(jk\, I_2 - I_3) \tag{2.20-a}$$

$$H_y(r) \simeq -\frac{Y_o\,\hat{k}'_{ca}\,C(\phi)(z - b')}{jk}\sin\phi\,(jk\, I_2 - I_3) \tag{2.20-b}$$

$$H_z(r) \simeq -\frac{Y_o\,\hat{k}'_{ca}\,C(\phi)}{jk}\left\{-(\rho - \alpha)(jk\, I_2 - I_3)\right\} \tag{2.20-c}$$

The approximate radial and azimuthal components of the fields can be obtained from (2.19-a, b, c) and (2.20-a, b, c) with the aid of (2.13-a, b).

The results are

$$E_\rho(r) \simeq \frac{C(\phi)}{jk}\left\{-(\rho - \alpha)(jk\, I_2 - I_3)\right\} \tag{2.21-a}$$

$$E_\phi(r) \simeq \frac{C(\phi)}{jk}\left\{jk\,\hat{k}'_{ca}\,I_1\right\} \tag{2.21-b}$$

$$E_z'(\xi) \simeq -\frac{C(o)}{jk}(z - b')(jk\, I_2 - I_3) \qquad (2.21\text{-c})$$

$$H_o'(\xi) \simeq -\frac{Y_o\, \hat{k}_{ca}'\, C(o)}{jk}(z - b')(jk\, I_2 - I_3) = Y_o\, \hat{k}_{ca}'\, E_z'(\xi) \qquad (2.22\text{-a})$$

$$H_z'(\xi) \simeq 0 \qquad (2.22\text{-b})$$

$$H_z'(\xi) \simeq -\frac{Y_o\, \hat{k}_{ca}'\, C(b)}{jk}\left\{-(\rho - \rho')(jk\, I_2 - I_3)\right\} = -Y_o\, k_{ca}'\, E_o'(\xi) \qquad (2.22\text{-c})$$

A discussion of the evaluation of the integrals I_n is presented in Appendix I.

3. Calculations of Received Signals

The calculation of the received signal consists of the following steps:

Step 1: Calculation of the fields from the cable at an arbitrary point (x, y, z) as if the cable were in infinite free space

Step 2: Determination of the plane wave spectral representation of the fields calculated in Step 1

Step 3: Evaluation of the effects of the presence of the ground on the spectral fields determined in Step 2

Step 4: Coordinate transformations on the superposition of the spectral fields calculated in Steps 2 and 3 in order to prepare for the use of that superposition as the input to the scattering process. The transformation is from the earth coordinate system (x, y, z or ρ, φ, z) to a system whose origin is at the center of the scatterer and whose z-axis is parallel to the direction of the propagation vector of the wave incident on the scatterer

Step 5: Calculation of the fields scattered toward an arbitrary point, using the Barber scattering program

Step 6: Evaluation of the ground-reflected scattered field components at an arbitrary point, again using the Barber scattering program

Step 7: Coordinate transformation of the scattered field component (direct plus ground-reflected) from scatterer-centered coordinates to earth coordinates

Step 8: Integration ofthe superposition of field components calculated in Steps 2, 3, 5, 6 and 7 at the antenna over the plane-wave spectral space to produce the total field at the antenna

The background analysis and discussion pertaining to Steps 3, 4, 5, 6, 7 and 8 was covered in Reference 1, Sections 5, 6, 7, 9, 3, and 10

respectively. Brief summaries of the key results and required revisions pertaining to each of the steps 3, 4, 5, 6, 7 and 8 are presented in the present report in Sections 3.2, 3.3, 3.4, 3.6, 3.5, and 3.7. Step 1, for which the procedures were revised in the new project, is described in Section 2 of the present report.

Step 2 is described in Reference 1, Sections 3, 4 and aided by the material in Appendices II and III. A brief summary of some new investigations of this issue is presented in Section 3.1 of the present report.

3.1 Plane-wave Spectral Representation of Fields

The representation of a general electric or magnetic field vector as a superposition of plane wave fields, known as the "plane-wave spectrum" of the field,[1,66,67] was discussed in considerable detail in Ref. 1, Sections 3 and 4 and Appendices II and III. Referring to Appendix II of Ref. 1 we repeat here the Fourier transform pair given by Eqs. (II.3) and (II.4), with slight modifications.

First, from (II.3) the field vector $\underline{V}(\underline{r})$ at the observation point $\underline{r} = (\rho, \phi, z)$ is expressed in terms of its "plane wave spectrum" by

$$\underline{V}(\underline{r}) = \underline{V}(\underline{\rho}, z) = \iint_{\substack{\beta\text{-space in} \\ \text{which } \beta_h^2 + \beta_z^2 = 1}} d^2\beta_h \, e^{jk\underline{\beta}_h \cdot \underline{\rho}} \left\{ e^{-jk|\beta_z|z} \underline{V}_-(\underline{\beta}_h) + e^{jk|\beta_z|z} \underline{V}_+(\underline{\beta}_h) \right\} \tag{3.1}$$

where

$\underline{\rho} = x\hat{\underline{x}} + y\hat{\underline{y}}$ = horizontal part of $\underline{r}$

$\underline{\beta}$ = unit propagation vector = $\beta_x\hat{\underline{x}} + \beta_y\hat{\underline{y}} \pm |\beta_z|\hat{\underline{z}}$

$\underline{\beta}_h = \beta_x\hat{\underline{x}} + \beta_y\hat{\underline{y}}$ = horizontal part of $\underline{\beta}$

$\beta_h = |\underline{\beta}_h| = \sqrt{\beta_x^2 + \beta_y^2}$ = magnitude of horizontal part of $\underline{\beta}$

$|\beta_z| = \sqrt{1 - \beta_h^2}$ = absolute value of vertical component of $\underline{\beta}$

$\phi_\beta = \tan^{-1}\left(\frac{\beta_y}{\beta_x}\right)$ = direction angle of horizontal component of $\underline{\beta}$

$\beta_x = \beta_h \cos\phi_\beta$

$\beta_y = \beta_h \sin\phi_\beta$

$d^2\underline{\beta} = d\beta_x\, d\beta_y$

$\underline{\tilde{V}}_+(\underline{\beta}_h)$ = Portion of plane-wave spectrum of $\underline{V}(\underline{r})$ corresponding to $e^{+jk|\beta_z|z}$ (upward propagating plane wave)

$\underline{\tilde{V}}_-(\underline{\beta}_h)$ = Portion of plane-wave spectrum of $\underline{V}(\underline{r})$ corresponding to $e^{-jk|\beta_z|z}$ (downward propagating plane wave)

Inversion of (3.2) yields

$$\underline{V}_{\pm}(\underline{\beta}_h) = \frac{\left(\frac{k}{2\pi}\right)^2}{jk(1 + |\beta_z|)} \int_{-\infty}^{\infty}\int d^2\rho \left\{ jk|\beta_z|\, \underline{V}(\underline{\rho}, 0) \pm \left(\frac{\partial \underline{V}(\underline{\rho}, z)}{\partial z}\right)_{z=0} \right\} e^{-jk\underline{\beta}_h \cdot \underline{\rho}} \tag{3.2}$$

where $d^2\rho = dx\, dy$

The work that was done on this project to calculate plane-wave spectral fields $\underline{E}^{\pm}(\underline{\beta}_h)$ from the cable fields $\underline{E}(\underline{\rho}, z)$ and $\frac{\partial \underline{E}(\underline{\rho}, z)}{\partial z}$ through (3.2) (an approach that was eventually abandoned; see Section 4) is detailed in Appendix II. Also described in Appendix II is the work done on an alternative to solution of (3.2) used to obtain an approximation to the plane-wave spectrum.

3.2 Ground Reflections

Reflection of a plane wave with wave propagation vector $k\underline{\beta}$ propagating in semi-infinite free-space bounded by the surface of the earth was discussed in Ref. 1, Section 5. The results are given in Eqs. (5.13-a, b). With small changes in notation, the results for the electric field (magnetic field results will not be needed here) can be written in the form

$$[\tilde{E}_r^{(+)}(\underline{\beta}_h)] = [R_E(\underline{\beta}_h)][\tilde{E}_i^{(-)}(\underline{\beta}_h)] \tag{3.3}$$

where

$$\tilde{E}_r^{(+)}(\underline{\beta}_h) = \begin{bmatrix} \tilde{E}_{rx}^{(+)} \\ \tilde{E}_{ry}^{(+)} \\ \tilde{E}_{rz}^{(+)} \end{bmatrix} = \text{Ground reflected field vector, propagating upward} \tag{3.3-a)'}$$

$$\tilde{E}_i^{(-)}(\underline{\beta}_h) = \begin{bmatrix} \tilde{E}_{ix}^{(-)} \\ \tilde{E}_{iy}^{(-)} \\ \tilde{E}_{iz}^{(-)} \end{bmatrix} = \text{Incident field vector, propagating downward} \tag{3.3-b)'}$$

$$R_{Ejk}(\underline{\beta}_h) = C_o(\underline{\beta}_h)\,\hat{R}_{Ejk}(\underline{\beta}_h) \tag{3.3-c)'}$$

$$\hat{R}_E(\underline{\beta}_h) = \begin{bmatrix} \beta_h^2 \cos 2\phi_\beta - |\beta_z| Y_z & \beta_h^2 \sin 2\phi_\beta & 0 \\ \beta_h^2 \sin 2\phi_\beta & -\beta_h^2 \cos 2\phi_\beta - |\beta_z| Y_z & 0 \\ 0 & 0 & \beta_h^2 - |\beta_z| Y_z \end{bmatrix}$$

$$= \text{ground-reflection matrix} \tag{3.3-d)'}$$

$$C_o(\beta_h) = \left(\frac{\gamma_z - |\beta_z|}{\gamma_z + |\beta_z|}\right) \frac{1}{[\beta_h^2 + |\beta_z|\gamma_z]} \qquad (3.3\text{-e})'$$

$$\gamma_z = \sqrt{\nu^2 - \beta_h^2} \qquad (3.3\text{-f})'$$

where

$\nu = \nu_R + j\nu_I$ = complex refractive index of earth

and

$$\begin{matrix} \nu_R \\ \nu_I \end{matrix} = \sqrt{\frac{\epsilon_n}{2}} \sqrt{\pm 1 + \sqrt{1 + \left(\frac{\sigma}{\omega \epsilon_o \epsilon_n}\right)^2}} \qquad (3.3\text{-g})'$$

3.3 Fields Incident on the Scatterer-Coordinate Transformations

The coordinate transformations required to adapt the field components to the Barber scattering program are treated in Section 6 of Ref. 1. Figure 6.1 on Page 6-2 of Ref. 1 is repeated here (numbered Figure 3.3.1 in the present report) to illustrate the "lab frame" and "body frame" coordinates.

As is evident from Figure 3.3.1 the electric field vector of the incident wave is in the (x_L, y_L) plane of the "Lab frame." The direction of the z_B axis of the "body frame" (which is parallel to the long dimension of the spheroidal scatterer) is defined by spherical angles (θ_p, ϕ_p) referenced to the lab frame. Since the electric field has been referenced to the "ground frame" coordinates (x, y, z), it was necessary to develop transformations between the ground frame and the lab frame and also between the lab frame and body frame. These transformations were developed in Section 6 of Ref. 1.

The transformation matrices between body and lab frame, body and ground frame, and lab and ground frame (in both directions for each case) are given by (6.4-c, d)', (6.15-a, b)' and (6.17-a, b)' of Ref. 1 respectively. These are used to develop the expressions for the electric field components in the lab frame in terms of those in the ground frame. These expressions are given by (6.28-a, b, c)' in Ref. 1 and apply to plane wave spectral components of the fields. Written in matrix form, the expressions are

$$[\tilde{E}_{iL}] = [\tilde{X}_{LO}][\tilde{E}_{iO}] \tag{3.4}$$

where

Figure 3.3.1 Coordinate systems for Berber Scattering Program

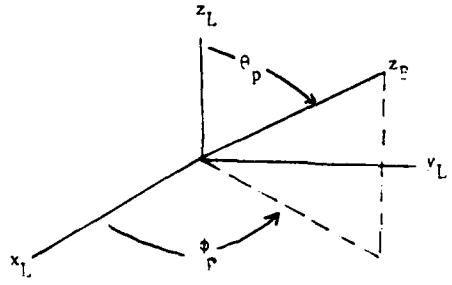

(a) Lab frame

(b) Direction of incident wave with respect to lab frame coordinates

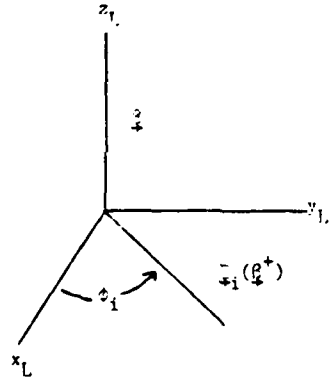

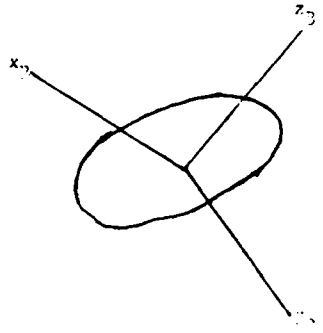

(c) Body frame

$$[\tilde{E}_{i0}] = \begin{bmatrix} \tilde{E}_{ix} \\ \tilde{E}_{iy} \\ \tilde{E}_{iz} \end{bmatrix} = \text{Spectral incident field vector in ground frame} \qquad (3.4\text{-a})'$$

$$[\tilde{E}_{iL}] = \begin{bmatrix} \tilde{E}_{ix_L} \\ \tilde{E}_{iy_L} \\ \tilde{E}_{iz_L} \end{bmatrix} = \text{Spectral incident field vector in lab frame} \qquad (3.4\text{-b})'$$

(Note that $\tilde{E}_{iz_L} = 0$, as is evident from Figure 3.3.1-b)

$$[T_{L0}] = \begin{bmatrix} (\cos\Theta_\beta \cos\Phi_\beta \cos\Phi_J - \sin\Phi_\beta \sin\Phi_J) & (\cos\Theta_\beta \sin\Phi_\beta \cos\Phi_J + \cos\Phi_\beta \sin\Phi_J) & -\sin\Theta_\beta \cos\Phi_J \\ -(\cos\Theta_\beta \cos\Phi_\beta \sin\Phi_J + \sin\Phi_\beta \cos\Phi_J) & -(\cos\Theta_\beta \sin\Phi_\beta \sin\Phi_J - \cos\Phi_\beta \cos\Phi_J) & \sin\Theta_\beta \sin\Phi_J \\ \sin\Theta_\beta \cos\Phi_\beta & \sin\Theta_\beta \sin\Phi_\beta & \cos\Theta_\beta \end{bmatrix} \qquad (3.4\text{-c})'$$

where Θ_β and Φ_β are the spherical polar and azimuthal angles respectively of the wave vector $\underline{\beta}$ in the ground frame and the angle Φ_J is defined in Eqs. (6.22-a, ..., c) of Ref. 1 for the two scattering processes treated, namely scattering directly into the antenna (Subscript A) and scattering toward the ground-reflection point (Subscript G):

$$\cos(\gamma_1)_A = \frac{\rho_{SA} \cos\theta_\beta \cos(\Phi_\beta - \Phi_{AS}) - (z_A - z_S) \sin\theta_\beta}{\sqrt{[\rho_{SA} \cos\theta_\beta \cos(\Phi_\beta - \Phi_{AS}) - (z_A - z_S) \sin\theta_\beta]^2 + [\rho_{SA} \sin(\Phi_\beta - \Phi_{AS})]^2}} \qquad (3.5\text{-a})$$

$$\sin(\phi_J)_A = \frac{-\rho_{SA} \sin(\phi_\beta - \phi_{AS})}{\sqrt{[\rho_{SA} \cos\phi_\beta \cos(\phi_\beta - \phi_{AS}) - (z_A - z_S) \sin\theta_\beta]^2 + [\rho_{SA} \sin(\phi_\beta - \phi_{AS})]^2}} \quad (3.5\text{-b})$$

$$\cos(\phi_J)_G = \frac{\rho_{SG} \cos\theta_\beta \cos(\theta_\beta - \phi_{GS}) + z_S \sin\theta_\beta}{\sqrt{[\rho_{SG} \cos\theta_\beta \cos(\phi_\beta - \phi_{GS}) + z_s \sin\theta_\beta]^2 + [\rho_{SG} \sin(\phi_\beta - \phi_{GS})]^2}} \quad (3.5\text{-c})$$

$$\sin(\phi_J)_G = \frac{-\rho_{SA} \sin(\phi_\beta - \phi_{GS})}{\sqrt{[\rho_{SG} \cos\theta_\beta \cos(\phi_\beta - \phi_{GS}) + z_S \sin\theta_\beta]^2 + [\rho_{SG} \sin(\phi_\beta - \phi_{GS})]^2}} \quad (3.5\text{-d})$$

where

$$\rho_{SA} = \sqrt{(x_A - x_S)^2 + (y_A - y_S)^2} \quad (3.5\text{-a})'$$

$$\phi_{SA} = \tan^{-1}\left[\frac{y_A - y_S}{x_A - x_S}\right] \quad (3.5\text{-b})'$$

$$\rho_{SG} = \sqrt{(x_G - x_S)^2 + (y_G - y_S)^2} \quad (3.5\text{-c})'$$

$$\phi_{SG} = \tan^{-1}\left[\frac{y_G - y_S}{x_G - x_S}\right] \quad (3.5\text{-d})'$$

$$x_G = \frac{x_A z_S + x_S z_A}{z_A + z_S} \quad (3.5\text{-e})'$$

$$y_G = \frac{y_A z_S + y_S z_A}{z_A + z_S}$$

and where (x_A, y_A, z_A), (x_G, y_G, z_G) and (x_S, y_S, z_S) are the ground frame-coordinates of the antenna, ground reflection point and scatterer center respectively. The angles ϕ_{AS} and ϕ_{GS} are respectively the azimuthal angles (in the ground frame) of the antenna relative to the scatterer center and the ground reflection point relative to the scatterer center (Eqs. (3.5-b)' and (3.5-d)'). The parameters ρ_{SA} and ρ_{SG} (Eqs. (3.5-a)' and (3.5-c)') are distances

between scatterer center and antenna and ground reflection point respectively, and (x_G, y_G) (Eqs. (3.5-e, f)') are the coordinates of the ground reflection point.

The required inputs to the Barber scattering program are the incident field amplitude (Eq. (6.33) of Ref. 1)

$$\tilde{E}_i = \sqrt{|\tilde{E}_{ix_L}|^2 + |\tilde{E}_{iy_L}|^2 + |\tilde{E}_{iz_L}|^2} \qquad (3.6\text{-a})$$

and the polarization angle of the incident field (Eq. (6.34) of Ref 1 and Figure 3.3.1 (b) of the present report)

$$\psi_i = \tan^{-1}\left(\frac{\pm|\tilde{E}_{iy_L}|}{|\tilde{E}_{ix_L}|}\right) \qquad (3.6\text{-b})$$

The quantities in (3.6-a, b) are obtained from Eqs. (3.4) with the aid of (3.4-a, ..., c)', (3.5-a, ..., d) and (3.5-a, ..., f)'.

The equations (3.6-a, b) were implemented on the computer as a part of the original project. This was done through a subroutine called "BIS." All of the Fortran statements in Subroutine BIS and the calls to BIS from the main program were checked as a part of the current project and it was confirmed that all of the programming was faithful to the analytical results summarized above. The analysis itself was also checked and found to be correct within the assumptions made in its development.

3.4 The Scattering Process

For the original project, the scattering process was modelled through the scattering program developed by Peter Barber.[50,52,57] This program, our study of alternative possibilities and the reasons why the Barber program was chosen as the means of modelling scattering from a human frame target, are discussed in detail in Section 7 of Reference 1. The theory behind the program is discussed in References 41, 45, 47, 50, 52, 57, 58, 60, 61.

Further investigation of alternatives was undertaken at the beginning of the present project. The possibility of changing to a simple short dipole scatterer was considered, as was the possibility of a simplified model in which the scatterer was treated as a small perturbation in constitutive parameters within the volume that it occupies. The small dipole was dismissed on the basis that the human frame dimension is comparable to a wavelength at the frequencies of interest and the short dipole is an extreme oversimplification. The second idea seemed to show some promise in reducing computer time (one of the principal weaknesses of the Barber program) but again it is not as accurate as the Barber program and the limited resources at our disposal did not allow the extensive software changes that would have been necessary to implement the idea for this application.

For the above reasons it was finally decided to continue to use the Barber program. Again, as in the original project, it was implemented as a subroutine called by the main program. Some small software were made in the calling format within the main program, but not in the Barber subroutine itself.

The Barber program models the scatterer as an electromagnetically uniform spheroid of length L_s and radius P_s, where L_s and $2P_s$ are assigned values

corresponding to the height and girth of a human body. The constitutive parameters for the scatterer are chosen at values representing a composite of the widely variable constitutive parameters of the various kinds of tissue found in the body (e.g., bone, skin, fatty tissue, muscle, blood). These values, carefully chosen by Professor Barber and his colleagues in connection with their studies of absorption of RF radiation by the human body, were transmitted to the Principal Investigator on our project. Those were the values used in our implementation of Barber's program.

The input to the scatterer in this program is assumed to be a linearly polarized plane wave. That is one of the major reasons for our use of the plane wave spectral representation of the fields incident on the scatterer (Section 3.1 of the present report). The approximation described in Section 4, which was eventually invoked in our final computations was a response to the difficulties encountered due to the use of the plane wave spectrum concept. Although the scheme described in Section 4 is not ideal, it is a means of approximation of the input to the scatterer that captures the most important features of plane wave fields. This is further discussed in Section 4.

3.5 Fields Emerging from the Scattering Process-Coordinate Transformation

The coordinate transformations required for the scattered fields were described in Ref. 1, Section 8. The geometry is illustrated in Figure 8.1 of Ref. 1, reproduced in the present report as Figure 3.5.1.

Figure 3.5.1

Scattering Geometry

$\hat{\beta}_S = \hat{\beta}_{SA}$ for scattering toward antenna

$\hat{\beta}_{SG}$ for scattering toward ground-reflection point

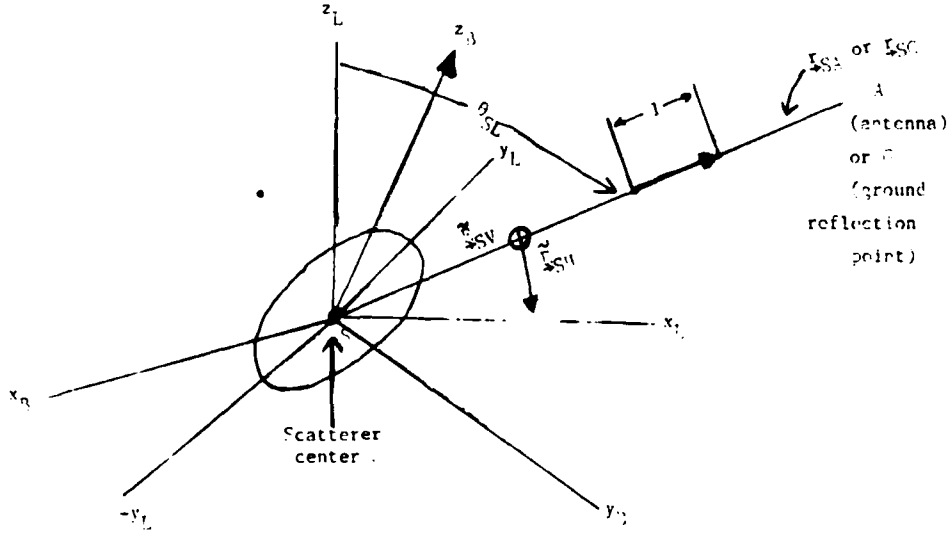

As evident from the figure, the scattered field is measured along the $(x_L - z_L)$ plane in the lab frame. The wave vector for the scattered field is called $\hat{\beta}_S$. The spherical polar angle of $\hat{\beta}_S$ in the lab frame is denoted by θ_{SL}. The outputs of the Barber scattering program are:

(1) the "vertically polarized" scattered field component $\tilde{E}_{SV}$, i.e., the component normal to the $(x_L - z_L)$ plane

(2) the "horizontally polarized" scattered field component $\tilde{E}_{SH}$, i.e., the component parallel to the $(x_L - z_L)$ plane.

The task to be performed is to obtain the scattered field components in the ground frame from the components in the lab frame. The transformation, developed in Section 8 of Ref. 1, is given by Eqs. (8.4-a, b, c) of Ref. 1, repeated below in matrix form with slightly modified notation:

$$[\tilde{E}_S^{(0)}] = [M_{0L}][\tilde{E}_S^{(L)}] \tag{3.7}$$

where

$$[\tilde{E}_S^{(0)}] = \begin{bmatrix} \tilde{E}_{SX} \\ \tilde{E}_{SY} \\ \tilde{E}_{SZ} \end{bmatrix} = \text{Ground-frame components of scattered field} \tag{3.7-a)'}$$

$$[\tilde{E}_S^{(L)}] = \begin{bmatrix} \tilde{E}_{SX_L} \\ \tilde{E}_{SY_L} \\ \tilde{E}_{SZ_L} \end{bmatrix} = \text{Lab-frame components of scattered field} \tag{3.7-b)'}$$

$$[M_{0L}] = \begin{bmatrix} (\cos\theta_\beta \cos\phi_\beta \cos\phi_J - \sin\phi_\beta \sin\phi_J) & -(\cos\theta_\beta \cos\phi_\beta \sin\phi_J + \sin\phi_\beta \cos\phi_J) & \sin\theta_\beta \cos\phi_\beta \\ (\cos\theta_\beta \sin\phi_\beta \cos\phi_J + \cos\phi_\beta \sin\phi_J) & -(\cos\theta_\beta \sin\phi_\beta \sin\phi_J - \cos\phi_\beta \cos\phi_J) & \sin\theta_\beta \sin\phi_\beta \\ -\sin\theta_\beta \cos\phi_J & \sin\theta_\beta \sin\phi_J & \cos\theta_\beta \end{bmatrix}$$

$$= [M_{L0}]^{-1} \tag{3.7-c)'}$$

The expressions (3.7) and (3.7-a, b, c)' are evaluated on the computer for each of the scattering processes "A" and "G," A being that applicable to scattering directly toward the antenna and G being that directed at the ground-reflection point.

The relationship between the lab-frame components of $\tilde{E}_S$ and the horizontally and vertically polarized components $\tilde{E}_{SV}$ and $\tilde{E}_{SH}$ is given in (3.3-a, b, c) of Ref. 1, cast in matrix form as follows:

$$[\tilde{E}_S^{(L)}] = [B][\tilde{E}_S^{(b)}] \tag{3.8}$$

where $[\tilde{E}_S^{(L)}]$ is given by (3.7-b)',

where

$$[\tilde{E}_S^{(b)}] = \begin{bmatrix} \tilde{E}_{SH} \\ \tilde{E}_{SV} \end{bmatrix} \tag{3.8-a)'}$$

and

$$[B] = \begin{bmatrix} \cos \Theta_{SL} & 0 \\ 0 & 1 \\ -\sin \Theta_{SL} & 0 \end{bmatrix} \tag{3.8-b)'}$$

and where $\cos \Theta_{SL}$ and $\sin \Theta_{SL}$ are given through (8.5-a, b) and (8.6-a, b, c) of Ref. 1.

Based on (3.7), (3.7-a, b, c)', (3.8) and (3.8-a, b) of the present report and Eqs. (8.5-a, b) and (8.6-a, b, c) of Ref. 1, the final computation of the scattered field components in the ground-frame in terms of $\tilde{E}_{SH}$ and $\tilde{E}_{SV}$ can be achieved. That result is given in (8.11-a, b, c) of Ref. 1. It is repeated below in matrix form:

$$[\tilde{E}_S^{(0)}] = [P][\tilde{E}_S^{(b)}] \tag{3.9}$$

where

$[\tilde{E}_S^{(0)}]$ and $[\tilde{E}_S^{(b)}]$ are given by (3.7-a)' and (3.8-a)' respectively and [P] is given by

$$[P] = \begin{vmatrix} [(\cos\Theta_\beta \cos\Phi_\beta \cos\Phi_J - \sin\Phi_\beta \sin\Phi_J)\cos\Theta_{SL} & [-(\cos\Theta_\beta \cos\Phi_\beta \sin\Phi_J \\ \quad - \sin\Theta_\beta \cos\Phi_\beta \sin\Theta_{SL}] & \quad + \sin\Phi_\beta \cos\Phi_J)] \\ [(\cos\Theta_\beta \sin\Phi_\beta \cos\Phi_J + \cos\Phi_\beta \sin\Phi_J)\cos\Theta_{SL} & [-(\cos\Theta_\beta \sin\Phi_\beta \sin\Phi_J \\ \quad - \sin\Theta_\beta \sin\Phi_\beta \sin\Theta_{SL}] & \quad - \cos\Phi_\beta \cos\Phi_J)] \\ [-(\sin\Theta_\beta \cos\Phi_J \cos\Theta_{SL} & [\sin\Theta_\beta \sin\Phi_J] \\ \quad + \cos\Theta_\beta \sin\Theta_{SL})] & \end{vmatrix} \tag{3.9-a)'}$$

where

$\cos\Phi_J$ and $\sin\Phi_J$ for both A and G processes are given by (3.5-a, ..., d) with the aid of (3.5-a, ..., f)'

and Eqs. (8.5-a, b) and (8.6-a, b, c) of Ref. 1)

$$\cos\Theta_{SL}^{(U)} = \frac{z_{LU}}{r_{SU}} \tag{3.9-b)'}$$

$$\sin\Theta_{SL}^{(U)} = \frac{|x_{LU}|}{r_{SU}} \tag{3.9-c)'}$$

where

(x_U, y_U, z_U) = rectangular coordinates of point U (3.9-d)'

$r_{SU} = \sqrt{(x_U - x_S)^2 + (y_U - y_S)^2 + (z_U - z_S)^2}$ = distance between scatterer center and point U (3.9-e)'

$$x_{LU} = (\cos\Theta_\beta \cos\Phi_\beta \cos\Phi_J - \sin\Phi_\beta \sin\Phi_J)(x_U - x_S) + (\cos\Theta_\beta \sin\Phi_\beta \cos\Phi_J + \cos\Phi_\beta \sin\Phi_J)(y_U - y_S) - \sin\Theta_\beta \cos\Phi_J (z_U - z_S) \tag{3.9-f)'}$$

$$z_{LU} = \sin \Theta_\beta \cos \Phi_\beta (x_U - x_S) + \sin \Theta_\beta \sin \Phi_\beta (y_U - y_S) + \cos \Theta_\beta (z_U - z_S) \qquad (3.6\text{-}8)'$$

and where U is either the antenna (Point A) or the ground reflection point (Point G).

In the original project, the equations above were implemented in a subroutine called "BOS." The analysis on which BOS is based, the Fortran in the subroutine itself and the calls to it from the main program were all examined thoroughly as a part of the current project. The analysis was found to be correct within the assumptions made and the programming was found to be consistent with the results of the analysis, so no changes were made in the software relating to the coordinate transformations at the output of the scattering process.

3.6 Effects of Ground Reflections on the Scattered Fields

The effects of ground reflections on the scattered fields was covered in Section 9 of Ref. 1. It is an adaptation of the theory discussed in Section 3.2 of the present report to the special case of a plane wave propagating in the direction from the scatterer center toward the ground reflection point. Although the scattered wave is actually a spherical wave, the ground-reflection process is modelled as if a plane wave were incident on the ground surface in a region containing the ground reflection point (i.e., the point at which the law of reflection is obeyed for the path from scatterer center to ground reflection point to antenna).

The wave vectors directed from the scatterer center S toward the ground-reflection point G, denoted by $\hat{s}^{-}_{SG}$ is given by Eqs. (9.12-b, c, e) in Ref. 1. The wave vector directed from the point G toward the antenna A, denoted by $\hat{s}^{+}_{GA}$, is given by Eqs. (9.12-f, g, i) in Ref. 1. The quantities Y^{-}_{SZ} and Y^{+}_{SZ} for these wave directions are given by (9.12-j, k) in Ref. 1.

The following equations, taken from Ref. 1 (Eqs. 9.12-a, ..., k), summarize the results of the analysis pertaining to ground reflection of the scattered fields:

$$x_G - x_S = \frac{z_A}{z_S + z_A}(x_A - x_S)$$

$$y_G - y_S = \frac{z_S}{z_S + z_A}(y_A - y_S)$$

$$z_G - z_S = -z_S$$

Coordinate of ground reflection point relative to scatterer center in terms of antenna and scatterer coordinates (3.10-a), (3.10-b), (3.10-c)

$$r_{SG} = \left(\frac{z_S}{z_S + z_A}\right)\sqrt{(x_A - x_S)^2 + (y_A - y_S)^2 + (z_A + z_S)^2} =$$

distance between scatterer center and ground reflection point in terms of antenna and scatterer coordinates (3.10-d)

$$\underline{\beta}_S^- = \hat{x}\,\beta_{Sx}^- + \hat{y}\,\beta_{Sy}^- + \hat{z}\,\beta_{Sz}^- = \frac{\underline{r}_{SG}}{r_{SG}} = \frac{\hat{x}(x_G - x_S) + \hat{y}(y_G - y_S) - \hat{z}(z_S)}{\sqrt{(x_G - x_S)^2 + (y_G - y_S)^2 + z_S^2}} \tag{3.10-e}$$

where

$$\left.\begin{aligned} \beta_{Sx}^- &= \left(\frac{z_S}{z_S + z_A}\right)\frac{(x_A - x_S)}{r_{SG}} \\ \beta_{Sy}^- &= \left(\frac{z_S}{z_S + z_A}\right)\frac{(y_A - y_S)}{r_{SG}} \\ \beta_{Sh}^- &= \sqrt{(\beta_{Sx}^-)^2 + (\beta_{Sy}^-)^2} \\ \beta_{Sz}^- &= \frac{-z_S}{r_{SG}} = -\sqrt{1 - (\beta_{Sh}^-)^2} \end{aligned}\right\}$$ components of wave vector for scattered wave incident on ground reflection point (3.10-f), (3.10-g), (3.10-h), (3.10-i)

$$\gamma_z^- = \sqrt{\nu^2 - (\beta_{Sh}^-)^2} \tag{3.10-j}$$

Parameters for ground-reflection point to antenna propagation

$$\left.\begin{aligned} x_A - x_G &= \frac{z_A}{z_A + z_S}(x_A - x_S) \\ y_A - y_G &= \frac{z_A}{z_A + z_S}(y_A - y_S) \\ z_A - z_G &= z_A \end{aligned}\right\}$$ Coordinates of antenna relative to ground reflection point in terms of antenna and scatterer coordinates (3.11-a), (3.11-b), (3.11-c)

$$r_{GA} = \frac{z_A}{z_A + z_S}\sqrt{(x_A - x_S)^2 + (y_A - y_S)^2 + (z_A + z_S)^2} =$$

distance between antenna and ground in terms of antenna and scatterer coordinates (3.11-d)

$$\underline{\beta}_S^+ = \hat{x}\,\beta_{Sx}^+ + \hat{y}\,\beta_{Sy}^+ + \hat{z}\,\beta_{Sz}^+ = \frac{\underline{r}_{GA}}{r_{GA}} = \frac{\hat{x}(x_A - x_G) + \hat{y}(y_A - y_G) + \hat{z}(z_A)}{\sqrt{(x_A - x_G)^2 + (y_A - y_G)^2 + z_A^2}} \tag{3.11-e}$$

where

$$\beta^+_{Sx} = \left(\frac{z_A}{z_S + z_A}\right)\frac{(x_A - x_S)}{r_{GA}} \qquad (3.11\text{-f})$$

$$\beta^+_{Sy} = \left(\frac{z_A}{z_S + z_A}\right)\frac{(y_A - y_S)}{r_{GA}} \qquad (3.11\text{-g})$$

$$\beta^+_{Sh} = \sqrt{(\beta^+_{Sx})^2 + (\beta^+_{Sy})^2} \qquad (3.11\text{-h})$$

$$\beta^+_{Sz} = \frac{z_A}{r_{GA}} = +\sqrt{1 - (\beta^+_{Sh})^2} \qquad (3.11\text{-i})$$

Components of wave vector for scattered wave reflected from ground and propagating toward antenna

$$\gamma^+_{Sz} = \sqrt{v^2 - (\beta^+_{Sh})^2} \qquad (3.11\text{-j})$$

Given Eqs. (3.10-a, ..., j) and (3.11-a, ..., j), we can apply the theory of ground reflection of plane waves summarized in Section 3.2. We invoke Eq. (3.3) in the form given by (9.13) in Ref. 1. The final expression for the ground-reflected scattered field vector at the antenna is:

$$[\tilde{E}_S^{(GA)}] = [R_E^{(GA)}][\tilde{E}_S^{(G)}] \qquad (3.12)$$

where

$$[\tilde{E}_S^{(GA)}] = \begin{bmatrix} \tilde{E}_{Sx}^{(GA)} \\ \tilde{E}_{Sy}^{(GA)} \\ \tilde{E}_{Sz}^{(GA)} \end{bmatrix} \qquad (3.12\text{-a})'$$

$[\tilde{E}_S^{(G)}] = [\tilde{E}_S^{(O)}]$ as given by (3.9) for the "G" scattering process (3.12-b)'

$$R_{Ejk}^{(GA)} = C_o(\beta^+_{hs})\,\hat{P}_{Ejk}^{(GA)} \qquad (3.12\text{-c})'$$

where

$$\hat{R}_E^{(GA)} = \begin{bmatrix} [(\beta_{Sh}^+)^2 \cos 2\phi_{S\beta}^+ - |\beta_{Sz}^+| \gamma_{Sz}^+] & [(\beta_{Sh}^+)^2 \sin 2\phi_{S\beta}^+] & 0 \\ [(\beta_{Sh}^+)^2 \sin 2\phi_{S\beta}^+] & [-(\beta_{Sh}^+)^2 \cos 2\phi_{S\beta}^+ - |\beta_{Sz}^+| \gamma_{Sz}^+] & 0 \\ 0 & 0 & [(\beta_{Sh}^+)^2 - |\beta_{Sz}^+| \gamma_{Sz}^+] \end{bmatrix}$$

and where

$$\phi_{S\beta}^+ = \tan^{-1}\left[\frac{\beta_{Sy}^+}{\beta_{Sx}^+}\right]$$

$$C_o(\beta_{hS}^+) = \left[\frac{\gamma_{Sz}^+ - |\beta_{Sz}^+|}{\gamma_{Sz}^+ + |\beta_{Sz}^+|}\right] \frac{1}{[(\beta_{Sh}^+)^2 + |\beta_{Sz}^+| \gamma_{Sz}^+]}$$

This portion of the analysis was not changed from its original form, but both the theory behind it and the computer software with which it was implemented were thoroughly checked and found to be correct.

3.7 Total Field at the Antenna

The integration of the components of the spectral field over spectral space (i.e., the space of the wave vector $\underline{\beta}$) to produce the components of the total (direct from cable plus ground-reflected plus scattered directly toward antenna plus ground-reflected scattered) field was described in detail in Reference 1, Section 10. This operation, which is actually a two-dimensional inverse Fourier transformation, is given generically by Eq. (10.1) in Section 10 of Reference 1, as follows:

$$E(\underline{r}) = \left(\frac{jk_o}{2\pi}\right)^2 \int\int_{(\beta\text{-space})} d^2\beta_h \, e^{jk_o \underline{\beta} \cdot \underline{r}} \, \tilde{E}(\beta_h) \tag{3.13}$$

where $\tilde{E}(\beta_h)$ is a component (e.g., x, y or z) of the total spectral field and $E(\underline{r})$ is the same component of the actual total field as a function of the position coordinates of the observation point. k_o is the free-space wave number and $d^2\beta_h$ denotes $d\beta_x \, d\beta_y$. Using the cylindrical coordinate representation of $\underline{\beta}$ (i.e., $\underline{\beta} = \beta_h(\hat{x} \cos\phi_\beta + \hat{y} \sin\phi_\beta) \pm |\beta_z|\hat{z}$) and noting that $|\beta_z| = \sqrt{1 - \beta_h^2}$, the integral (3.13) can be converted to the form

$$E(\rho, \phi, z) = \left(\frac{jk_o}{2\pi}\right)^2 \int_0^{2\pi} d\phi_\beta \int_0^1 d\beta_h \beta_h \, \tilde{E}^+(\beta_h, \phi_\beta) e^{jk_o[\rho\beta_h \cos(\phi_\beta - \phi) + z\sqrt{1 - \beta_h^2}]} \tag{3.14}$$

where it is noted that only the "upgoing" spectral wave (i.e., $\beta_z = + |\beta_z|$) enters the computation, because both direct (from cable) and ground-reflected spectral waves incident on the scatterer are upgoing.

The procedure for integrating (3.14) in the original project was to first evaluate the β_h integral numerically and then evaluate the ϕ_β integral by stationary phase methods. It was recognized that a compromise in accuracy was incurred in certain parameter regimes through the use of stationary phase. However, the expenditure of computer time in performing a more rigorous

numerical integration on ϕ_3 is prohibitive. Consequently it was decided to continue to use stationary phase for the ϕ_β-integration in the present project.

There was some improvement in the technique for carrying out this double integration, however. A new numerical integration procedure was adopted for the β_h integral that is very fast and requires only 12 points to attain great accuracy over the range from $\beta_h = 0$ to $\beta_h = 1$. That technique was used in the computations that were done using the plane-wave spectrum approach. In Section 4, a new approach not requiring this integration is described, and the latter approach was used to obtain our final numerical results. Hence the issue of how the integration is performed becomes academic with respect to the actual results presented in Section 5.

4. Approximation of Field at Scatterer as a Single Plane Wave

In Appendix II the difficulties experienced in trying to implement the plane-wave spectrum approach are described in some detail. In response to these difficulties, a new scheme was devised, in which the plane-wave spectrum approach was abandoned in favor of an approach wherein the field incident on the scatterer is approximated as a single plane wave (i.e., not as a superposition of plane waves) Obviously this constitutes a sacrifice in realism, because the field incident on the scatterer from the cable is not a plane wave. However, the scattering is determined by the incident field within the volume occupied by the scatterer. The incident field pattern outside the scatterer volume does not affect the scattered wave. Thus if the variation of the incident field resembles that of a plane wave coming from a particular direction within the scatterer volume, regardless of its behavior outside that volume, then it can be so approximated for purposes of determining the scattered wave fields.

Various ways of generating a plane wave approximation at the scatterer were contemplated. The major problem was to determine a proper direction for the incoming "approximate plane wave." It was decided that the optimal direction to assume was that in which the power flows, i.e., the direction of the Poynting vector for the total field from the cable, i.e., the fields whose rectangular components are given by (2.19-a, b, c) and (2.20-a, b, c). The procedure was to

(1) Calculate the Poynting vector for the total $\underset{\sim}{E}$ and $\underset{\sim}{H}$ fields from the cable at an arbitrary observation point $\underset{\sim}{r} = (\rho, \phi, z)$. This computation is

$$\underset{\sim}{P} = \frac{1}{2} \text{Re} \left(\underset{\sim}{E} \times \underset{\sim}{H}^* \right) \tag{4.1}$$

or in component form

$$P_x = \frac{1}{2} \text{Re} \left(E_y H_z^* - E_z H_y^* \right) \tag{4.1-a)'}$$

$$P_y = \frac{1}{2} \text{Re} \left(E_z H_x^* - E_x H_z^* \right) \tag{4.1-b)'}$$

$$P_z = \frac{1}{2} \text{Re} \left(E_x H_y^* - E_y H_x^* \right) \tag{4.1-c)'}$$

where E_x, E_y, E_z, H_x, H_y and H_z are given by (2.19-a), (2.19-b), (2.19-c), (2.20-a), (2.20-b) and (2.20-c) respectively.

(2) Calculate the amplitude of the Poynting vector

$$P_o = \sqrt{P_x^2 + P_y^2 + P_z^2} \tag{4.2}$$

where P_x, P_y, P_z are obtained from (4.1-a, b, c)'.

(3) Assume the normalized propagation vector $\underset{\sim}{\beta}$ for the assumed plane-wave incident on the scatterer to be in the direction of the Poynting vector at the center of the scatterer. Since $\underset{\sim}{\beta}$, by definition, must have unit magnitude, this implies that the components of $\underset{\sim}{\beta}$ are given by

$$\beta_x = \frac{P_x}{P_o} \text{ at scatterer center} \tag{4.3-a}$$

$$\beta_y = \frac{P_y}{P_o} \text{ at scatterer center} \tag{4.3-b}$$

$$\beta_z = \frac{P_z}{P_o} \text{ at scatterer center} \tag{4.3-c}$$

The calculations of the components of $\underset{\sim}{\beta}$ are made from (4.3-a, b, c) with the components of $\underset{\sim}{P}$ calculated from (4.1-a, b, c)' and P_o from (4.2).

(4) The values of β_x, β_y, β_z obtained from (4.3-a, b, c) are used as inputs to the Barber scattering program, in order to define the direction of the plane-wave assumed to be incident on the scatterer.

It should be noted that the approximation used here is based on the determination of the direction of power flow only at the exact center of

the scatterer. The actual direction of the Poynting vector will be different at different points on the scatterer, but we are in effect assuming that the incident wave can be approximated by a linearly polarized plane electromagnetic wave.

The properties of the assumed plane wave are as follows:

(1) the amplitude of a component of the electric field of the incident plane wave is the amplitude of that component of the actual electric field at the center of the scatterer

(2) the incident plane wave is propagating in the direction of the Poynting vector (i.e., direction of power flow) of the actual fields at the center of the scatterer

(3) the spatial direction of the electric field of the incident plane wave is the spatial direction of the actual electric field at the center of the scatterer

Assumption (2) guarantees that the assumed plane wave will be transverse, because it forces the propagation direction as defined by β to be normal to both electric and magnetic field vectors at the center of the scatterer. Although the phase fronts of the field may have some significant curvature within the scatterer volume if that volume is comparable to a cubic wavelength, and the variation of phase in the assumed propagation direction $\hat{\xi}$ is not exactly the same as that of a plane wave, the approximate wave field is that of a transverse linearly polarized wave in the region near the center of the scatterer. To repeat the point made above about the nature of the assumed plane wave, if the propagation direction as defined by $\hat{\xi}$ is parallel to the Poynting vector at the scatterer center, then $\hat{\xi}$ must be normal to both the electric and magnetic field vectors at the scatterer center, guaranteeing that the assumed plane wave is transverse throughout the volume of the scatterer.

It is also linearly polarized in that region, because the direction of the electric field of the incident wave will be assumed to be that at the scatterer center. That direction is fixed as that of the actual total electric field from the cable at that point.

Software was written to implement the computations of P_x, P_y, P_z from (4.1-a, b, c), (2.19-a, b, c) and (2.20-a, b, c), the subsequent computation of P_o from (4.2) and computation of β_x, β_y, β_z from (4.3-a, b, c). The end products of these computations are the components of $\hat{\beta}$, which define a propagation direction of the assumed plane wave incident on the scatterer and which are inputted into the Barber scattering program. The electric field amplitude and direction (in a plane normal to $\hat{\beta}$) for that plane wave, assumed to be those of the actual computed field at the scatterer center, are also delivered to the Barber scattering program as the amplitude and polarization direction of the incident plane wave. The phase of the incident plane wave's electric field at the scatterer center is assumed to be the same as that of the actual field at the scatterer center and to vary along the propagation direction (i.e., in the direction parallel to $\hat{\beta}$) as does that of a plane wave propagating in the direction of $\hat{\beta}$.

This plane wave approximation is assumed to hold within the scatterer region for both the direct field from the cable and the ground-reflected field. The latter is also approximated as a plane wave and its direction within the scatterer volume is assumed to be the same as that of the wave directly from the cable. This is a valid approximation, because the source of the field is (for all practical purposes) at ground level and hence the ground reflection point can be located at the source with negligible error. The elevation of the cable slots relative to ground level is $h' \approx .0039$, less than 1 centimeter above ground; hence for the scatterer center at its lowest possible point within the parameter regime of interest in this study

(e.g., the case of the crawling intruder, where the height of the scatterer center is 25 cm.), the ground reflection point is extremely close to the cable. To show this note that the distance between the cable and the ground reflection point is (See Figure 4.1)

$$\ell = d\left(\frac{h_1}{h_1 + h_2}\right) \tag{4.4}$$

where d is the radial distance between the cable and the scatterer center, h_1 is the height of a cable slot and h_2 is the height of the scatterer center. For the crawling intruder at the furthest radial distance in our computations (where d = 6.5 m, h_1 = .0089 m, h_2 = .25 m), the radial distance from the cable to the ground-reflection point is only about 22.5 cm and it is still smaller for larger scatterer heights and smaller scatterer distances. To put this another way, the ground-reflected wave at the scatterer center appears to originate at the image-point shown in Figure 4.1, which isabout .89 cm. below ground level. The tangents of the elevation angles of $\underset{\sim}{\beta}$ and $\underset{\sim}{\beta}'$ (the angles β and β' respectively in Figure 4.1), in the "worst case" alluded to above, are

$$\beta = \tan^{-1}\left(\frac{h_2 - h_1}{d}\right) \simeq .0369 \text{ rdn} = 2.115 \text{ degrees} \tag{4.5-a}$$

$$\beta' = \tan^{-1}\left(\frac{h_2 + h_1}{d}\right) \simeq .0398 \text{ rdn} = 2.281 \text{ degrees} \tag{4.5-b}$$

The difference in angle between the propagation vectors of the direct and ground-reflected (assumed) plane-waves in the worst case is only .166 degrees, hence for practical purposes the propagation directions for these two waves can be considered parallel.

Based on the above arguments, the ground-reflected wave impinging on the scatterer is modelled as a plane wave propagating in the direction of

Figure 4.1

Geometry of Ground Reflection for Plane-Wave Approximation

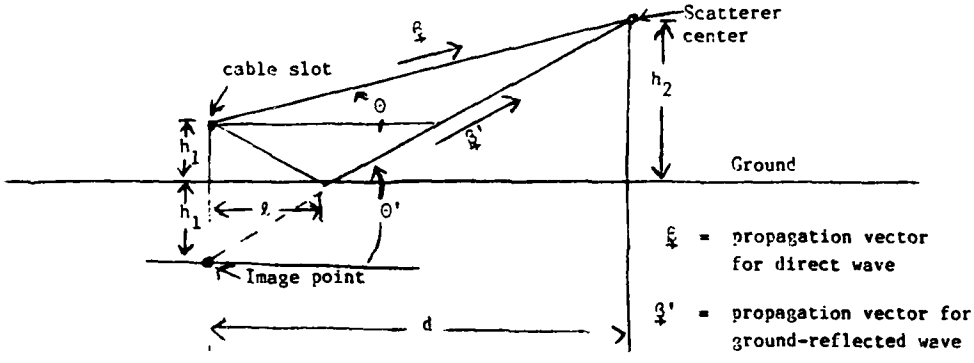

the Poynting vector for the total field from the cable at the scatterer center. The amplitude and phase of the components of that wave at the scatterer center are those obtained through the ground-reflection transformation equations (3.3) and (3.3-a, b, ..., f, g)', where the parameters (β_h, ϕ_β) used in (3.3-c, d, e, f)' are otained from (β_x, β_y, β_z) as calculated from (4.3-a, b, c).

5. Results and Conclusions

In this section the numerical results are presented (Subsection 5.1) and then discussed (Subsection 5.2).

5.1 Numerical results

Numerical computations were made of:

(1) The rectangular components of the (direct and ground-reflected) electric fields at various observation points near the cable in the absence of a scatterer (i.e., the "illuminating fields" in the region where the scatterer would be located)

(2) The rectangular components of the (direct plus ground-reflected) electric field at the antenna in the absence of a scatterer

(3) The rectangular components of the contributions to the field at the antenna due to the presence of the scatterer (wave scattered directly into the antenna plus ground-reflected scattered wave at the antenna)

(4) The rectangular components of the total field (direct-wave-plus-ground reflected wave plus direct scattered wave plus ground-reflected scattered wave) at the antenna

The format for these computations was essentially the same as that in Reference 1, Section 11. For the set of computations (1), the amplitudes of the rectangular component of the electric field were computed for eight values of ρ, the radial coordinate at the observation point, at a fixed value of the azimuthal coordinate ϕ and the height z. For one particular set of results presented, z is set at 0.5 meters and ϕ is set at 0°, 90°, 180° or 270°. For another set of results presented, ρ is set at 0° and z is set at 1, 1.5, 2 and 2.5 meters. For each fixed pair of values of ρ and z, a

set of runs was made for ρ = 17.5, 19.0, 20.5, 22.0, 23.5, 25.0, 26.5 and 28.0. In each case, the quantities $|E_x|$, $|E_y|$, $|E_x|$, $|E_x|^2$, $|E_y|^2$, $|E_z|^2$ and $|E_x|_{dB} = 20 \log_{10} |E_x|$, $|E_y|_{dB}$ and $|E_z|_{dB}$ were computed.

The computations (2) were also of the absolute amplitudes, squared amplitudes and amplitudes in decibels of the rectangular components of the electric field, but at a single point, the location of the antenna. The assumed antenna coordinates are ρ = 0 and z = 1.

The format for the computations (3) and (4) was exactly the same as that for the computations (1). Of course, the coordinate values ρ, ϕ and z, which were the coordinates of the observation point in computations (1), are now the coordinates of the center of the scatterer. The coordinates of the observation point in computations (3) and (4) are those assumed for the antenna, ρ = 0 and z = 1.

The purpose of the computations (1) is to determine the amplitudes of the components of the fields that illuminate the scatterer as its distance from the cable varies. The cable is at ρ approximately equal to 24 meters; hence the radial distance of the observation point from the cable is varied from 6.5 meters inside (ρ = 17.5) to 4.0 meters outside (ρ = 28).

Computations (2) and (3) were done for the purpose of separating out the contributions to the fields at the antenna location from the cable (both direct and ground-reflected) and the contributions from the scatterer. Computations(4) are those of the end-product of this study, the total field due to cable, ground reflections and scatterer.

Since the antenna used in the system of direct interest is vertical and therefore responds only to the vertical electric field component, plots are presented only for the vertical field components in Computations (3).

Tabulated results are presented for all field components.

For the computations (3) and (4), three cases are considered, as in Reference 1. The first case is the "radial walk," where the spheroid that represents the human frame target has its long axis in the vertical direction as it moves between $\rho = 17.5$ and $\rho = 28.0$. The second case is the "radial crawl," where the spheroid's axis is in the horizontal direction and pointed in the radial direction as it traverses the path between $\rho = 17.5$ and $\rho = 28.0$. The third case is the "radial walk on stilts," where the upright "man" is elevated by 1 meter relative to ground level, implying the use of 1 meter-high stilts to elude detection.

The tables below (Tables 5.1, 5.2, 5.3) constitute an account of the numerical results for Computations (1), (3) and (4). The results are all presented in decibels relative to a reference level of 1 v/m. In each column, the peak value (if it exists) is indicated by surrounding the number by a rectangle.* The results for Computation (2), the fields at the antenna without the scatterer, are:

$$|E_x|_{dB} = -112$$

$$|E_y|_{dB} = -110$$

$$|E_z|_{dB} = -146 \qquad (5.1)$$

---

* In some cases, there is no clearly definable peak value, in which case there is no such indication.

Plots of some of the above results are presented in Figures 5.1 through 5.24. The plots are as follows:

page 5.10, Fig. 5.1 Illuminating field component: $|E_x|$dB vs. ρ, $z = 0.5$, $\phi = 0°$

" 5.11 " 5.2 " " " " " " " " " " " 90°

" 5.12 " 5.3 " " " " " " " " " " " 180°

" 5.13 " 5.4 " " " " " " " " " " " 270°

" 5.14 " 5.5 " " " $|E_y|$dB vs. ρ, $z = 0.5$, $\phi = 0°$

" 5.15 " 5.6 " " " " " " " " " " " 90°

" 5.16 " 5.7 " " " " " " " " " " " 180°

" 5.17 " 5.8 " " " " " " " " " " " 270°

" 5.18 " 5.9 " " " $|E_z|$dB vs. ρ, $z = 0.5$, $\phi = 0°$

" 5.19 " 5.10 " " " " " " " " " " " 90°

" 5.20 " 5.11 " " " " " " " " " " " 180°

" 5.21 " 5.12 " " " " " " " " " " " 270°

" 5.22 " 5.13 Scattered " " $|E_z|$dB " " Radial walk, z=1 ϕ=0°

" 5.23 " 5.14 " " " " " " " " " " " 90°

" 5.24 " 5.15 " " " " " " " " " " " 180°

" 5.25 " 5.16 " " " " " " " " " " " 270°

" 5.26 " 5.17 " " " " " " Radial crawl, z=0.25 ϕ=0°

" 5.27 " 5.18 " " " " " " " " " " " 90°

" 5.28 " 5.19 " " " " " " " " " " " 180°

" 5.29 " 5.20 " " " " " " " " " " " 270°

" 5.30 " 5.21 " " " " " " Radial Walk, z=2 ϕ=0° on stilts

" 5.31 " 5.22 " " " " " " " " " " " 90°

" 5.32 " 5.23 " " " " " " " " " " " 180°

" 5.33 " 5.24 " " " " " " " " " " " 270°

Table 5.1

Illuminating Field Components at Various Observation Points - No Scatterer, No Ground Reflections

(a) $|E_x|$ dB z=0.5

ρ	φ=0°	φ=90°	φ=180°	φ=270°
17.5	-101	-99	-102	-100
19.0	-98	-97	-100	-98
20.5	-95	-95	-96	-96
22.0	-89	-88	-89	-89
23.5	-81	-76	-83	-77
25.0	-82	-79	-84	-81
26.5	-90	-91	-91	-92
28.0	-97	-97	-98	-98

(b) $|E_y|$ dB z=0.5

φ=0°	φ=90°	φ=180°	φ=270°
-99	-101	-100	-103
-96	-99	-98	-100
-94	-96	-95	-97
-87	-88	-88	-90
-76	-82	-77	-83
-79	-83	-80	-84
-90	-91	-91	-92
-96	-98	-98	-99

(c) $|E_z|$ dB z=0.5

φ=0°	φ=90°	φ=180°	φ=270°
-123	-124	-125	-125
-119	-119	-120	-121
-112	-113	-114	-114
-100	-100	-102	-102
-82	-82	-83	-84
-89	-89	-90	-91
-104	-105	-106	-106
-115	-116	-117	-117

(d) φ = 0°

ρ	z=1.0	z=1.5	z=2.0	z=2.5
17.5	-101	-101	-101	-102
19.0	-99	-99	-100	-100
20.5	-96	-97	-98	-99
22.0	-90	-92	-95	-98
23.5	-88	-94	-99	-104
25.0	-86	-91	-95	-99
26.5	-91	-93	-95	-98
28.0	-97	-98	-99	-100

(e) φ = 0°

z=1.0	z=1.5	z=2.0	z=2.5
-99	-99	-99	-99
-96	-97	-97	-97
-94	-94	-95	-95
-88	-90	-92	-93
-79	-83	-87	-90
-81	-84	-88	-91
-91	-93	-94	-95
-96	-96	-96	-96

(f) φ = 0°

z=1.0	z=1.5	z=2.0	z=2.5
-117	-114	-112	-110
-113	-110	-108	-106
-107	-104	-103	-102
-96	-95	-95	-96
-82	-85	-86	-90
-86	-87	-89	-91
-99	-98	-97	-98
-110	-107	-105	-104

Table 5.2

Scattered Field Components at Antenna

	(a) Radial Walk $\lvert E_x \rvert$dB				(b) Radial Walk $\lvert E_y \rvert$dB				(c) Radial Walk $\lvert E_z \rvert$dB			
ρ	φ=0°	φ=90°	φ=180°	φ=270°	φ=0°	φ=90°	φ=180°	φ=270°	φ=0°	φ=90°	φ=180°	φ=270°
17.5	-125	-168	-134	-173	-156	-145	-154	-150	-131	-143	-132	-148
19.0	-123	-167	-135	-144	-156	-143	-153	-154	-130	-141	-130	-162
20.5	-122	-175	-148	-148	-152	-145	-150	-158	-129	-146	-129	-165
22.0	-128	-162	-128	-168	-139	-129	-145	-149	-138	-135	-129	-149
23.5	-118	-140	-117	-146	-131	-127	-150	-140	-139	-124	-129	-125
25.0	-123	-140	-135	-107	-139	-120	-151	-108	-115	-124	-129	-134
26.5	-142	-144	-154	-156	-175	-130	-174	-132	-147	-132	-155	-143
28.0	-144	-112	-152	-157	-175	-110	-180	-134	-146	-134	-152	-152
	(d) Radial Crawl $\lvert E_x \rvert$dB				(e) Radial Crawl $\lvert E_y \rvert$dB				(f) Radial Crawl $\lvert E_z \rvert$dB			
17.5	-136	-144	-135	-146	-168	-127	-170	-127	-143	-127	-143	-127
19.0	-135	-144	-134	-144	-166	-126	-171	-125	-142	-125	-143	-125
20.5	-133	-141	-132	-142	-167	-127	-169	-126	-137	-125	-142	-124
22.0	-134	-134	-130	-133	-151	-121	-168	-119	-137	-129	-139	-119
23.5	-91	-134	-115	-125	-113	-110	-152	-97	-98	-114	-133	-100
25.0	-106	-165	-130	-177	-126	-121	-142	-153	-106	-143	-113	-159
26.5	-116	-160	-122	-155	-136	-131	-144	-136	-120	-146	-125	-139
28.0	-126	-164	-126	-163	-150	-154	-149	-139	-135	-146	-129	-146

Table 5.2 (continued)

	(g) Radial Walk on Stilts $\lvert E_x \rvert$ dB				(h) Radial Walk on Stilts $\lvert E_y \rvert$ dB				(i) Radial Walk on Stilts $\lvert E_z \rvert$ dB			
ρ	φ=0°	φ=90°	φ=180°	φ=270°	φ=0°	φ=90°	φ=180°	φ=270°	φ=0°	φ=90°	φ=180°	φ=270°
17.5	-124	-164	-145	-149	-144	-145	-149	-160	-142	-145	-135	-164
19.0	-125	-165	-157	-152	-140	-144	-148	-161	-149	-145	-135	-174
20.5	-129	-183	-137	-177	-138	-149	-147	-164	-141	-152	-137	-174
22.0	-129	-155	-128	-165	-138	-131	-148	-156	-141	-136	-142	-158
23.5	-123	-153	-126	-146	-133	-140	-155	-145	-129	-135	-143	-136
25.0	-116	-152	-151	-140	-143	-133	-134	-130	-124	-133	-134	-141
26.5	-131	-144	-162	-166	-153	-135	-175	-131	-133	-140	-146	-170
28.0	-141	-147	-165	-174	-158	-129	-169	-139	-137	-146	-144	-190

Table 5.3

Total Field Components at Antenna

	(a) Radial walk $\lvert E_x \rvert_{dB}$				(b) Radial walk $\lvert E_y \rvert_{dB}$				(c) Radial walk $\lvert E_z \rvert_{dB}$			
ρ	φ=0°	φ=90°	φ=180°	φ=270°	φ=0°	φ=90°	φ=180°	φ=270°	φ=0°	φ=90°	φ=180°	φ=270°
17.5	-112	-112	-113	-112	-109	-110	-110	-110	-131	-140	-134	-160
19.0	-112	-112	-113	-112	-109	-110	-110	-110	-129	-139	-132	-148
20.5	-111	-112	-112	-112	-110	-110	-110	-110	-129	-146	-131	-147
22.0	-112	-112	-111	-112	-110	-110	-110	-110	-139	-134	-130	-142
23.5	-109	-112	-109	-112	-111	-109	-110	-110	-136	-124	-130	-125
25.0	-110	-112	-112	-107	-110	-112	-110	-105	-115	-123	-129	-133
26.5	-112	-112	-112	-112	-110	-110	-110	-111	-161	-133	-146	-153
28.0	-112	-112	-112	-112	-110	-109	-110	-110	-140	-132	-148	-149
	(d) Radial Crawl				(e) Radial Crawl				(f) Radial Crawl			
17.5	-112	-112	-113	-112	-110	-109	-110	-111	-144	-126	-148	-126
19.0	-112	-112	-113	-112	-110	-109	-110	-108	-139	-125	-147	-126
20.5	-112	-112	-113	-112	-110	-110	-110	-109	-138	-125	-147	-124
22.0	-113	-113	-112	-113	-110	-111	-110	-113	-136	-130	-140	-119
23.5	-91	-112	-114	-114	-105	-105	-110	-99	-90	-115	-135	-100
25.0	-111	-112	-111	-112	-111	-112	-110	-110	-106	-139	-113	-146
26.5	-115	-112	-114	-112	-110	-109	-110	-110	-120	-141	-124	-141
28.0	-111	-112	-114	-112	-110	-110	-110	-110	-133	-154	-128	-142

Table 5.3 (continued)

	(g) Radial Walk on Stilts				(h) Radial Walk on Stilts				(i) Radial Walk on Stilts			
17.5	-111	-112	-112	-112	-110	-110	-110	-110	-144	-143	-137	-145
19.0	-111	-112	-112	-112	-110	-110	-110	-110	-142	-142	-137	-146
20.5	-111	-112	-112	-112	-110	-110	-110	-110	-138	-145	-139	-146
22.0	-111	-112	-111	-112	-110	-110	-110	-110	-138	-137	-138	-145
23.5	-111	-112	-112	-112	-110	-110	-110	-110	-129	-137	-140	-138
25.0	-108	-112	-112	-112	-110	-110	-110	-109	-123	-131	-132	-147
26.5	-112	-112	-112	-112	-110	-109	-110	-110	-135	-146	-149	-147
28.0	-112	-112	-112	-112	-110	-109	-110	-110	-135	-140	-151	-146

FIGURE 5.1

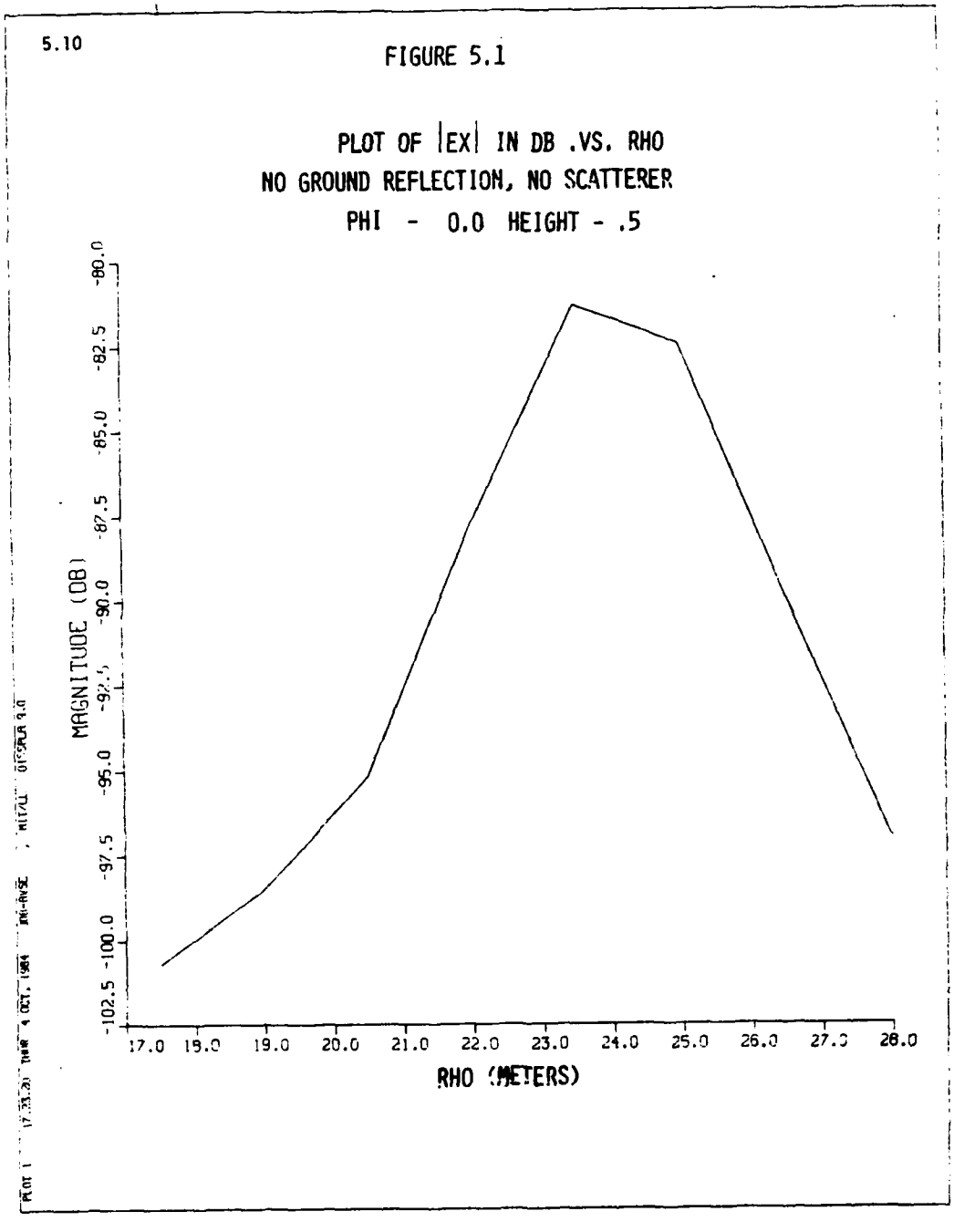
PLOT OF |EX| IN DB .VS. RHO
NO GROUND REFLECTION, NO SCATTERER
PHI - 0.0 HEIGHT - .5
MAGNITUDE (DB)
-80.0
-82.5
-85.0
-87.5
-90.0
-92.5
-95.0
-97.5
-100.0
-102.5
17.0
18.0
19.0
20.0
21.0
22.0
23.0
24.0
25.0
26.0
27.0
28.0
RHO (METERS)

FIGURE 5.2

PLOT OF |EX| IN DB .VS. RHO
NO GROUND REFLECTION, NO SCATTERER
PHI - 90.0 HEIGHT - .5

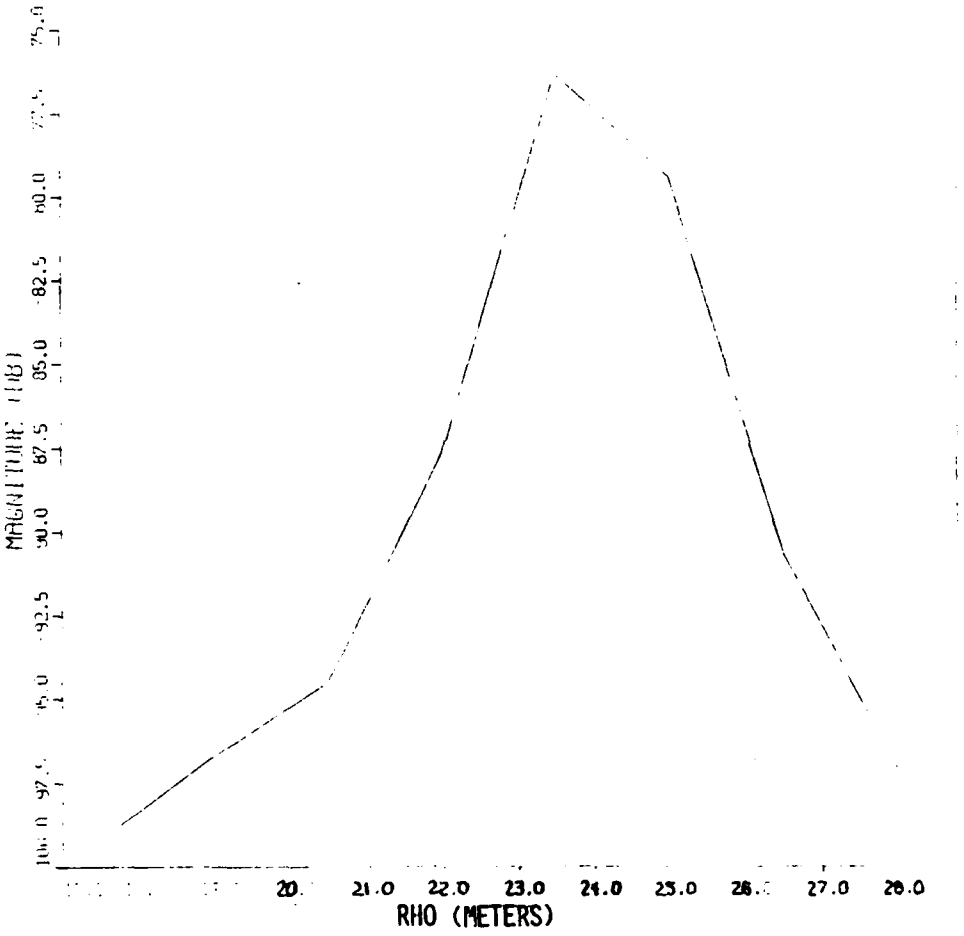

FIGURE 5.3

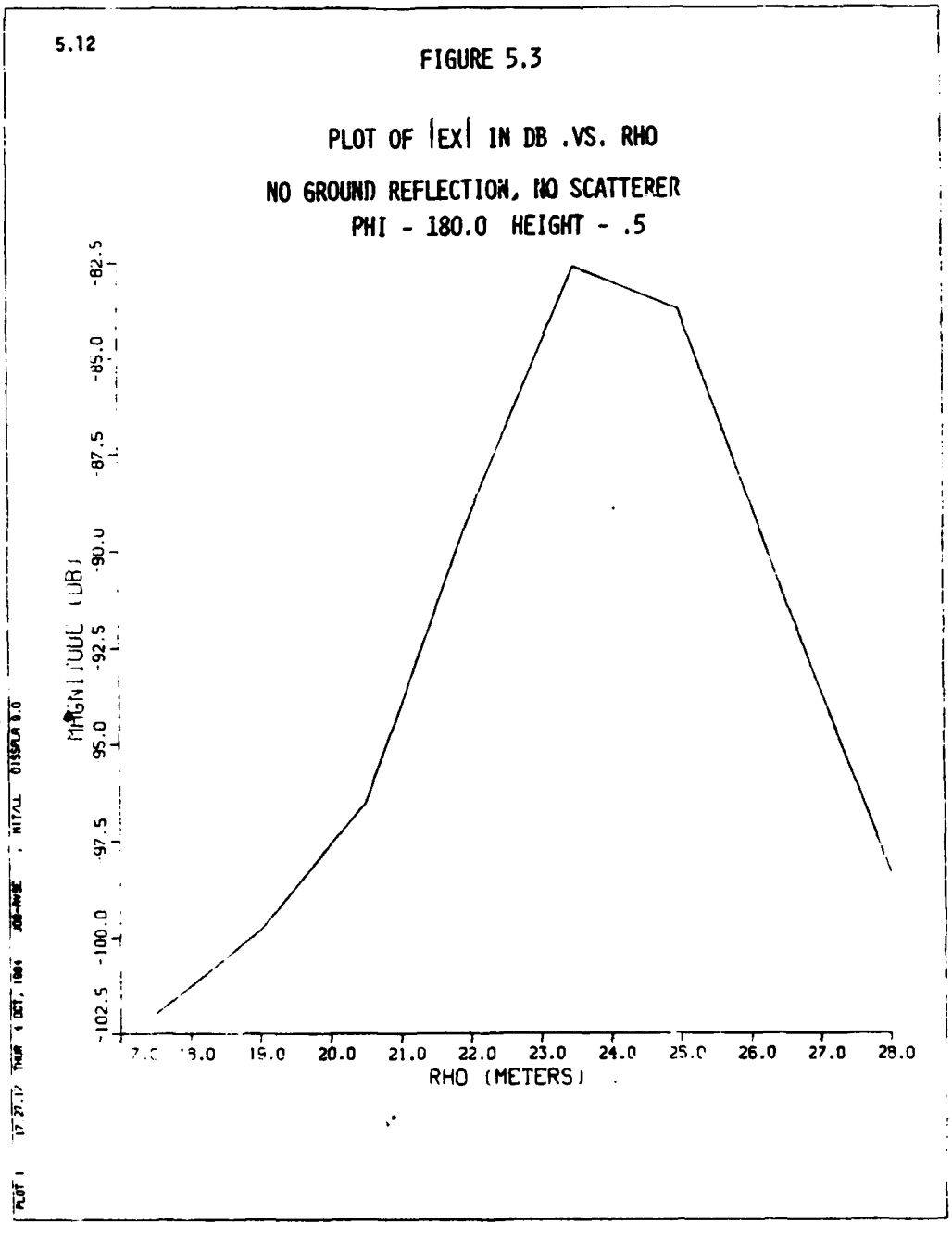
PLOT OF |EX| IN DB .VS. RHO
NO GROUND REFLECTION, NO SCATTERER
PHI - 180.0 HEIGHT - .5
MAGNITUDE (DB)
-82.5
-85.0
-87.5
-90.0
-92.5
-95.0
-97.5
-100.0
-102.5
19.0
20.0
21.0
22.0
23.0
24.0
25.0
26.0
27.0
28.0
RHO (METERS)

FIGURE 5.4

PLOT OF |EX| IN DB .VS. RHO
NO GROUND REFLECTION, NO SCATTERER
PHI - 270.0 HEIGHT - .5

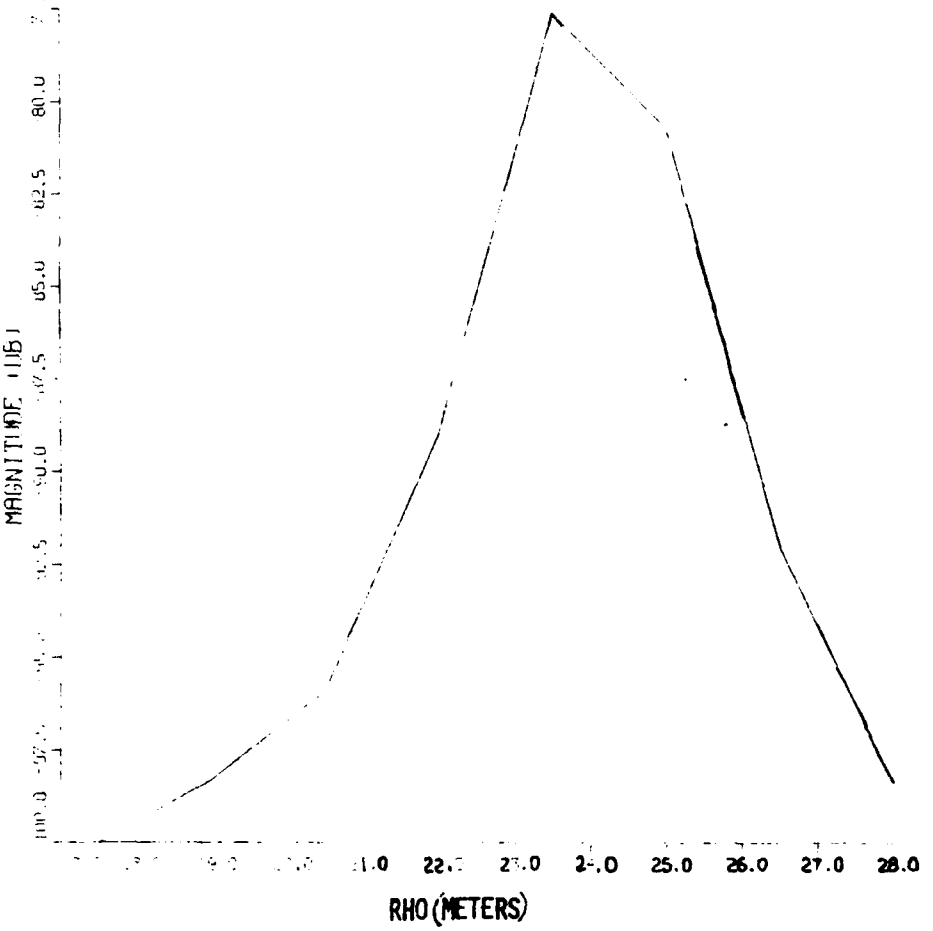

FIGURE 5.5

PLOT OF |EY| IN DB .VS. RHO

NO GROUND REFLECTION, NO SCATTERER

PHI - 0.0 HEIGHT - .5

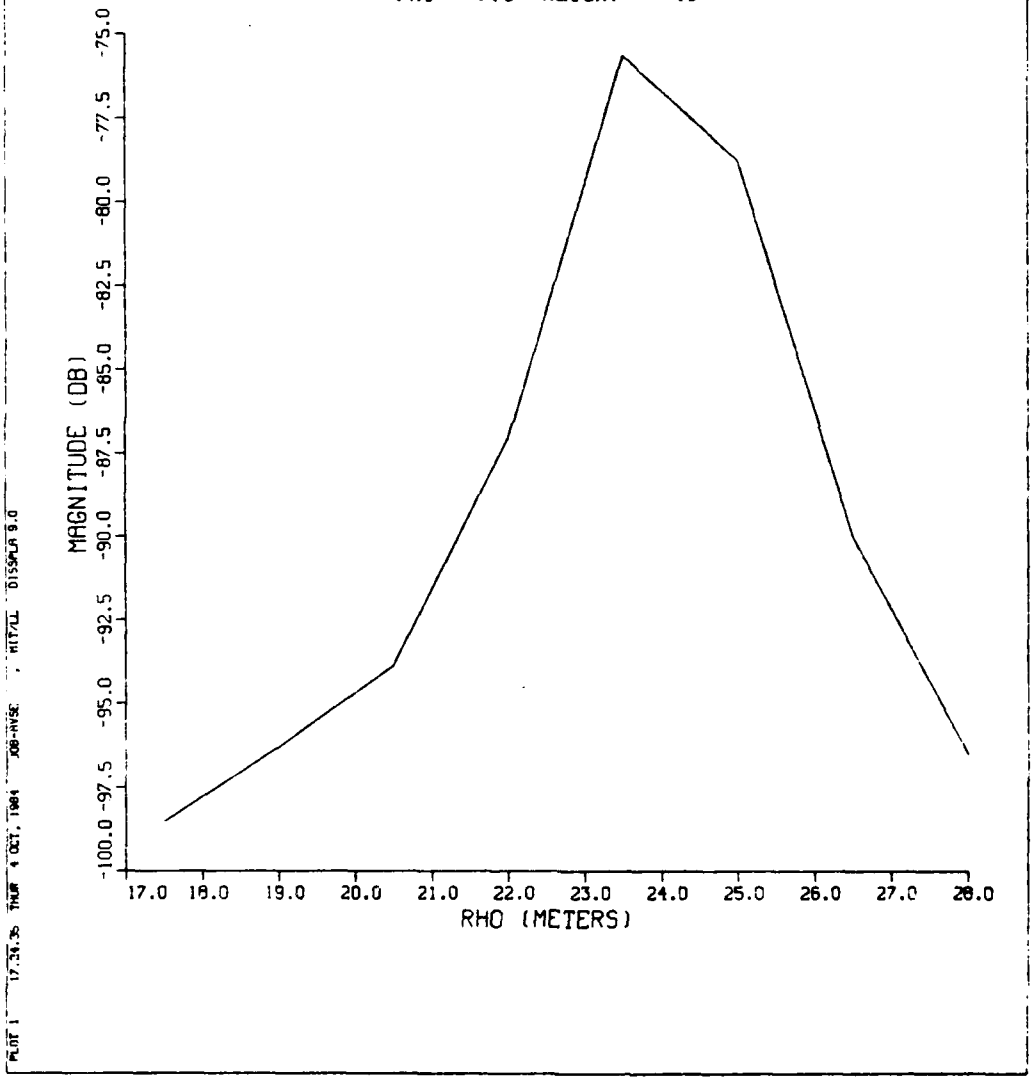

FIGURE 5.6

PLOT OF |EY| IN DB .VS. RHO
NO GROUND REFLECTION, NO SCATTERER
PHI - 90.0 HEIGHT - .5

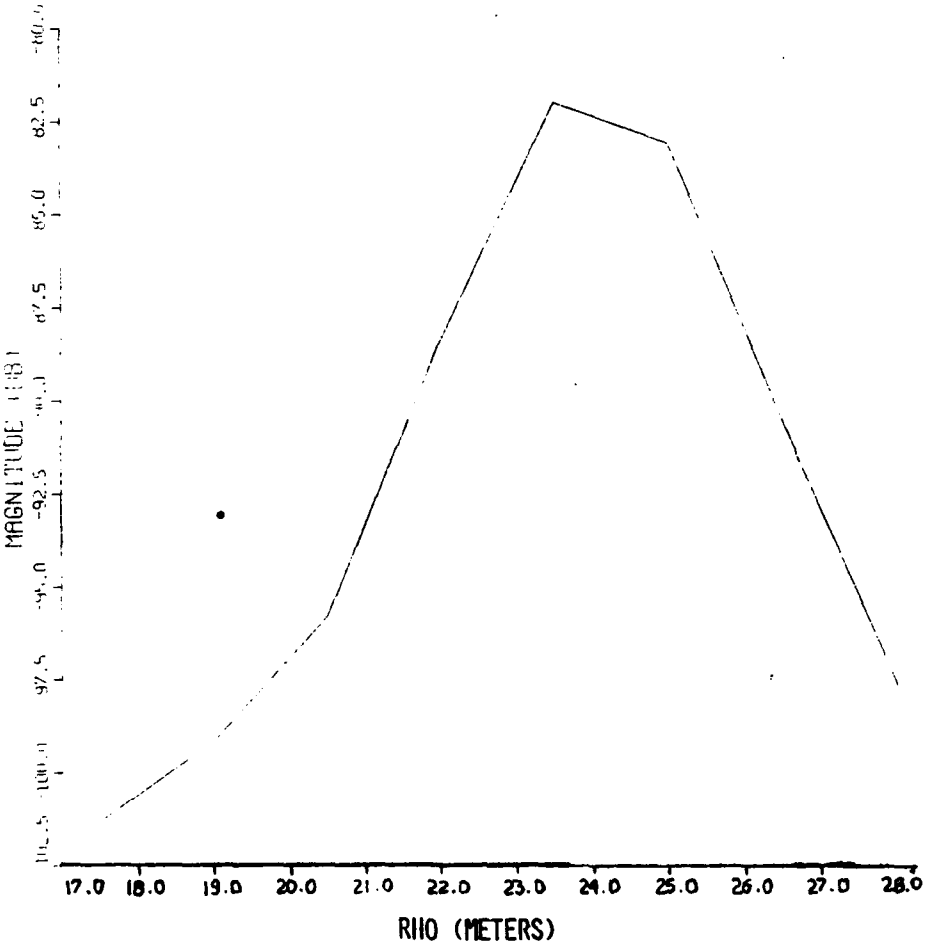

FIGURE 5.7

PLOT OF |EY| IN DB .VS. RHO
NO GROUND REFLECTION, NO SCATTERER
PHI - 180.0 HEIGHT - .5

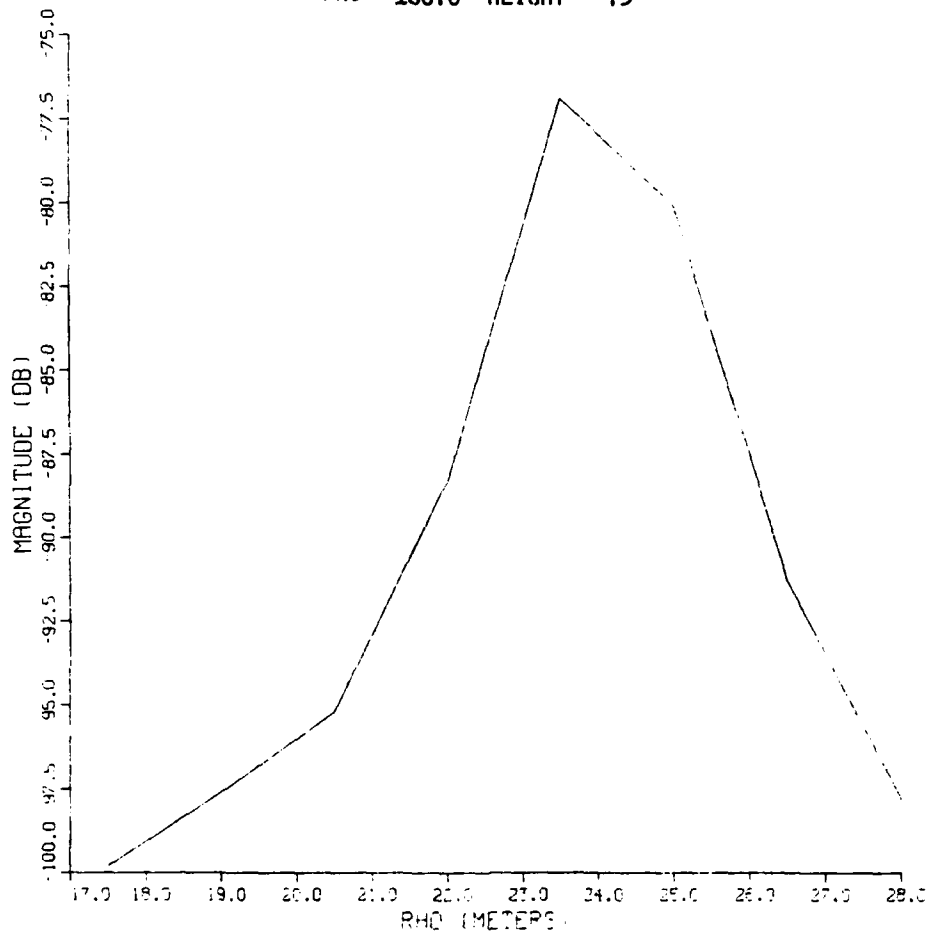

FIGURE 5.8

PLOT OF |EY| IN DB .VS. RHO
NO GROUND REFLECTION, NO SCATTERER
PHI - 270.0 HEIGHT - 5

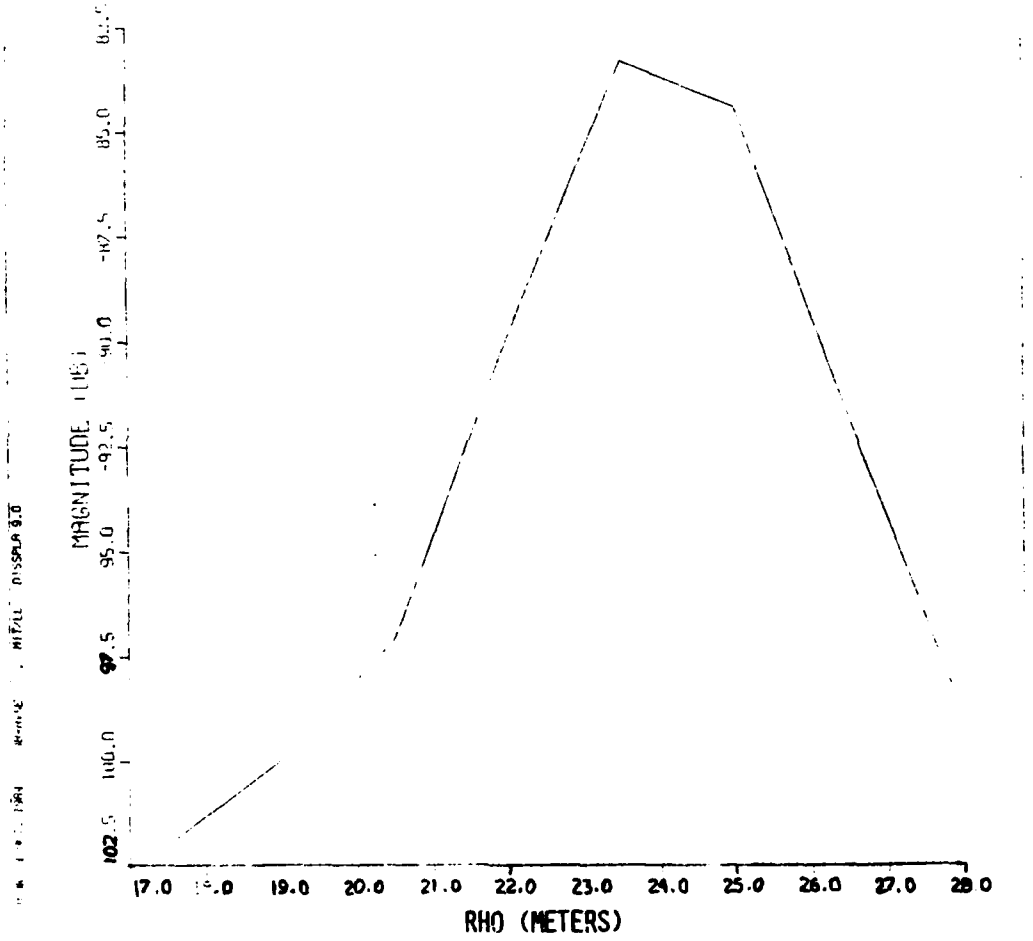

FIGURE 5.9

PLOT OF |EZ| IN DB .VS. RHO
NO GROUND REFLECTION, NO SCATTERER
PHI - 0.0 HEIGHT - .5

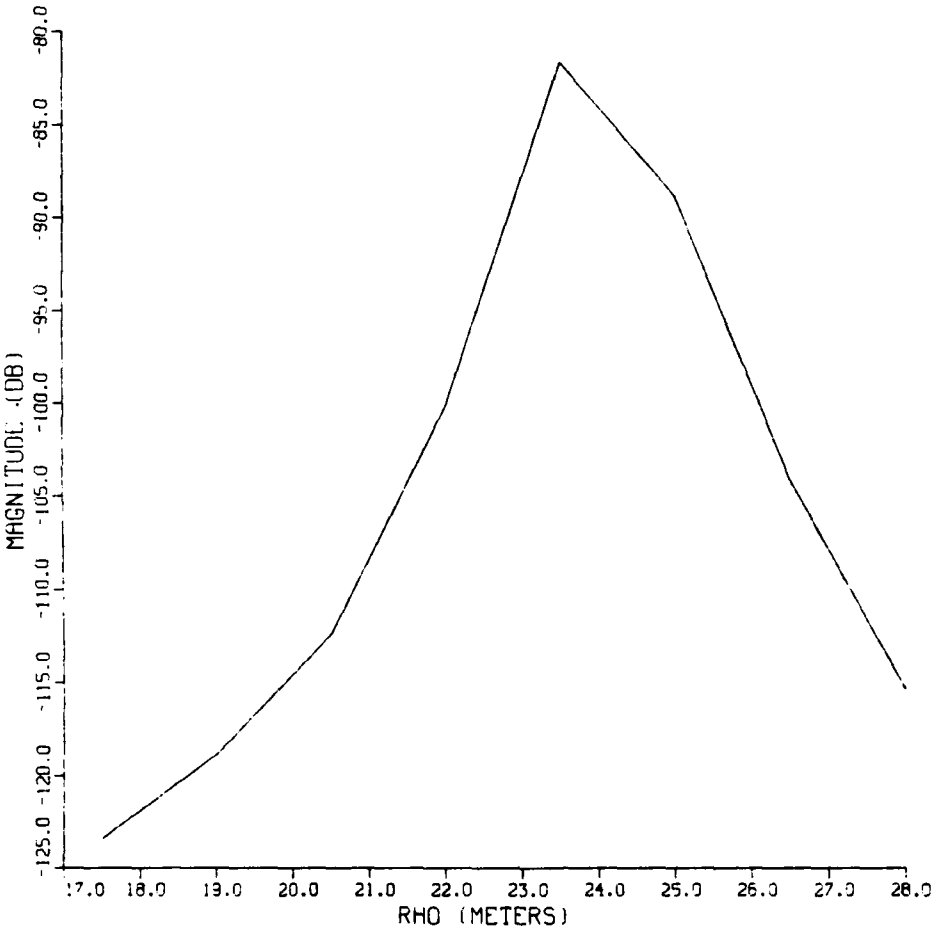

FIGURE 5.10

PLOT OF |EZ| IN DB .VS. RHO

NO GROUND REFLECTION, NO SCATTERER

PHI - 90.0 HEIGHT - .5

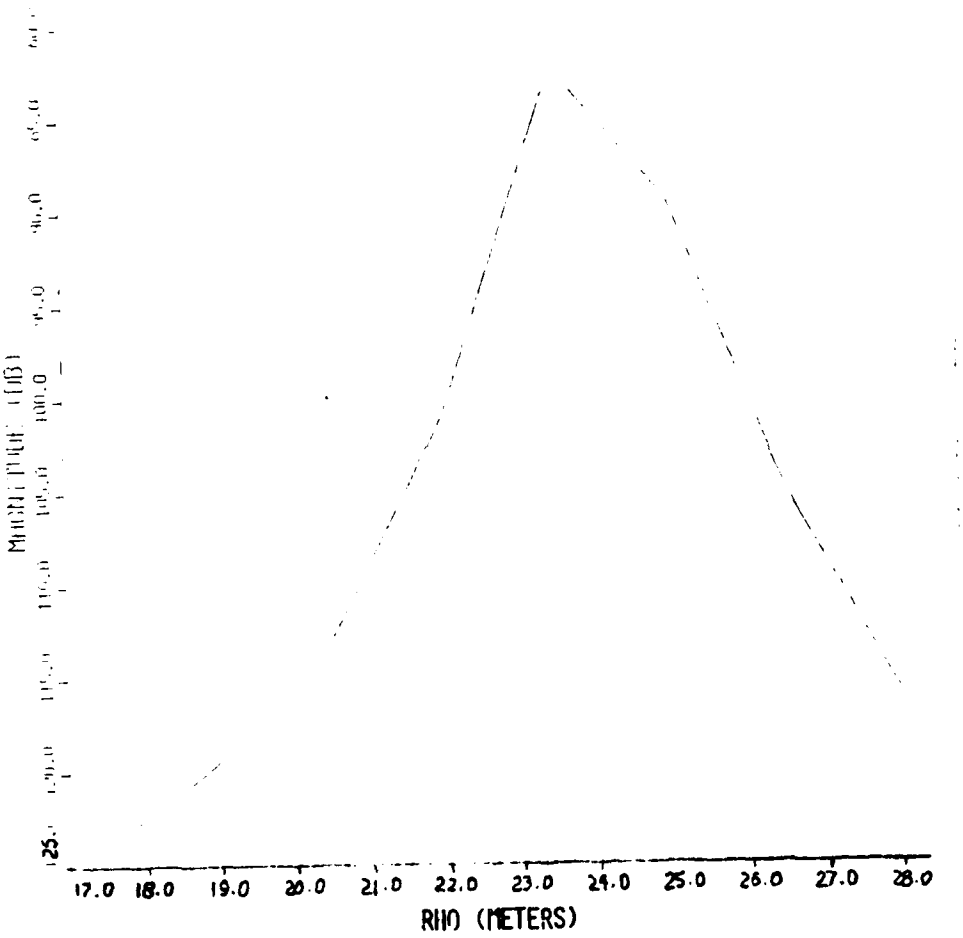

FIGURE 5.11

PLOT OF |EZ| IN DB .VS. RHO

NO GROUND REFLECTION, NO SCATTERER

PHI - 180.0 HEIGHT - .5

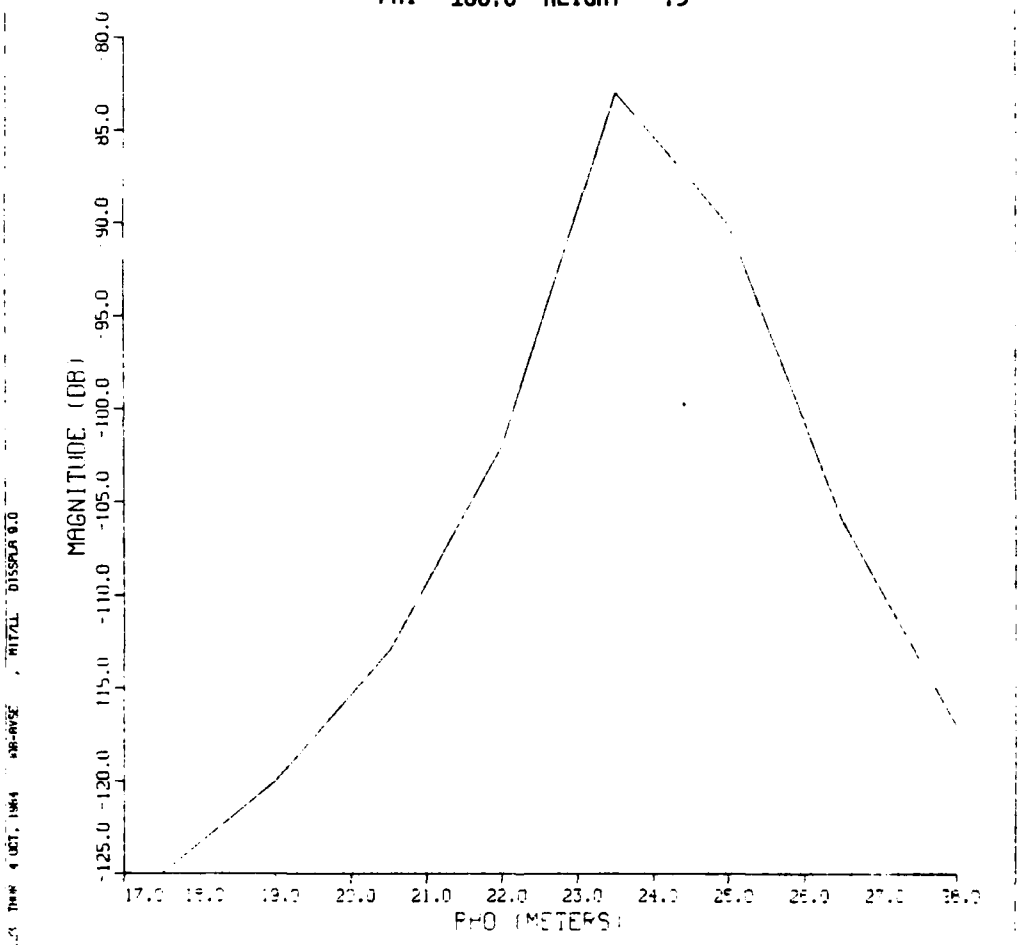

FIGURE 5.12

PLOT OF |EZ| IN DB .VS. RHO
NO GROUND REFLECTION, NO SCATTERER
PHI - 270.0 HEIGHT - .5

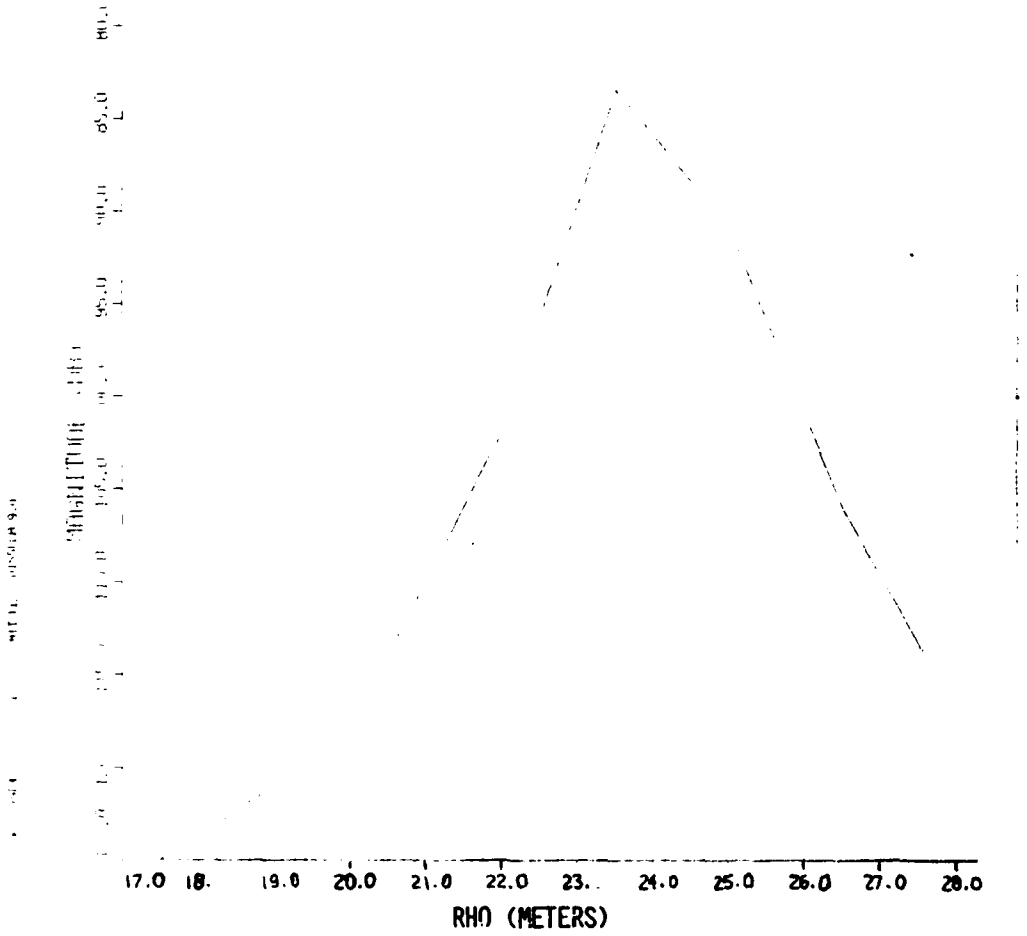

FIGURE 5.13

|Ez| dB VS. ρ

RADIAL WALK

HEIGHT - 2 PHI - 0.0

SCATTERED FIELDS ONLY
(DIRECT PLUS GROUND REFLECTED)

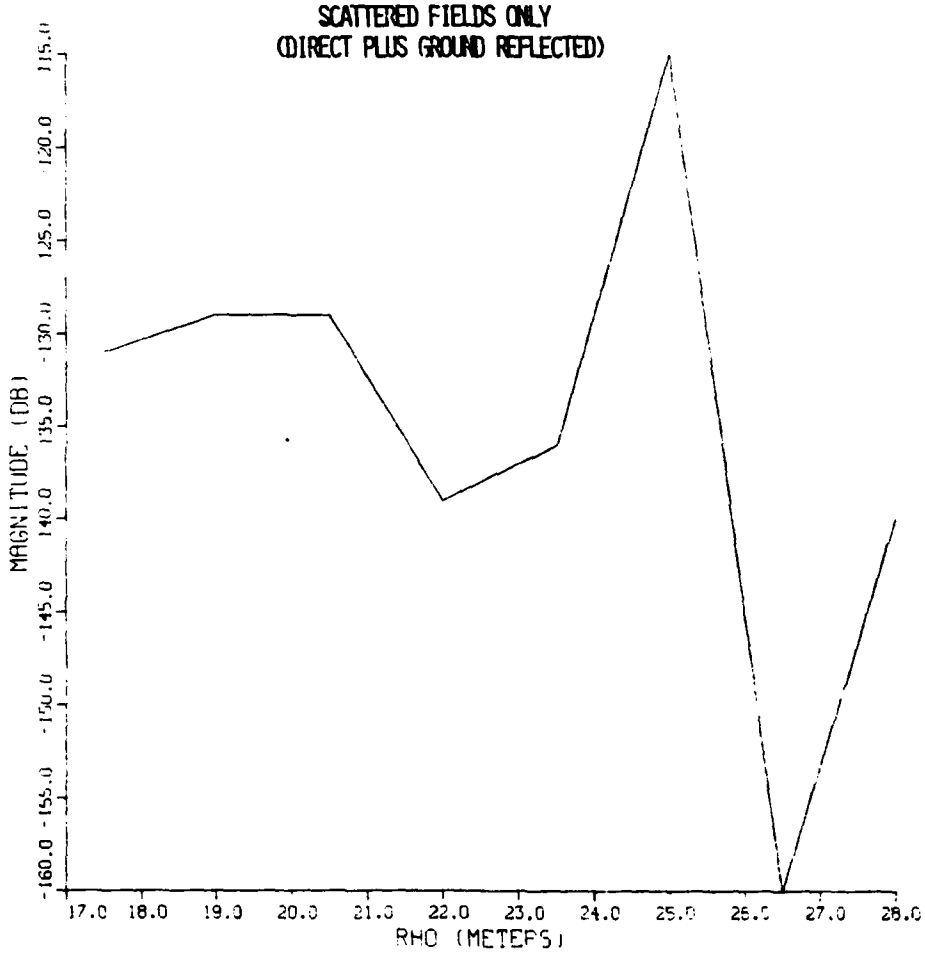

FIGURE 5.14

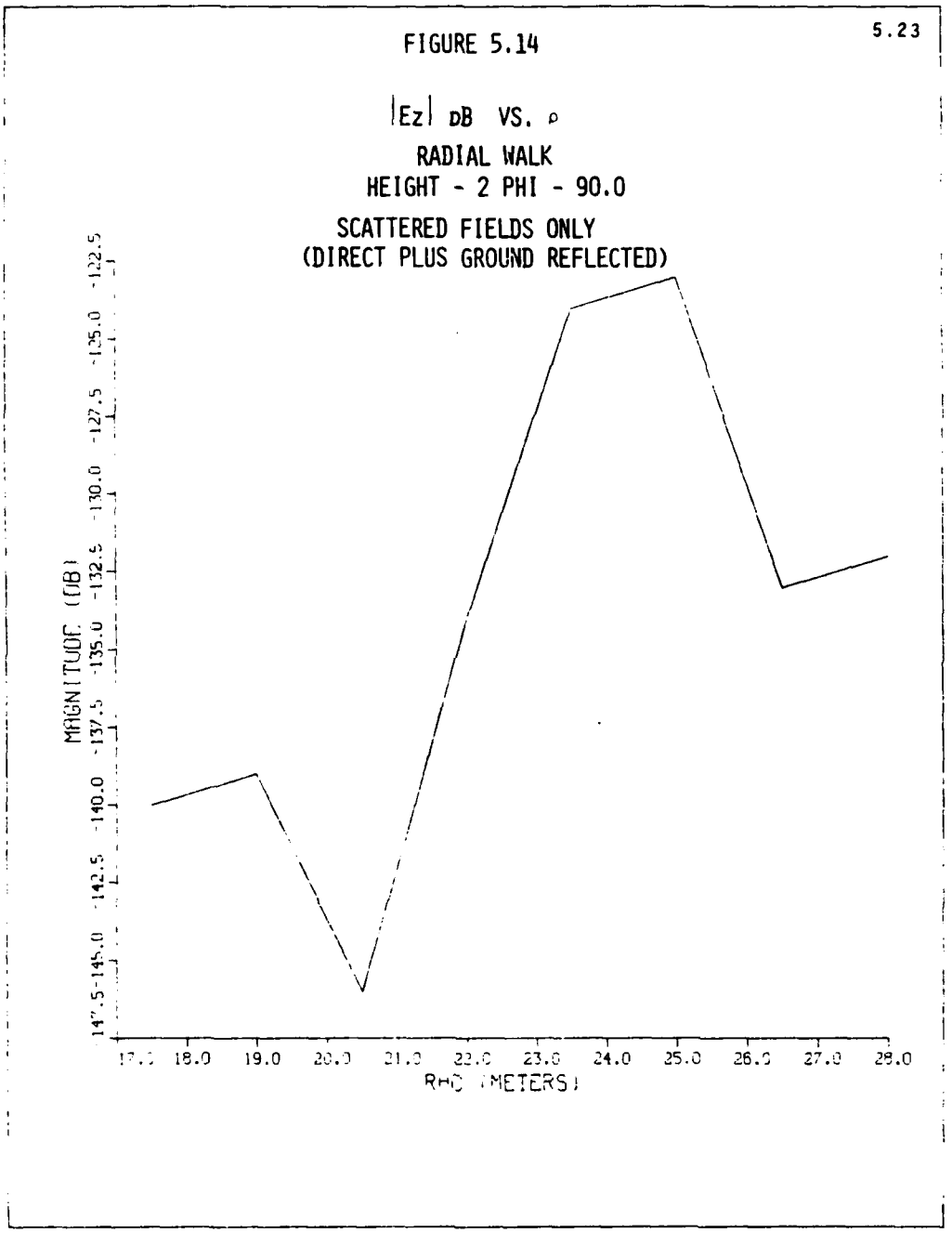
|Ez| dB VS. ρ
RADIAL WALK
HEIGHT - 2 PHI - 90.0
SCATTERED FIELDS ONLY
(DIRECT PLUS GROUND REFLECTED)
MAGNITUDE (dB)
-122.5
-125.0
-127.5
-130.0
-132.5
-135.0
-137.5
-140.0
-142.5
-145.0
17.0
18.0
19.0
20.0
21.0
22.0
23.0
24.0
25.0
26.0
27.0
28.0
RHO (METERS)

FIGURE 5.15

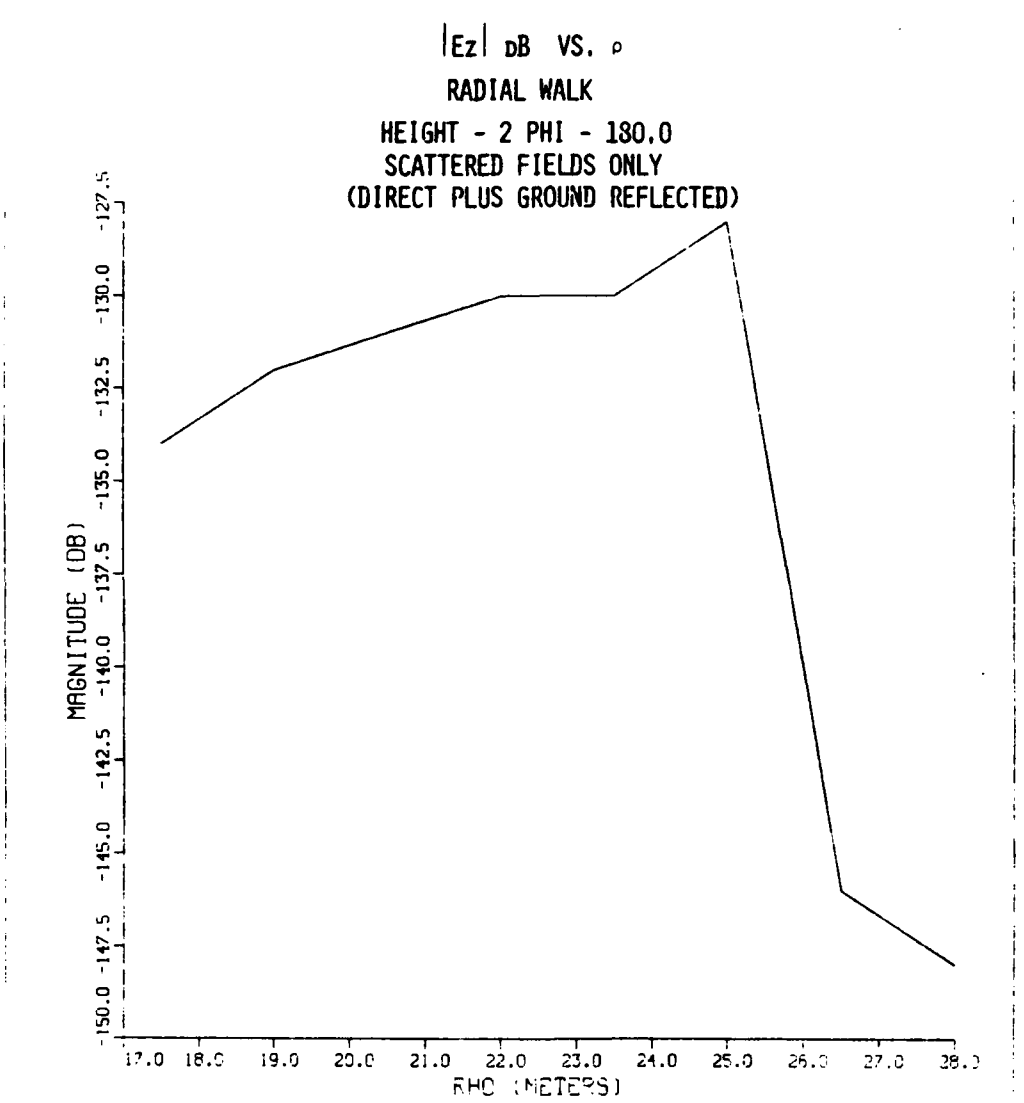
|Ez| dB VS. ρ
RADIAL WALK
HEIGHT - 2 PHI - 180.0
SCATTERED FIELDS ONLY
(DIRECT PLUS GROUND REFLECTED)
MAGNITUDE (DB)
-127.5
-130.0
-132.5
-135.0
-137.5
-140.0
-142.5
-145.0
-147.5
-150.0
17.0
18.0
19.0
20.0
21.0
22.0
23.0
24.0
25.0
26.0
27.0
28.0
RHO (METERS)

FIGURE 5.16

|Ez| dB VS. ρ

RADIAL WALK

HEIGHT - 2 PHI - 270.0
SCATTERED FIELDS ONLY
(DIRECT PLUS GROUND REFLECTED)

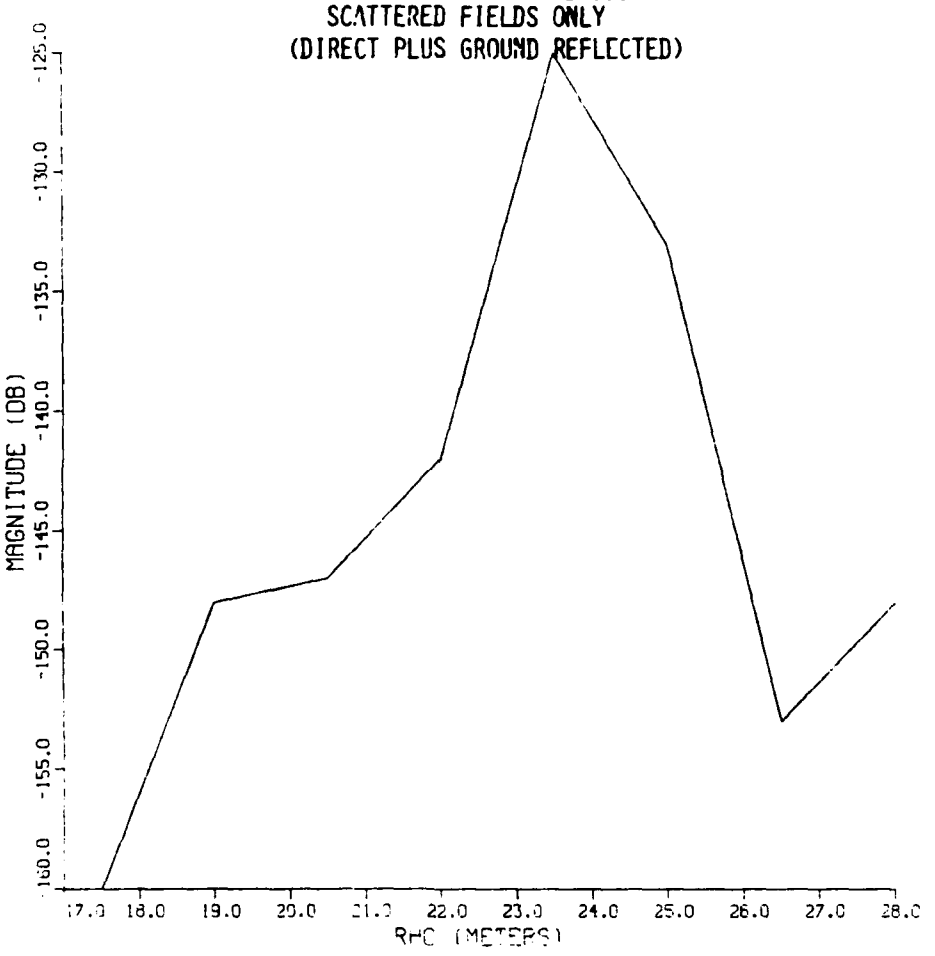

FIGURE 5.17

$|E_z|$ dB VS. ρ

CRAWLING SCATTERER
Z - .25 PHI - 0.0
SCATTERED FIELDS ONLY
(DIRECT PLUS GROUND REFLECTED)

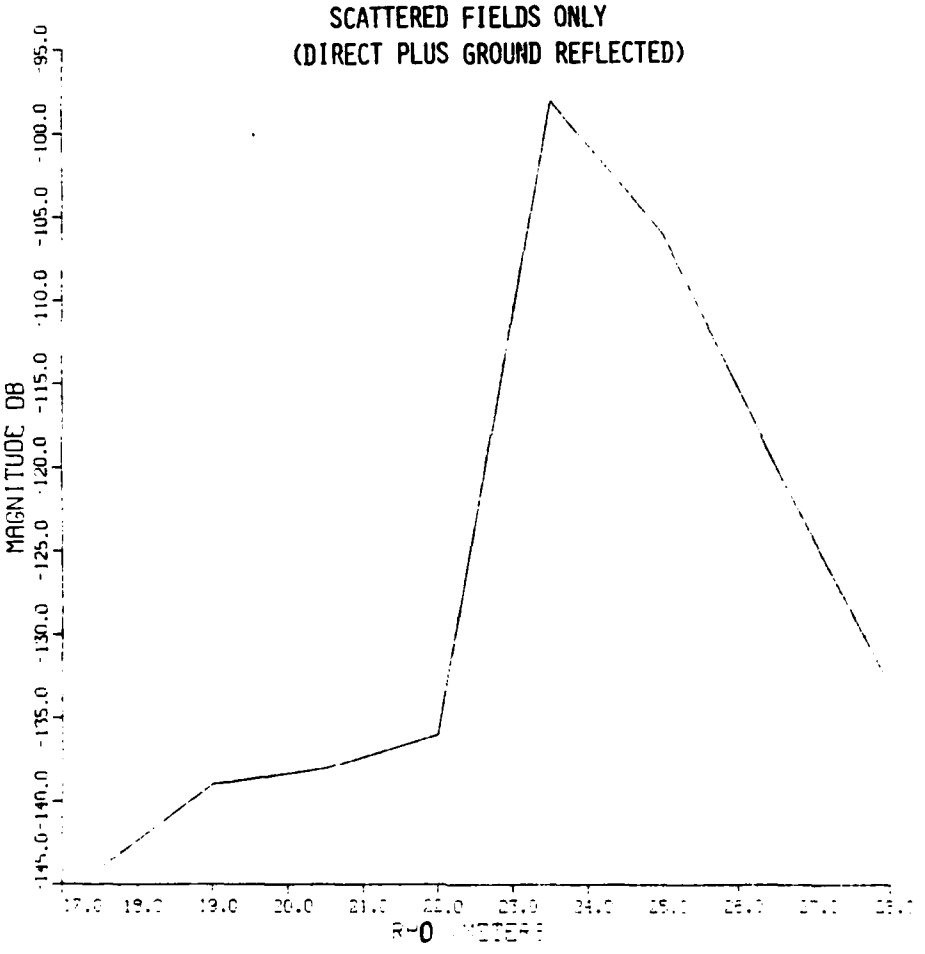

FIGURE 5.18

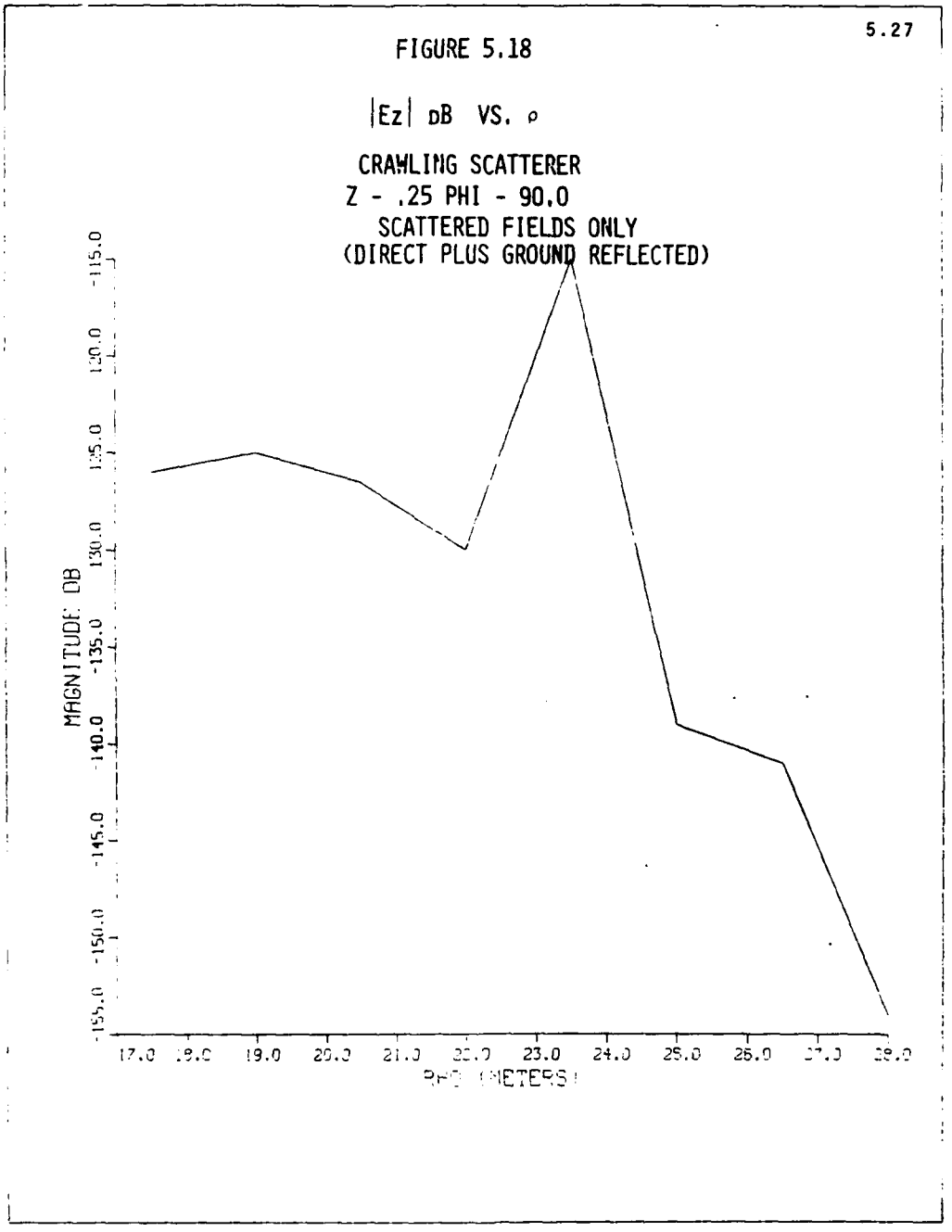
|Ez| dB VS. ρ
CRAWLING SCATTERER
Z - .25 PHI - 90.0
SCATTERED FIELDS ONLY
(DIRECT PLUS GROUND REFLECTED)
MAGNITUDE DB
-115.0
-120.0
-125.0
-130.0
-135.0
-140.0
-145.0
-150.0
-155.0
17.0
18.0
19.0
20.0
21.0
22.0
23.0
24.0
25.0
26.0
27.0
28.0
RHO (METERS)

FIGURE 5.19

$|E_z|$ dB VS. ρ

CRAWLING SCATTERER
Z - .25 PHI - 180.0
SCATTERED FIELDS ONLY
(DIRECT PLUS GROUND REFLECTED)

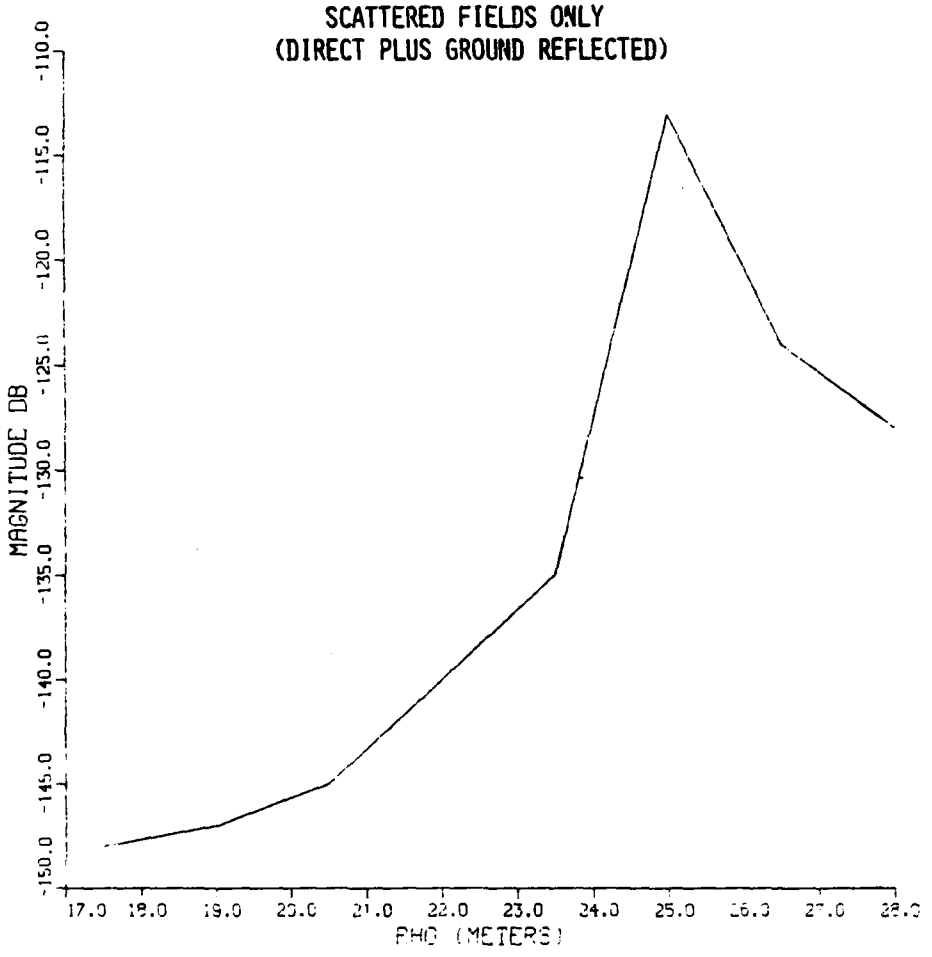

FIGURE 5.20

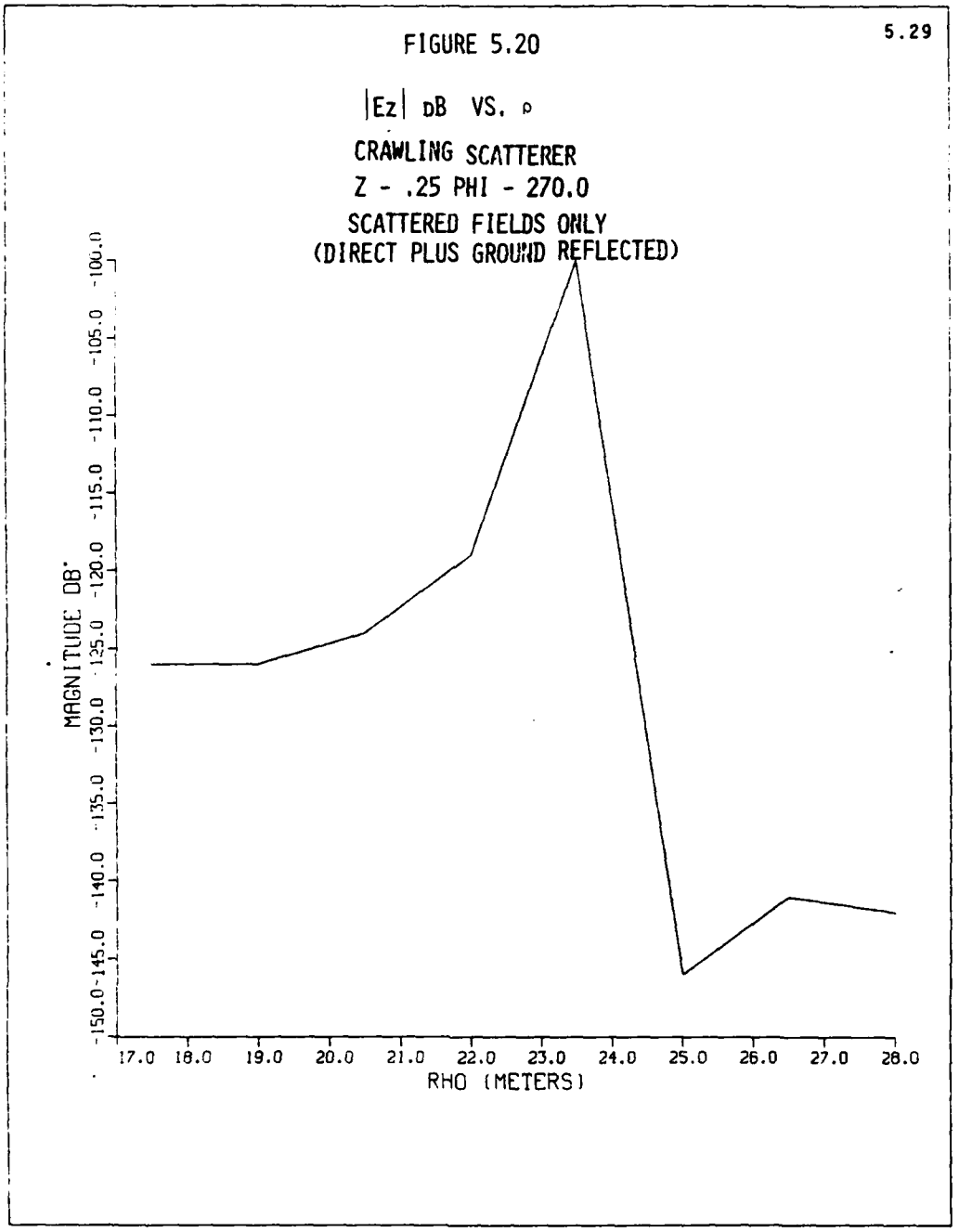
|Ez| dB VS. ρ
CRAWLING SCATTERER
Z - .25 PHI - 270.0
SCATTERED FIELDS ONLY
(DIRECT PLUS GROUND REFLECTED)
MAGNITUDE DB
-100.0
-105.0
-110.0
-115.0
-120.0
-125.0
-130.0
-135.0
-140.0
-145.0
-150.0
17.0
18.0
19.0
20.0
21.0
22.0
23.0
24.0
25.0
26.0
27.0
28.0
RHO (METERS)

FIGURE 5.21

$|E_z|$ dB VS. ρ

RADIAL WALK ON STILTS
PHI - 0.0
SCATTERED FIELDS ONLY
(DIRECT PLUS GROUND REFELECTED)

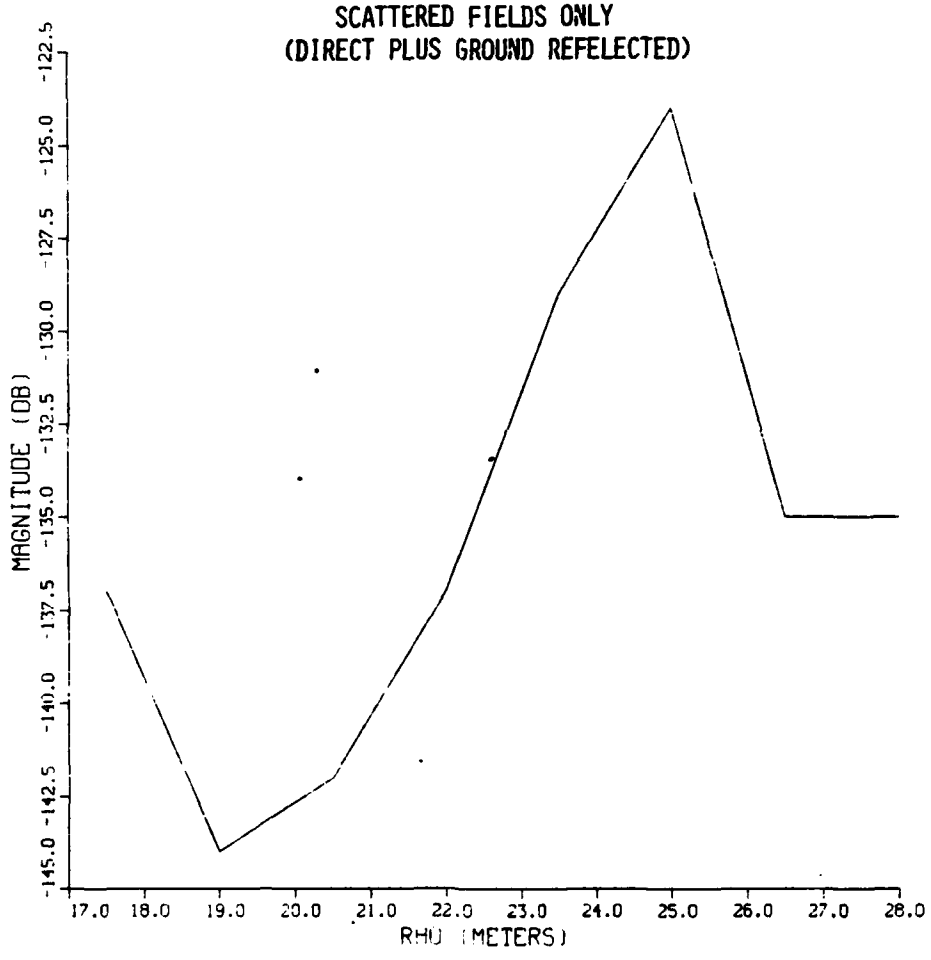

FIGURE 5.22

$|E_z|$ dB VS. ρ

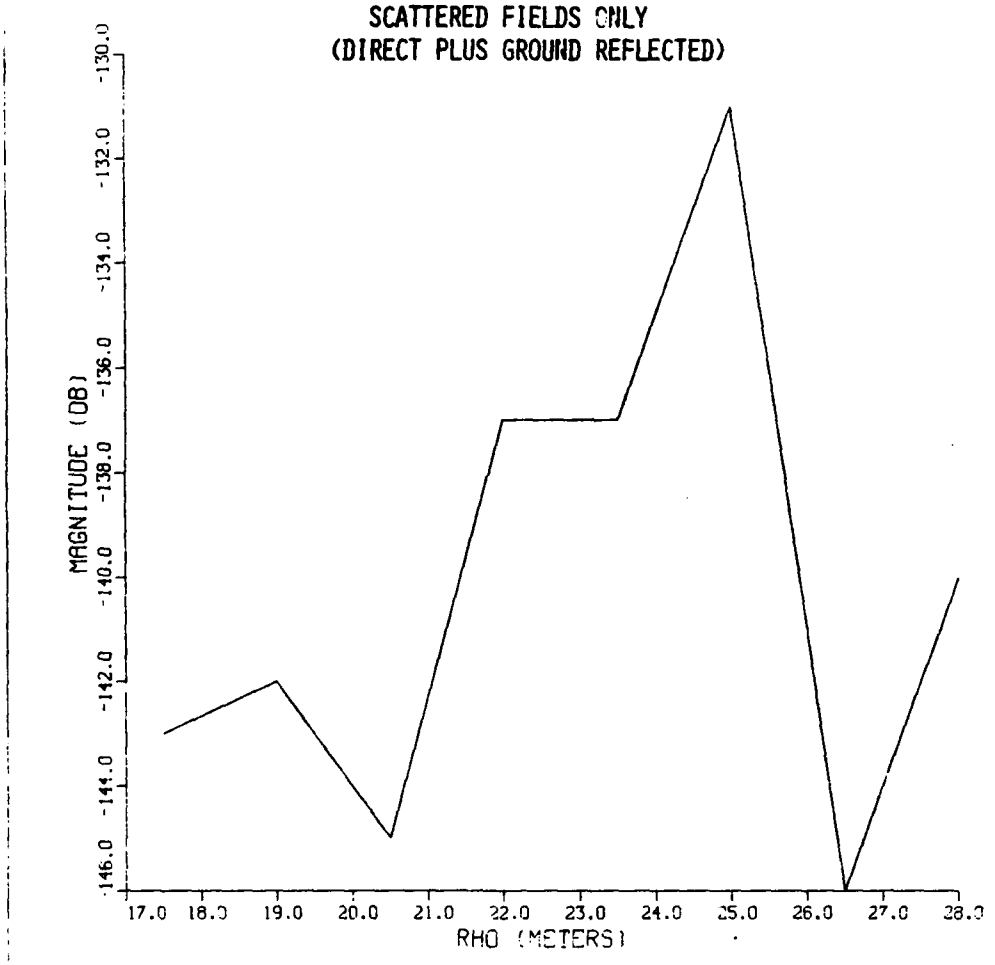

FIGURE 5.23

$|E_z|$ dB VS. ρ

RADIAL WALK ON STILTS
PHI - 180.0
SCATTERED FIELDS ONLY
(DIRECT PLUS GROUND REFLECTED)

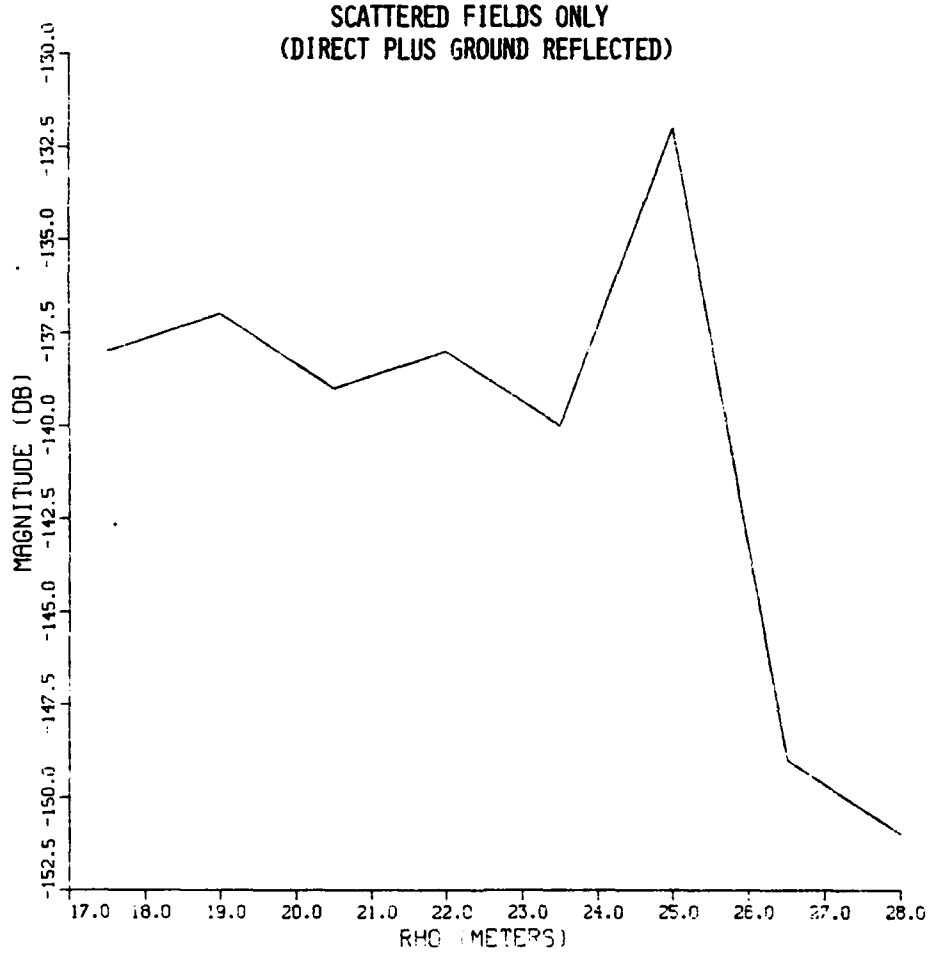

FIGURE 5.24

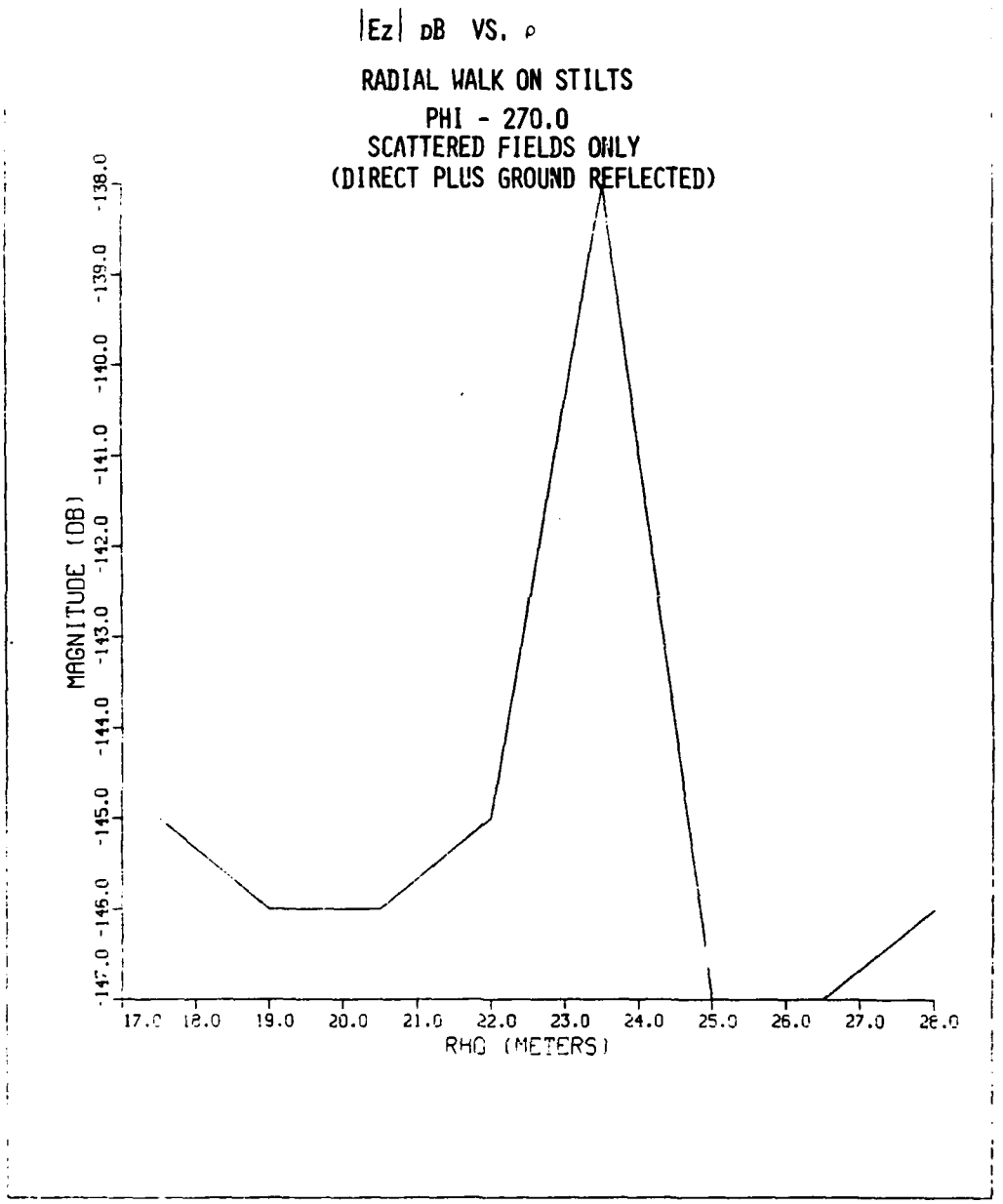
|Ez| dB VS. ρ
RADIAL WALK ON STILTS
PHI - 270.0
SCATTERED FIELDS ONLY
(DIRECT PLUS GROUND REFLECTED)
MAGNITUDE (DB)
-138.0
-139.0
-140.0
-141.0
-142.0
-143.0
-144.0
-145.0
-146.0
-147.0
17.0
18.0
19.0
20.0
21.0
22.0
23.0
24.0
25.0
26.0
27.0
28.0
RHO (METERS)

5.2 Discussion of results

5.2.1 The illuminating fields

Consider first the components of the "illuminating electric field" with no ground reflections, as given in Table 5.1 and Figures 5.1-5.12. These results are from computations of the amplitudes of the quantities in Eqs. (2.19-a, b, c). Since these results involve the integrals around the cable, we cannot say that the fields originate from any one particular portion of the cable. However, intuitively (aided by the discussions in Appendix I, especially Section I-C) it is evident that at points very close to the cable, the major contribution to the fields should come from the slots closest to the observation point, i.e., those slots where ϕ' is very close to ϕ. Using that intuitive idea, the rough dependence on $\delta = \sqrt{\Delta^2 + (z - z')^2}$ (where $\Delta = \ell - \rho$) the distance from the cable slot corresponding to $\phi' = \phi$, should be easy to establish. First, the factors $(jk\, I_z - I_3)$ that appear in all the electric field components of (2.19-a, b, c) can be thought of as varying roughly as $\frac{1}{\delta^2}\sqrt{1 + \frac{1}{(k\delta)^2}}$. In E_x and E_y, there is a factor proportional to Δ multiplying $(jk\, I_2 - I_3)$ in one of the terms. Thus the factors $\Delta(jk\, I_2 - I_3)$ in the cos ϕ and sin ϕ terms in E_x and E_y respectively should vary roughly as $\frac{\Delta}{\delta^2}\sqrt{1 + \frac{1}{(k\delta)^2}}$. The sin ϕ term of E_x and the cos ϕ term of E_y should vary roughly as $\frac{1}{\delta}$. Based on these considerations, we should be able to conclude from (2.19-a, b, c) that

At $\phi = 0°$ or $\phi = 180°$

$$|E_x| \simeq C\,\frac{|\Delta|}{\delta^2}\sqrt{1 + \frac{1}{(k\delta)^2}} \qquad (5.2\text{-a})$$

$$|E_y| \simeq C \frac{|\hat{k}'_{ca}|}{\delta} \qquad (5.2\text{-b})$$

$$|E_z| \simeq C \frac{|z - b'|}{\delta^2} \sqrt{1 + \frac{1}{(k\delta)^2}} \qquad (5.2\text{-c})$$

At $\phi = 90°$ or $\phi = 270°$

$$|E_x| \simeq \frac{C|\hat{k}'_{ca}|}{\delta} \qquad (5.2\text{-d})$$

$$|E_y| \simeq \frac{C|\Delta|}{\delta^2} \sqrt{1 + \frac{1}{(k\delta)^2}} \qquad (5.2\text{-e})$$

$$|E_z| \simeq \frac{C|z - b'|}{\delta^2} \sqrt{1 + \frac{1}{(k\delta)^2}} \qquad (5.2\text{-f})$$

The eqs (5.2-a, ..., f) tend to corroborate the results in Table 5.1. The major trends observed in Table 5.1, Parts (a), (b), (c) are:

(1) The peak values of all three field amplitudes always occur at $\rho = 23.5$ m.

(2) At $\rho = 23.5$, where peak values occur, the y-components of the field amplitudes at $\phi = 90°$, 180° and 270° are nearly the same as the x-components at $\phi = 0°$, 90° and 180° respectively, i.e., the x and y components appear to interchange their roles at 90° intervals.

(3) At other values of ρ, the x and y field amplitudes show very weak dependence on ϕ.

(4) At $\rho = 23.5$, peaks of the z-field amplitude are roughly the same as those of the x and y components.

(5) At other values of ρ, the z-component values are considerably lower than the x and y component values.

Some of these effects are discussed more quantitatively below. From (5.2-a, ..., f), we conclude that, if cable attenuation is neglected

$$|E_x|_{\phi=0° \text{ or } 180°} \gtrsim |E_y|_{\phi=90° \text{ or } 270°} \tag{5.3-a}$$

$$|E_y|_{\phi=0° \text{ or } 180°} \gtrsim |E_x|_{\phi=90° \text{ or } 270°} \tag{5.3-b}$$

$$|E_z|_{\phi=0° \text{ or } 180°} \gtrsim |E_z|_{\phi=90° \text{ or } 270°} \tag{5.3-c}$$

$$\eta_1 = \frac{|E_x|_{\phi=0° \text{ or } 180°}}{|E_x|_{\phi=90° \text{ or } 270°}} \gtrsim \frac{|E_y|_{\phi=90° \text{ or } 270°}}{|E_y|_{\phi=0° \text{ or } 180°}} = \frac{|\Delta|}{|k'_{ca}|\delta}\sqrt{1 + \frac{1}{(k\delta)^2}} \tag{5.3-d}$$

$$\eta_2 = \frac{|E_z|_{\phi=0° \text{ or } 180° \text{ or } 90° \text{ or } 270°}}{|E_x|_{\phi=0° \text{ or } 180°}} = \frac{|E_z|_{\phi=0° \text{ or } 180° \text{ or } 90° \text{ or } 270°}}{|E_y|_{\phi=90° \text{ or } 270°}} = \frac{|z - b'|}{|\Delta|} \tag{5.3-e}$$

Most of the effects predicted by (5.3-a, b, c) are borne out qualitatively in the computed results shown in Table 5.1 (a), (b), (c). In particular, the independence of $|E_z|$ on the angle ϕ as predicted by (5.3-c) is borne out by Table 5.1, Part (c) and the tendency of $|E_x|$ and $|E_y|$ to interchange at intervals of 90° are borne out by Table 5.1, Parts (a) and (b).

Using the numerical values of parameters assigned in the computations in (5.3-d) and (5.3-e), we have the following approximate results predicted by (5.3-d) and (5.3-e), indicated in the tabulation below:

In every case in this tabulation $k \cong 1.05$, $|\hat{k}'_{ca}| \cong \sqrt{1.7} = 1.3$, $|z - b'| = .5$, $|\Delta| = |o - \mathcal{R}|$, $\delta = \sqrt{\Delta^2 + (z - b')^2}$.

ρ	$\lvert\Delta\rvert$	δ	$\frac{1}{\delta}$	$\frac{\lvert\Delta\rvert}{\lvert k'_{ca}\rvert\delta}$	$\frac{1}{(k\delta)^2}$	$\sqrt{1 + \frac{1}{(k\delta)^2}}$	η_1	η_2	$(\eta_1)_{dB}$	$(\eta_2)_{dB}$
23.5	.5	.707	1.414	.544	.476	1.21	.667	1	-3.5	0
25.0	1.0	1.12	.893	.687	.759	1.33	.913	.5	-.79	-6.0
20.5 or 26.5	3.0	3.0	.333	.769	.111	1.05	.807	.1667	-1.93	-15.6
17.5	6.0	6.0	.1667	.769	.027	1.01	.777	.083	-2.19	-21.6

The ratio $(\eta_1)_{dB}$ in Table 5.1 is about -5 dB at $\rho = 23.5$, as compared with -3.5 dB as in the tabulation below. The computational results given in Table 5.1 for $(\eta_1)_{dB}$ at $\rho = 25.0$, (20.5 or 26.5) and 17.5 are (-3 to -4 dB), (0 to -2 dB) and (-1 to -3 dB) respectively. The corresponding values on the tabulation above are -.71 dB, -1.86 dB and -2.19 dB respectively.

The computed values of the ratio $(\eta_2)_{dB}$ for $\rho = 23.5$, 25.0, (20.5 or 26.5) and 17.5 respectively are (0 to -1 dB), (-5 to -10 dB), (-14 to -17 dB) and (-23 to -25 dB) respectively. The corresponding values on the tabulation above are 0 dB, -6 dB, -15.6 dB and -21.6 dB respectively.

For the most part (i.e., except for the result η_1 at $\rho = 25.0$), these results indicate that the illumination of the scatterer situated within about 6 meters radial distance from the cable on either side are primarily due to the slots near the scatterer location, i.e., the rough estimates culminating in the tabulation above, which are based on the approximation that the field comes entirely from the cable slot at $\rho' = \rho$, come remarkably close to the results given in Table 5.1, (a), (b), (c) which take account of contributions from all portions of the cable.

The remaining dependence on ϕ in (2.19-a, b, c) arises through the cable attenuation factor $e^{-\alpha\ell\phi}$ which is present in $C(\phi)$. This number in dB is $-8.68\,\alpha\ell\phi$. With the values $\alpha = .002$, $\ell = 24$, the decibel difference at 90° intervals due to this factor is about $.417\,\frac{\pi}{2}$ or .65 dB. Thus the variation with ϕ due to this attenuation factor over the entire cable is about 2.6 dB, corresponding to a 180° variation of about 1.3 dB. That helps explain the small decrease (between 1 and 2 dB) in field amplitudes between 0° and 180° and between 90° and 270°. Otherwise the variations between the $|E_x|$ and $|E_y|$ results for $\phi = (0°, 180°)$ and those for $\phi = (90°, 270°)$ appear to be due to the factors $\cos\phi$ and $\sin\phi$ in (2.19-a) and (2.19-b). Because of

these factors, the computed values of $|E_y|_{dB}$ at $\phi = 90°$, 180° and 270° are nearly indentical with those of $|E_x|_{dB}$ at 0°, 90° and 180° respectively.

From Table 5.1 (c), it is evident that there is no significant dependence of $|E_z|$ on ϕ except for the small (1 - 2 dB) difference between values of ϕ separated by 180° due to the attenuation factor alluded to above. Otherwise, as indicated by the absence of ϕ-dependence in Eq. (2.19-c), the amplitude has nearly perfect cylindrical symmetry.

We now consider the variation of the illuminating fields with the height of the observation point z at $\phi = 0°$ (Table 5.1 (d), (e), (f)). As z varies from 1 to 2.5, the peaks gradually disappear and in general the variation of field amplitude becomes increasingly flattened. This is clearly due to the fact that the dependence of field strength on horizontal distance from the cable is weakened as the vertical distance increases. The mathematical dependence of field strength on these two components of the separation distance is contained in the distance R, which is essentially the square-root of the sum of squares of horizontal and vertical distance from the cable. As the vertical distance is increased, the contribution from the horizontal distance is increasingly "swamped out" by that involving the vertical distance.

Finally, we observe by comparing Parts (a) and (b) of Table 5.1 with Part (c) of that same table that there is appreciable difference between the vertical and horizontal field amplitudes in the regions near the peak values but that the vertical amplitudes decay more rapidly as the observation point recedes from the cable. The reason is easily determined from Eqs. (2.19-a, b, c). The vertical field decays roughly as $\frac{1}{\delta^2}$ and the horizontal fields as $\frac{1}{\delta}$ as the distance from the cable increases. Thus, while their values are comparable near the cable, the vertical fields decay more rapidly with distance from the cable.

5.2.2 The scattered fields

We now turn to the results for the scattering contribution to the field components at the antenna (Table 5.2 and Figures 5.13-5.24).

First, we consider the variation with ρ for fixed ϕ and z. There are three sources of this variation, as follows:

(1) The variation of the fields illuminating the scatterer with the distance from the cable. This was discussed in Section 5.1 and is summarized in Eqs. (5.2-a, ..., f). If the effect of ground reflections on the illuminating fields is included, these results will be changed but the variation with distance from the cable will not be radically different.

(2) The factor $\frac{1}{r_{SA}}$ on the wave scattered directly into the antenna and the factor $\frac{1}{(r_{SG} + r_{GA})}$ on the ground-reflected scattered wave, where r_{SA} is the distance between scatterer center and antenna location, r_{GA} is the distance between ground-reflection point and antenna, and r_{SG} is the distance between scatterer and ground-reflection point.

(3) The dependence of the direction of the wave scattered into the antenna (relative to the direction of the incident wave) on the distance between the cable and scatterer and on whether the scatterer is inside or outside the cable.

The three effects (1), (2) and (3) above are all present in the scattered wave, but the mathematical relationships are too complicated to determine exactly the relative role of each of them. However, it is possible to intuitively infer some of this information at least qualitatively.

Consider first the effect (1). From the discussions in Section 5.1, we should expect that, due to effect (1), since the scattered field amplitude

is roughly proportional to the illuminating field amplitude at the scatterer center, the scattered field amplitude will reach its peak near $\rho = 24$ meters. This is shown to be the case for all the outputs shown in Table 5.2, (a) through (i). The peak is reached either at $\rho = 23.5$ or $\rho = 25$ in every case. This means that (since computations are made at 1.5 meter intervals) the true peak is somewhere near $\rho = 24$, i.e., when the scatterer center is directly over the cable. If Effect (1) were the predominant agent in determining the variation with ρ, we would also expect that the 1 - 2 dB assymmetry due to attenuation (as discussed in Section 5.1) would enter into the results However, the way in which these features would appear is quite complicated. There is a contribution to any scattered field component from the x, y and z-components of the illuminating fields, so the precise dependence of the scattered field on ρ would be a composite of those arising from each illuminating field component. Since the scatterer is assumed to be isotropic, however, the horizontal and vertical components of the scattered field would be affected primarily by the horizontal and vertical components respectively of the incident fields; hence the ρ-variation of the amplitude of each scattered field component should contain some of the features of the corresponding component of the incident field. The extent to which this is true, however, depends sensitively on the direction angle of the scattered field. For example, the vertical component of the illuminating E-field will certainly give rise to some horizontal components of the scattered E-field except possibly in the case of absolutely pure backscatter or pure forward scatter, which could only occur for a very rare geometry of cable, scatterer and antenna.

The effect (1) should cause rates of decay of field strength somewhere between $\frac{1}{\rho}$ and $\frac{1}{\rho^3}$ as the scatterer moves away from the cable in either direction. The tabulation below provides a rough idea of what rate of decay one might

expect due to this mechanism. The 0 dB level is taken to be at ρ = 23.5 in every case.

ρ	δ (approximately, neglecting z)	$\left(\frac{1}{\delta}\right)_{dB} = -20 \log_{10}$	$\left(\frac{1}{\delta^2}\right)_{dB}$	$\left(\frac{1}{\delta^3}\right)_{dB}$
17.5	6.5	-22	-44	-66
19.0	5.0	-20	-40	-60
20.5	3.5	-17	-34	-51
22.0	2.0	-12	-24	-36
23.5	0.5	0	0	0
25.0	1.0	-6	-12	-18
26.5	2.5	-14	-28	-42
28.0	4.0	-18	-36	-54

Another feature of the variation of the illuminating fields with distance from the cable is a difference between the illumination mechanism inside the cable circle and that outside the circle. Inside the circle, the cable appears concave, while outside the circle, it appears convex. Thus at a given distance from the cable, a larger portion of the cable illuminates the scatterer than would be the case at that same distance outside the circle. Moreover, inside the circle, the phases from the illuminating slots should be more nearly equal. This should introduce an asymmetry resulting in larger illuminating field strength at a given distance from the cable inside the circle relative to that observed at that same distance outside the circle.

The effect (2) should be weak relative to (1) in determining the field variation with ρ and is easy to estimate. Considering the scattering directly into the antenna when the scatter is inside the cable circle, the factor $\frac{1}{r_{SA}}$ introduces an <u>increase</u> in field strength as the scatterer moves away from the cable and toward the antenna. This effect is opposite to that due to Effect (1), which is a <u>decrease</u> in field strength as the scatterer moves

AD-A164 925 INTRUDER POLARIZATION(U) NORTHEASTERN UNIV BOSTON MA 2/2
H RAEMER ET AL. DEC 85 RADC-TR-85-234 F30602-81-C-0169

UNCLASSIFIED F/G 17/9 NL

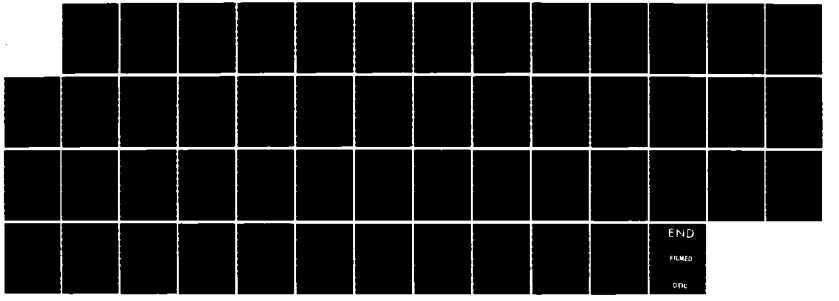

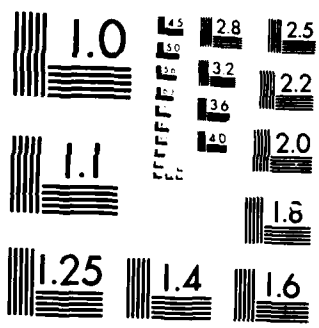

further inside the circle. The magnitude of this effect is roughly 20 $\log_{10} r_{SA}$. The numbers roughly follow the tabulation below, neglecting the effect of the vertical coordinate z

$\rho = r_{SA}$	$-20 \log_{10} r_{SA}$
23.5	-27.4
22.0	-26.8
20.5	-26.2
19.0	-25.6
17.5	-24.9

The variation between the values of ρ for which computations are made is only about 0.6 dB. The entire variation between 17.5 and 23.5 is only about 2.5 dB.

As the scatterer recedes from the cable when it is outside the circle, the effect is to <u>decrease</u> the field strength. The tabulation below applies to that case

$\rho = r_{SA}$	$-20 \log_{10} r_{SA}$
25.0	-28.0
26.5	-28.5
28.0	-28.9

In this case, the rate of decay of the field is about .4 or .5 dB for each 1.5 meter increase in ρ.

This effect is roughly the same for the ground-reflected scattered field, since the size of $(r_{SC} + r_{CA})$ is not very different from that of r_{SA}. As evidenced by the above tabulations, it <u>does</u> introduce a small asymmetry between values of ρ inside and outside the cable circle. The effect should be to <u>reduce</u> the rate of decay of field strength as the scatterer moves away from

the cable inside the circle and to increase the rate of decay as it moves away from the cable outside the circle. In both cases, this asymmetry effect should be quite small compared to the effects (1) and (3), the latter to be discussed below.

Finally we consider the effect (3). If we think of the scatterer as being illuminated primarily by fields from the nearest slots, then as the scatterer moves away from the cable inside the circle, the scattering into the antenna direction becomes increasingly more like forward scatter. As it recedes from the cable outside the circle, the effect more nearly resembles backscatter. In either case, when the scatterer is very close to the cable, it is illuminated primarily from below and hence the scattered wave into the antenna is at a wide angle from the incident wave. Since backscatter is likely to be much stronger than forward scatter, we should expect that this mechanism will produce a higher rate of decay as the scatterer moves away from the cable inside the circle than that which occurs as it recedes outside the circle. That asymmetry in ρ around the cable is exactly opposite to the one caused by the effect (2).

The results on rate of decay of field strength as the scatterer recedes from the cable are quite erratic and show no clear trends that would indicate whether mechanisms (1), (2), or (3) are the predominant ones. The rates of decay vary from small values commensurate with mechanisms (1) and (2) to enormous values that appear to bear no obvious relationship to the mechanisms we have discussed here. Sometimes the field decays from its peak value more rapidly inside the circle than it does outside the circle and sometimes the opposite trend holds. This is not surprising in view of the complexity of the calculations made here. Each quantity calculated is a coherent sum of two complex quantities, the field component of the wave scattered directly into the antenna and that of the scattered wave reflected from the ground

and then propagating toward the antenna. These two complex quantities are of comparable magnitude (as shown by computations we have carried out in which these two constituents are calculated separately) and their relative phase is very sensitive to small changes in parameter values. Hence the resultant amplitudes can range from values near zero to values nearly twice the amplitude of the direct wave field.

In addition to this, the scattering process itself for this frequency range is highly sensitive to angle and should produce some erratic or noise-like" effects with small changes in geometry.

At this point, having discussed the variation with ρ for fixed ϕ and z, we will discuss the azimuthal asymmetry in the results. There were certain azimuthal trends observed in the illuminating fields, presented in Table 5.1 and discussed in Section 5.1. For those horizontal field components the amplitudes at $\phi = 0°$ and $\phi = 180°$ were nearly the same, as were those at $\phi = 90°$ and $\phi = 270°$, the latter being larger than the former for $|E_x|$ and smaller than the former for $|E_y|$. The z-components were more nearly azimuthally uniform. Small decreases in amplitude as ρ increases due to cable attenuation were also present in all components of the illuminating fields. All of this was amenable to explanation through the equations for the illuminating fields.

Since the scattered fields are proportional to the illuminating fields, we searched for the same azimuthal trends in the former as were observed in the latter. Some of these trends are present but not necessarily consistently. However, except for some wild fluctuations probably attributable to coherent addition of two roughly-equal size complex numbers the tendency is for the x-directed field components at $\phi = 0°$ and $\phi = 180°$ to be roughly comparable to each other and to the y-directed components at $\phi = 90°$ and $\phi = 270°$. The same comparison exists (again very roughly) between $|E_y|$ at $\phi = 90°$ and

270° and $|E_y|$ at $\phi = 0°$ and 180°. However, the z-components $|E_z|$ appear to exhibit much more azimuthal asymmetry than their counterparts for the illuminating fields, which were nearly symmetrical. There is also more azimuthal asymmetry in all components of the scattered fields than was present in their counterparts in the illuminating fields.

A possible partial reason for this additional asymmetry in all the components is the fact that, at $\phi = 0°$ and $\phi = 180°$, the scattered field components E_x contain large contributions from E_y and E_z of the incident fields and the scattered field components E_z contain large contributions from incident E_x and E_z. Also, at $\phi = 90°$ and $\phi = 270°$, scattered E_y has contributions from incident E_y and E_z contributions. Thus asymmetries in E_x and E_y in the illuminating field will find their way into E_z in the scattered field and will also introduce greater asymmetries into scattered E_x and E_y.

Now we must examine the differences between the results for the radial walk ($z = 1$, upright scatterer, Table 5.2, (a), (b), (c)), the radial crawl ($z = 0.25$, prone scatterer, Table 5.2, (d), (e), (f)) and the radial walk on stilts ($z = 2$, upright scatterer, Table 5.2, (g), (h), (i)).

Aside from the trends already commented upon, which tend to be common to all three cases, there are some general comparative tendencies observed which appear to be consistent with intuitive expectations.

First comparing the radial walk on stilts ($z = 2$) with the radial walk ($z = 1$), the corresponding field component amplitude for the former tends to be smaller than that for the latter. This is sometimes strikingly true and sometimes the reverse holds, so one cannot say that trend is absolutely consistent. But it is true more often than not and tends to be accentuated by proximity to the cable, i.e., it is more likely to be true for the peak values than for the values 4 - 6 meters from the cable. An explanation is that the effect of the height (the value of z) is much more pronounced very

near the cable, being comparable to the horizontal distance from the cable, and becomes nearly negligible 6 meters from the cable, where the height in both cases is small compared with the horizontal distance from the cable.

The same observations can be made concerning comparison between the radial crawl ($z = 0.25$) and the radial walk ($z = 1$). For most of the points at which computations were made, the radial crawl gives larger values than the radialwalk. This is particularly true of the peak values, which are nearly always significantly larger for the crawling case than for the walking case. The field magnitudes 3 - 6 meters away from the cable, however, are not always larger for the crawling case and are sometimes somewhat smaller. To some extent, this can be attributed to the smaller sensitivity of the amplitude in the crawling case to the height z. Since z for the crawler is one-fourth of its value for the walker, it becomes negligible compared to the horizontal distence from the cable when the latter is only about 2 meters. Hence over much of the range of θ, the comparative amplitudes in the two cases have very little to do with the comparative values of the height z. Within two meters of the cable, however, there is a significant dependence of the amplitude on z, and than helps to explain the fact that peak values of amplitude are nearly always significantly higher for the crawling case.

Aside from the comparison involving the height, alluded to above, the remainder of the comparison between crawling and walking cases relates to the difference in the angular orientation of the scatterer in the two cases. In the walking case, the scattering tends to be "broadside" whereas in the crawling case it tends to be in the spheroid's longitudinal direction. The scattering in the latter case tends to be weaker than that in the former case; hence for some scatterer positions, the fact that the illuminating field is stronger in the crawling case (because the center of the crawler is lower and therefore closer to the cable than that of the walker at the

same horizontal distance from the cable) is offset by the fact that the scattering is stronger for the walker due to its orientation. That is more likely to be true far from the cable, where the height difference has little effect. Thus while the height is likely to play the dominant role near the cable, the orientation should be more important further from the cable, which might explain why the scattered field is sometimes significantly larger for the walker especially at positions far from the cable.

As a final observation, we note that the horizontal and vertical components of the scattered field amplitudes are, on the average, not radically different, although they do exhibit some erratic behavior (e.g., in some cases there are large differences in the peak values for different components, where vertical is sometimes larger and sometimes smaller than the horizontal components). The probable causes of the erratic or noise-like nature of some of the results have already been discussed, alluding to the sensitivity of the scattering process to small changes in geometry and coherent addition of complex numbers with sensitive relative phase as the major mechanisms causing this behavior.

5.2.3 Total Fields

The computed results for the components of the total field at the antenna (fields without the scatterer plus those due to the presence of the scatterer) are shown in Table 5.3.

Discussion of the fields due to the presence of the scatterer was covered in Section 5.2.2. The computed field components at the antenna in the absence of the scatterer are given by (5.1) and are -112 dB, -110 dB and -146 dB for the x, y and z-electric field amplitudes respectively.

These values were determined by a very accurate numerical technique. That technique and some approximate calculations of the field components are discussed in Appendix I, where the fact that the horizontal components at the antenna is much larger than the vertical component is explained. The remaining discussion in this section will be confined to comments on the parameter regimes in which the field component amplitudes given by (5.1) for the case where the scatterer is not present are comparable in magnitude to those given in Table 5.2 for the contributions due to the presence of the scatterer. In those regimes there is a significant effect attained through coherent addition of the antenna fields in the absence of the scatterer and those due to the scatterer's presence. In many regimes the scatterer-free components given by (5.1) overwhelm the scattered fields and the results show the scatterer to be undetectable. For other regimes, the components given by (5.1) are overwhelmed by the scattered fields and the values in Table 5.3 are almost exactly the same as the corresponding values in Table 5.2.

To initiate the discussion, we summarize the results in the tabulation below (obtained from Tables 5.1 and 5.2 with the aid of Eq. (5.1)) which indicates the points of detectability of the scatterer, denoted by D and

characterized by the fact that the presence of the scatterer changes the field component at the antenna by at least 4dB; an increment below 4 dB should be considered as "noise." As a subclass of these points, we also indicate points where the scatterer contribution to the field overwhelms the field component that would be seen in the absence of the scatterer, i.e., introduces an increment of at least ± 10 db; these points are denoted by DA. Points where there are no perceptable changes in the antenna signal due to the presence of the scatterer, i.e., where the scatterer is "not detectable" (i.e., ≤ 10 dB change) are denoted by ND. Finally, those points where there is a small but barely perceptable change in the signal level due to the scatterer's presence (i.e., "barely detectable" scatterer) are denoted by BD; between 1 dB and 4 dB change due to presence of scatterer).

Radial walk

	$\lvert E_x \rvert$				$\lvert E_y \rvert$				$\lvert E_z \rvert$			
ρ	φ=0°	φ=90°	φ=180°	φ=270°	φ=0°	φ=90°	φ=180°	φ=270°	φ=0°	φ=90°	φ=180°	φ=270°
17.5	ND	"	ND	ND	ND	ND	ND	ND	DA	D	DA	DA
19.0	ND	"	"	"	"	"	"	"	DA	D	DA	BD
20.5	ND	"	"	"	"	"	"	"	DA	ND	DA	ND
22.0	ND	"	"	"	"	"	"	"	DA	DA	DA	BD
23.5	BD	"	BD	"	"	"	"	"	DA	DA	DA	DA
25.0	ND	"	ND	D	"	BD	"	D	DA	DA	DA	DA
26.5	ND	"	"	ND	"	ND	"	ND	DA	DA	BD	DA
28.0	ND	"	"	"	"	"	"	"	D	DA	BD	BD

Radial crawl

	$\lvert E_x \rvert$				$\lvert E_y \rvert$				$\lvert E_z \rvert$			
ρ	φ=0°	φ=90°	φ=180°	φ=270°	φ=0°	φ=90°	φ=180°	φ=270°	φ=0°	φ=90°	φ=180°	φ=270°
17.5	ND	ND	ND	ND	ND	ND	ND	ND	BD	DA	BD	DA
19.0	"	"	"	"	"	"	"	BD	D	DA	BD	DA
20.5	"	"	"	"	"	"	"	ND	D	DA	BD	DA
22.0	"	"	"	"	"	"	"	BD	DA	DA	D	DA
23.5	DA	"	BD	BD	D	D	"	DA	DA	DA	DA	DA
25.0	ND	"	ND	ND	ND	BD	"	ND	DA	D	DA	ND
26.5	BD	"	BD	BD	"	ND	"	"	DA	D	DA	BD
28.0	ND	"	BD	BD	"	"	"	"	DA	D	DA	D

Radial walk on stilts

	$\lvert E_x \rvert$				$\lvert E_y \rvert$				$\lvert E_z \rvert$			
ρ	φ=0°	φ=90°	φ=180°	φ=270°	φ=0°	φ=90°	φ=180°	φ=270°	φ=0°	φ=90°	φ=180°	φ=270°
17.5	ND	ND	ND	ND	ND	ND	ND	ND	BD	BD	D	ND
19.0	"	"	"	"	"	"	"	"	D	D	D	ND
20.5	"	"	"	"	"	"	"	"	D	ND	D	ND
22.0	"	"	"	"	"	"	"	"	D	D	D	ND
23.5	"	"	"	"	"	"	"	"	DA	D	D	D
25.0	D	"	"	"	"	"	"	"	DA	DA	D	ND
26.5	"	"	"	"	"	"	"	"	DA	ND	BD	ND
28.0	"	"	"	"	"	"	"	"	DA	D	D	ND

The issue of detectability of the "intruder" is that of the comparison between the amplitude of a field component at the antenna when the scatterer is present relative to the amplitude of that same field component when the scatterer is not present. In some cases the total field amplitude is reduced rather than increased due to the presence of the scatterer. The reduction will occur if the amplitudes with and without the scatterer are

of comparable magnitude and the relative phase angle of these two quantities is between 90° and 270°, while an enhancement occurs when that angle is between -90° and +90°.

In the existing system, the antenna is vertical and hence the z-component of the electric field is the only component of interest. However, there is no reason (in principle) that horizontal components could not be used for detection with an antenna that respond to those components. Therefore, it is worthwhile as a part of this study to consider the horizontal components of the field in addressing the detectability issue.

The overall conclusion that would follow from the results shown here is that the dtectability of the intruder with horizontal fields in all three of the cases considered is nonexistent or very poor. In a few cases involving the radial walk or radial crawl and one case with radial walk on stilts, the scatterer is barely detectable at a point near the cable, but in nearly all cases it is not detectable.

If the vertical field component is used for detection, as in the actual system, the conclusions that would follow from the results is that the intruder is easily detectable for the radial walk and radial cases, but somewhat less detectable or undetectable for the "radial walk on stilts" case.

Since we have experimental results for comparison only for the vertical electric field component, no further comments on this topic will be made concerning the horizontal field components. The experimental results for the vertical antenna usually show values of the amplitude of the scattered signal at the antenna somewhere between 0 and 10 dB above the signal in the absence of the scatterer. Our analytical results usually show a larger incremental signal due to the scatterer than indicated by the experimental

results, i.e., for the radial walk, the peak scattered signal values are between 17 and 31 dB higher than the antenna signal in the absence of the scatterer. For the radial crawl, they are between 13 and 48 dB higher and for the radial walk on stilts, they are between 10 and 22 dB higher. When a scatterer is a few meters away from where the peak values occur, the incremental signal due to the scatterer is much more nearly comparable to that without the scatterer.

However, although the qualitative behavior of the signals due to the scatterer appears to be roughly as expected, the most prominent quantitative descrepancy appears to be excessively high values of the scattered signal relative to the signal in the absence of the scatterer. This is either because

(1) The calculated field amplitude at the antenna in the absence of the scatterer is too low, or

(2) The calculated field amplitude due to the scatterer is too high.

Explanation (1) seems less likely than Explanation (2). The field amplitude at the antenna in the scatterer's absence was a straightforward and simple quantity to calculate and presented no major computational problems. The calculation is discussed in Appendix I, where approximate methods are shown and where highly accurate numerical integration methods that were actually used to obtain the results are alluded to. In doing this computation, the effect of the ground reflections was found not to be as significant as in the case of the fields illuminating the scatterer, i.e., the fields at the antenna with or without ground reflections are comparable in magnitude. The effect ground reflections could have had would be in the direction of reduction of the antenna field due to destructive interference between direct and ground-reflected signals, or in the direction of an

enhancement no greater than 3 dB due to constructive interference. Therefore, although weakness in accounting for ground reflections is a possible cause of inaccuracy in this result, the effect of improving that part of the calculation might have been in the wrong direction, i.e., the direction of reduction rather than enhancement, or at best an enhancement of less than 6 dB.

Explanation (2) is more likely. It appears that the spheroid used to model the intruder, with the parameter values we have chosen, is too good a scatterer. Once a decision had been made on the choice of parameter values and the format for the computations, there was inadequate time or resources to make changes in these values and thereby determine empirically which values would provide the best fit to experimental results. Therefore the computations were all made with these same values. The values chosen were:

L_s = Length of spheroid = 2 meters

a_s = Radius of spheroid = 0.25 meters

ε_s = Permittivity of spheroid = .4089 (10^{-3}) farads/meter = 46.2 ε_0

σ_s = Conductivity of spheroid = .592 mhos/meter

Each one of these parameters could have been chosen to have a smaller value, which would have produced a smaller scattered field. The values L_s and σ_s are actually larger than those corresponding to a man of average size (L_s is equivalent to 6.56 feet, extremely tall for a man and $2a_s$ is equivalent to 1.64 feet, extremely wide for a man).

The chosen values of ε_s and σ_s were based on consultations with Professor Barber and are based on composite values from constituents of the human body. There is probably wide variability in the optimal choices of the constitutive parameters for this scattering model. Reduction in either or both values would have reduced the scattered fields. The other unknown

is the correspondance between the actual height and girth of a human frame and the proper height and radius of a spheroidal scatterer used to model a human frame.

The summarize the point of the discussion above, some degree of "cut and try" choice of the scatterer parameters L_s, R_s, ε_s and σ_s might be necessary to match the calculated received signal at the antenna to experimental results before the model could be used to predict results of changes in system design parameters. Other parameter values used in the computations are much easier to choose, because they are usually fixed by the geometry of the system.

There are many approximations used in this model, and there are noise-like fluctuations in some of the computations due to the sensitivity of the scattering model to the geometry and to coherent addition of complex numbers. The relative phases of the contributions might be subject to numerical errors and the results are extremely sensitive to these relative phases. There are also fluctuations in the experimental results (e.g., fluctuations as the angle ϕ changes in the "circumferential walk" results), so it is no surprise that such fluctuations occur in the analytical results. However, general trends, such as the peaking of the signal when the scatterer is near the cable and decaying as it recedes from the cable, are present in the results. It is concluded that this analytical model and associated computer program could be used to predict the effects on performance of changes in environmental parameters (i.e., different types of soil and design parameters e.g., different cable dimensions or antenna positions or orientations) or intruder parameters (i.e., height, girth and constitutive parameters of scatterer). In its present form, the computer program contains wide flexibility in parameter value choices and is not excessively computer-time intensive.

REFERENCES

1. H. R. Raemer, "Analysis of the Polarization dependence of the interaction between human frame targets and radio frequency sensor fields," RADC-TR-81-244, Final Technical Report, RADC Contract F30602-78-C-0102, November, 1981.

2. H. R. Raemer, "Field analysis of a class of RF intrusion sensor systems," presented and published in Symposium Digest, IEEE AP-S/URSI Symposium, Los Angeles, CA, June, 1981.

3. N. V. Karas, P. Franchi, R. L. Fante, and J. L. Poirier, "An RF Intrusion Sensor for Isolated Resources," RADC-TR-77-118, In-House Report, March, 1977.

4. J. L. Poirier, N. V. Karas, J. A. Antonucci, and M. Szczytko, "VHF Intrusion Detection: A Technique for Parked Aircraft," RAD-TR-77-384, In-House Report, November, 1977.

5. N. V. Karas, J. L. Poirier, J. Antonucci and M. Szczytko, "A VHF Intrusion Detection Technique for Isolated Resources," RADC-TR-78-177, In-House Report, July, 1978.

6. N. V. Karas, J. A. Antonucci, and M. Szczytko, "A VHF Intruder Detection System: Tests on a C-5A Aircraft," RADC-TR-78-230, In-House Report, November, 1978.

7. J. S. Rochefort, R. Sukys and N. C. Poirier, "An Area Instrusion Detection and Alarm System," RADC-TR-78-258, Final Technical Report, November, 1978.

8. J. L. Poirier and M. Kushner, "Analysis of the Response of an RF Intruder Protection System," RADC-TR-79-17, In-House Report, January, 1979.

9. J. L. Poirier, "Effect on Multiple Receiving Antennas on the Response of an RF Intrusion Sensor," RADC-TR-79-42, In-House Report, February, 1979.

10. J. L. Poirier, "An Evaluation of Some Factors Affecting the Choice of Operating Frequency of a Guided Wave Radar for Intruder Detection," [illegible].

11. J. L. Poirier, "Estimation of the Zone of Detection of the Single Wire Individual Resource Protection Sensor," [illegible].

12. J. L. Poirier, "Leaky coaxial cable resource protection sensor performance analysis," IEEE Trans. AES, Vol. AES-18, Pp. 275-285, May, 1982.

13. P. W. Chen and G. O. Young, "Ported coax intrusion detection sensor," IEEE Trans. AP-S, Vol. AP-32, No. 12, December, 1984, Pp. 1313-1317.

14. G. Goubau, "Surface waves and their application to transmission lines," J. Appl. Phys., 21, No. 11, November, 1950, pp. 1119-1128.

15. H. M. Barlow and J. Brown, "Radio Surface Waves," International Monographs on Radio, Oxford at the Clarendon Press, 1962.

16. Veena Rawat, "Unorthodox Transmission Lines for Continuous Access Guided Communication (CAGC)," Ph.D. Thesis, Queen's University, Kingston, Ontario, Canada, July, 1973.

References (cont'd)

17. P. Yoh, R. Esposito, R. Gagnon and R. Kodis, "Measurements of leaky coaxial cables and possible applications to train communications," Report No. FRA-ORO and O-74-43, U.S. Dept. of Transportation, May, 1974.

18. D. J. Cree and L. J. Giles, "Practical performance of radiating cables," The Radio and Electronic Engineer, 45 No. 5, May 1975, pp. 215-223.

19. P. P. Delogne and M. Safak, "Electromagnetic theory of the leaky coaxial cable," The Radio and Electronic Engineer, 45 No. 5, May, 1975, pp. 233-240.

20. D. J. R. Martin, "A general study of the leaky feeder principle," The Radio and Electronic Engineer, 45, No. 5, May, 1975, pp. 205-214.

21. J. R. Wait and D. A. Hill, "Propagation along a braided coaxial cable in a circular tunnel," IEEE Trans. on Microwave Theory and Techniques, MTT-23, No. 5, May, 1975, pp. 401-405.

22. D. C. Chang, "A general theory on small, radiating apertures in the outer sheath of coaxial cable," Scientific Report No. 19, ONR Contract No. N0014-76-C-0318, July, 1976.

23. D. C. Chang, "Some comments on the time-causal characteristics of leaky and surface waves," RADC TR-76-374, Interim Technical Report, December, 1976.

24. D. C. Chang, "Modal Characteristics of Single and Dual Wires Located Over a Dissipative Earth," RADC-TR-77-108, Final Report, March, 1972.

25. J. L. Mason, "Performance Characteristics of Leaky Coaxial Cables," Status Report No. 3, September 26, 1978, Status Report No. 4, December 28, 1978, USAF Contract No. F19628-77-C-0249, CCC Contract Serial No. 7SU77-00317, Tech. Rep. RADC-TR-79-340, ADA087475, Hanscom AFB, MA, 1980.

26. A. S. de C. Fernandes, "Propagation characteristics of a loose braid coaxial cable in free space," The Radio and Electronic Engineer, Vol. 49, No. 5, May, 1979, pp. 255-260.

27. Bulletin 1058A, Radiax Slotted Coaxial Cable, Andrew Corp., Oakland Park, Illinois.

28. N N Wang, J. H. Richmond and R. J. Garbacz, "Leaking ported coaxial cable embedded at a uniform depth in a lossy half-space," EM Sci. Lab., Ohio State University, Columbus, OH, Final Report 712949-3, 1981

29. D. S. Saxon, "Tensor scattering matrix for the electromagnetic field," Phys. Rev. Vol. 100, No. 6, December, 1955, pp. 1771-1775.

30. A. Anne, "Scattering and absorption of microwaves by dielectric objects: The biological significance and hazards to mankind," Ph.D. Thesis, Univ. of Pennsylvania, July, 1963.

31. A. C. Lind, R. T. Wang and J. M. Greenberg, "Microwave scattering by nonspherical particles," Applied Optics, Vol. 4, No. 12, December, 1965, pp. 1555-1561.

References (cont'd)

32. P. C. Waterman, "Symmetry, unitarity and geometry in electromagnetic scattering," Phys. Rev. D.3, 1971, pp. 825-839.

33. C. C. Johnson and A. W. Guy, "Nonionizing electromagnetic wave effects in biological materials and systems," Proc. IEEE, Vol. 60, 1972, pp. 692-718.

34. A. J. Poggio and E. K. Miller, "Integral equation solutions of three-dimensional scattering problems," Computer Techniques for Electromagnetics, R. Mittra, Ed., Pergamon Press, New York, 1973, pp. 159-264.

35. W. T. Joines and R. J. Spiegel, "Resonance absorption of microwaves by the human skull," IEEE Trans. on Biomedical Engineering, Vol. BME-21, 1974, pp. 46-48.

36. O. P. Gandhi, "Polarization and frequency effects on whole animal absorption of RF energy," Proc. IEEE, Vol. 62, No. 8, August, 1974, pp. 1171-1175.

37. B. Peterson and S. Strom, "T-matrix formulation of electromagnetic scattering from multilayered scatterers," Phys. Rev. D., Vol. 10, No. 8, pp. 2670-2684, October 15, 1974.

38. S. Asano and G. Yamamoto, "Light scattering by a spheroidal particle," Applied Optics, January, 1975, pp. 29-49.

39. C. H. Durney, C. C. Johnson and H. Massoudi, "Long-wavelength analysis of plane-wave irradiation of a prolate spheroid model of man," IEEE Trans. on Microwave Theory and Techniques, Vol. MTT-23, No. 2, February, 1975, pp. 246-253.

40. D. E. Beischer and V. R. Reno, "Microwave energy distribution measurements in proximity to man and their practical applications," Annals of N. Y. Acad. Sci., Vol. 247, February 28, 1975, pp. 473-480.

41. P. W. Barber, "Numerical study of electromagnetic power deposition in biological tissue bodies," presented URSI Annual Meeting, Boulder, Colorado, 1975.

42. G. W. Hohmann, "Three-dimensional polarization and electromagnetic modeling," Geophysics, Vol. 40, 1975, pp. 309-324.

43. C. C. Johnson, C. H. Durney, and H. Massoudi, "Long wavelength electromagnetic power absorption in prolate spheroidal models of man and animals," IEEE Trans. on Microwave Theory and Techniques, Vol. MTT-23, September, 1975, pp. 739-747.

44. O. P. Gandhi, "Frequency and orientation effects on whole animal absorption of EM waves," IEEE Trans. on Biomedical Engineering, Vol. BME 22, No. 11, November, 1975, p. 536.

45. P. Barber and C. Yeh, "Scattering of light by arbitrarily shaped dielectric bodies," Applied Optics, Vol. 14, December, 1975, pp. 2864-2872.

References (cont'd)

46. C. C. Johnson, C. H. Durney, P. W. Barber, H. Massoudi, S. J. Allen and J. C. Mitchell, "Radio Frequency Radiation Dosimetry Handbook," USAF Report SAM-TR-76-35, 1976.

47. P. W. Barber, "Numerical study of electromagnetic power deposition in biological tissue bodies," and "Biological effects of electromagnetic waves," Vol. II, U. S. Government Printing Office, 1976, pp. 119-134.

48. K. M. Chen and B. S. Guru, "Induced EM field and absorbed power density inside human torsos by 1 to 500 MHz EM waves," Technical Report No. 1, NSF Grant EMG 74-12603, 1976.

49. H. E. King and J. L. Wong, "Effects of a human body on a dipole antenna at 450 and 900 MHz," IEEE Trans. on Antennas and Propagation, Vol. AP-25, No. 3, May, 1977, pp. 376-379.

50. P. W. Barber, "Resonance electromagnetic absorption by nonspherical dielectric objects," IEEE Trans. Microwave Theory and Techniques, Vol. MTT-25, May, 1977, pp. 373-381.

51. K. M. Chen and B. S. Guru, "Internal EM field and absorbed power density on human torsos induced by 1-500 MHz EM waves," IEEE Trans. on Microwave Theory and Techniques, Vol. MTT-25, September, 1977, pp. 746-756.

52. P. W. Barber, "Electromagnetic power deposition in prolate spheroid models of man and animals at resonance," IEEE Trans. on Biomedical Engineering, Vol. BME 24, September, 1977, pp. 513-521.

53. M. J. Hagmann, O. P. Gandhi, and C. H. Durney, "Upper bound on cell size for moment-method solutions," IEEE Trans. on Microwave Theory and Techniques, Vol. MTT-25, October, 1977, pp. 831-832.

54. M. J. Hagmann, O. P. Gandhi, and C. H. Durney, "Numerical calculation of electromagnetic energy deposition for a realistic model of man," URSI International Symposium on Biological Effects of Electromagnetic Waves, Airlie, VA., October, 1977.

55. D. P. Nyquist, K. M. Chan, and B. S. Guru, "Coupling between small thin-wire antennas and a biological body," IEEE Trans. on Antennas and Propagation, Vol. AP-25, No. 6, November, 1977, pp. 863-866.

56. O. P. Gandhi, E. L. Hunt and J. A. D'Andrea, "Electromagnetic power deposition in man and animals with and without ground and reflector effects," Radio Science, Vol. 12, November/December, 1977, pp. 39-47.

57. P. W. Barber, "Scattering and absorption efficiencies for nonspherical dielectric objects - biological models," IEEE Trans. on Biomedical Engineering, Vol. BME-25, No. 2, March, 1978, pp. 155-159.

58. C. H. Durney, C. C. Johnson, P. W. Barber, H. Massoudi, M. F. Iskandor, J. L. Lords, D. K. Ryser, S. J. Allen, J. C. Mitchel, "Radio Frequency Radiation Dosimetry Handbook," (Second Edition), SAM-TR-78-22, June, 1978.

References (cont'd)

59. M. J. Hagmann, "Numerical Studies of Electromagnetic Energy by Man," Ph.D. Thesis, University of Utah, 1978.

60. M. J. Hagmann, O. P. Gandhi, and C. H. Durney, "Improvement of convergence in moment-method solutions by the use of interpolants," IEEE Trans. on Microwave Theory and Techniques, Vol. MTT-26, No. 11, November, 1978, pp. 904-908.

61. P. W. Barber, O. P. Gandhi, M. J. Hagmann and I. Chatterjee, "Electromagnetic absorption in a multilayered model of man," IEEE Trans. on Biomedical Engineering, Vol. BME-26, No. 7, July, 1979, pp. 400-405.

62. P. W. Barber, "Electromagnetic power deposition in an inhomogeneous man model," Final Report, NSF Award Number 76-15641, Bioengineering, Award Period: 9-1-76 to 8-31-79.

63. A. K. Tripathi and H. Lee, "Absorption characteristics of prolate spheroidal model of man and animals at and near resonance," EPA-600/1-79-025, U. S. Environmental Protection Agency, Research Triangle Park, North Carolina, 1979, p. 21.

64. O. P. Gandhi, "State of the knowledge for electromagnetic absorbed dose in man and animals," Proc. IEEE, Vol. 68, No. 1, January, 1980, pp. 24-32.

65. C. H. Durney, "Electromagnetic dosimetry for models of humans and animals: a review of theoretical and numerical techniques," Proc. IEEE, Vol. 69, No. 1, January, 1980, pp. 33-49.

66. J. A. Stratton, "Electromagnetic Theory," McGraw-Hill, New York, 1941.

67. P. C. Clemmow, "The Plane Wave Spectrum Representation of Electromagnetic Fields," Oxford, New York, Pergamon Press, 1966.

Appendix I

Details on Integration Around the Cable

Superposition of the field contributions from slots around the cable is accomplished through the evaluation of the integrals I_n, given by (2.17-a, b, c) with the aid of (2.18). In this appendix we present some of the details concerning approximations for this integral (and for the field components) when the observation point is close to the antenna (Section I-A) and when it is close to the cable (Section I-B). In Section I-C, the numerical solution for aribtrary location of the observation point is briefly discussed. In Section I-D, we discuss some methods such as stationary phase which can be used to evaluate the integrals approximately for arbitrary observation point locations.

I-A Approximations for Observation Points Near the Antenna

From the definition of ρ below Eqs (2.1-a, b)

$$\rho = \sqrt{a^2 + \rho^2 - 2a\rho\cos\phi' + (z - b')^2} \tag{I-1}$$

The approximation that applies to observation points near the antenna is

$$\rho \ll a \tag{I-2}$$

Applying (I-2) to (I-1) and retaining only first order terms in $(\frac{\rho}{a})$, we have

$$\rho \simeq a - \rho\cos\phi' \tag{I-3}$$

where it is implied that

$$|z - b'| \ll a \tag{I-4}$$

which is true for all cases of interest in this study.

Neglecting the second term in (I-5 in the amplitude ($e^{-jk\ell}/\ell^n$) and retaining it in the phase, we can write the integrals I_n from (2.17-a, b, c) with the aid of the approximation (2.18) as follows:

$$I_n \simeq \frac{e^{jk\ell}}{n} \int_0^{2\pi} d\theta' \, e^{-jk\rho \cos\theta' - (jk\hat{\ell}_{ce} + \alpha)\ell\theta'} \qquad \text{(I-5)}$$

Using the Bessel function relationship (See Eqs. (4.32-a, b) in Ref. 1)

$$e^{-jk\rho \cos\theta'} = \sum_{p=-\infty}^{\infty} J_p(k\rho) e^{jp(\theta' - \pi/2)} \qquad \text{(I-5)}$$

we can integrate each term of (I-5) exactly, with the result

$$I_n \simeq \frac{e^{jk\ell}}{\ell^n} \sum_{p=-\infty}^{\infty} J_p(k\rho)(-j)^p \int_0^{2\pi} d\theta' \, e^{j(p - [k\hat{\ell}_{ca} + \alpha]\ell)\theta'}$$

$$= \frac{e^{jk\ell}}{\ell^n} \sum_{p=-\infty}^{\infty} (-j)^p J_p(k\rho) \frac{(e^{j(p - [k\hat{\ell}_{ca} - j\alpha]\ell)2\pi} - 1)}{j(p - [k\hat{\ell}_{ca} - j\alpha]\ell)} \qquad \text{(I-6)}$$

In the case where the observation point is at the exact center of the cable configuration, i.e., $\rho = 0$, the Bessel functions other than $J_0(0)$ vanish and the integral (I-5) is

$$I_n \simeq \frac{e^{jk\ell}}{\ell^n} \left[\frac{1 - e^{-(jk\hat{\ell}_{ca} + \alpha)\ell 2\pi}}{(jk\hat{\ell}_{ca} + \alpha)} \right] \qquad \text{(I-7)}$$

This is the case that applies when one calculates the field at the antenna when the antenna is placed at the exact center of the cable configuration.

The easiest way to calculate the field components for this case is to begin by using (2.10-a, b, c) and (2.11-a, b, c) to calculate the components of the fields due to a single slot at angle θ'. We rewrite these equations in terms of θ', not in terms of x and θ', thus removing the

apparent dependence on the observation point's azimuth angle ϕ. In this particular case the fields are independent of ϕ (true for no other case) and the formulation in terms of ϕ, useful in all other cases should be replaced by a formulation in which all quantities are expressed directly in terms of ϕ' rather than in terms of ϕ and ϕ'.

The desired forms of (2.10-a, b, c) and (2.11-a, b, c), using the approximation

$$kR \gg 1 \tag{I-8}$$

(implied by (I-2), (I-3) and the known value of ℓ) can be approximated by the expressions

$$\underset{\substack{x\\y\\z}}{E}(\xi, \xi') \simeq C(\phi') \frac{e^{jk\ell}}{\ell} \underset{\substack{x\\y\\z}}{\hat{}}(\xi, \xi') \tag{I-9-a}$$

$$\underset{\substack{x\\y\\z}}{H}(\xi, \xi') \simeq -C(\phi') \frac{e^{jk\ell}}{\ell} Y_o \hat{z}'_{ca} \underset{\substack{x\\y\\z}}{\hat{}}(\xi, \xi') \tag{I-9-b}$$

where

$$\underset{\substack{x\\y\\z}}{\hat{}}(\xi, \xi') = \begin{Bmatrix} \cos\phi' - \hat{k}'_{ca} \sin\phi' \\ \hat{k}'_{ca} \cos\phi' + \sin\phi' \\ -\left(\frac{z - b'}{\ell}\right) \end{Bmatrix}$$

$$\underset{\substack{x\\y\\z}}{\hat{H}}(\xi, \xi') = \begin{Bmatrix} \left(\frac{z - b'}{\ell}\right) \cos\phi' \\ \left(\frac{z - b'}{\ell}\right) \sin\phi' \\ 1 \end{Bmatrix}$$

$$C(\phi') = -\frac{2}{\pi} jkL_s \, \hat{}_s \, e^{-(jk\hat{z}_{ca} + \alpha)b'}$$

Integrating (I-9-a, b) from $\phi' = 0$ to $\phi' = 2\pi$ and invoking the approximation (2.18) in evaluating these integrals, we obtain (approximately) the form (I-7) for all the integrals, leading to the result

$$\underset{z}{\overset{x}{E}}(0, \phi, z) \; - \; - \frac{E_o \, jkL_s''s}{4\pi} \frac{e^{jk\ell}}{\ell} \underset{z}{\overset{x}{E}}(0, \phi, z) \qquad \text{(I-10-a)}$$

$$\underset{z}{\overset{x}{H}}(0, \phi, z) \; - \; \frac{Y_o \, k'_{ca} \, E_o \, jkL_s''s}{4\pi} \frac{e^{jk\ell}}{\ell} \underset{z}{\overset{x}{H}}(0, \phi, z) \qquad \text{(I-10-b)}$$

where

$$\begin{matrix} E_x \\ E_y \\ E_z \end{matrix} = \Gamma \begin{Bmatrix} 1 \\ \hat{\phi}_{ca} \\ -\left(\frac{z - b'}{\ell}\right) \end{Bmatrix}$$

$$\begin{matrix} H_x \\ H_y \\ H_z \end{matrix} = \Gamma \begin{Bmatrix} \left(\frac{z - b'}{\ell}\right) \\ 0 \\ 1 \end{Bmatrix}$$

$$\Gamma = \frac{1 - e^{-(jk\hat{\phi}_{ca} + \alpha)\ell 2\pi}}{(jk\hat{\phi}_{ca} + \alpha)\ell}$$

The results (I-10-a, b) provide convenient approximations that can be used for comparison with the numerically evaluated field components obtained for the case where the scatterer is absent and ground reflections are not accounted for.

These results show the predominant electric field components in the horizontal direction and the predominant magnetic field component in the z-direction. The latter result appears to be due to the fact that the magnetic field in the cable slots is azimuthally directed (i.e., azimuth with respect to the cable itself, not the circle on which the cable is

laid), resulting in a predominantly vertical component of $\underline{E}$.

The relative magnitudes of the approximate electric field amplitudes as given by (I-10-a) are:

$$\left(\frac{|E_y|}{|E_x|}\right)_{dB} = 20 \log_{10} \sqrt{\frac{\varepsilon_{ca}}{\varepsilon_0}} = +2.3 \text{ dB} \qquad \text{(I-11)}$$

$$\left(\frac{|E_z|}{|E_x|}\right)_{dB} = 20 \log_{10} \left|\frac{z - b'}{\alpha}\right| = -33.5 \text{ dB} \qquad \text{(I-11)}$$

The results obtained from the rigorous computations using a highly accurate numerical integration technique (See Section I-C) are given by 5.1 and are (rounded off to the nearest integer)

$$\left(\frac{|E_y|}{|E_x|}\right)_{dB} \simeq (-110) - (-112) = 2 \text{ dB} \qquad \text{(I-12-a)}$$

$$\left(\frac{|E_z|}{|E_x|}\right)_{dB} \simeq (-146) - (-112) = -34 \text{ dB} \qquad \text{(I-12-b)}$$

Since the integration carried out in this appendix for the case $\rho = 0$ is exact, it is hardly surprising that the agreement between (I-12-a, b) and (I-11-a, b) is so good. However, it is still useful to establish that agreement because it serves to strengthen confidence in the numerical method used to evaluate the integrals in the general case.

I-3 Approximation for Observation Points Near the Cable

The important area of interest for the scatterer location in this study is the region near the cable. To determine the fields at the scatterer location, therefore, it is useful to focus on the approximations valid in this region.

To study this region, we define the parameter

$$\Delta = a - \rho \tag{I-13}$$

which is the radial distance from the cable, positive inside the cable and negative outside the cable.

Re-writing (I-1) in terms of Δ, we obtain

$$r = 2a\sqrt{\left(1 - \frac{\Delta}{a}\right)}\sqrt{\sin^2\left(\frac{\theta'}{2}\right) + \left(\frac{\Delta^2 + (z - b')^2}{4a^2\left(1 - \frac{\Delta}{a}\right)}\right)} \tag{I-14}$$

The approximation that holds in the region of interest is

$$\left|\frac{\Delta}{a}\right| \ll 1 \tag{I-15}$$

Unfortunately it is difficult to use this approximation effectively unless θ' is large enough so that the second term inside the radical in (I-14) is small compared with the first term. As the angle θ' increases, this condition becomes increasingly valid.

There are three regions of interest with respect to the dependence of r on the angle θ'. To discuss this, we define the second term inside the radical in (I-12) as

$$n^2 = \frac{\Delta^2 + (z - b')^2}{4a^2\left(1 - \frac{\Delta}{a}\right)} \tag{I-16}$$

With parameter value assignments used in our computations (i.e., $|z - b'| \cong 1$, $a \cong 24$), the following tabulation indicates the magnitude of n for values of $|\Delta|$ from 0 to 6

Δ	n^2	n
-6	.0129	.113
-4	.0063	.079
-2	.0021	.045
-1	.0010	.032

Δ	η^2	η
0	.0004	.020
1	.0009	.030
2	.0024	.049
4	.0089	.094
6	.0213	.146

The three regions alluded to above are:

$$R1: \quad \sin^2 \frac{\Theta'}{2} \ll \eta^2; \; R \simeq \sqrt{\Delta^2 + (z - b')^2} \qquad \text{(I-17-a)}$$

$$R2: \quad \sin^2 \frac{\Theta'}{2} \approx \eta^2; \; R \text{ is as given by (I-14)} \qquad \text{(I-17-b)}$$

$$R3: \quad \sin^2 \frac{\Theta'}{2} \gg \eta^2; \; R \simeq 2\ell\sqrt{1 - \frac{\lambda}{\ell}}\left|\sin \frac{\Theta'}{2}\right| \qquad \text{(I-17-c)}$$

Noting that, in general, if $x \ll 1$, then $\sqrt{1 + x^2} \simeq 1 + \frac{x^2}{2}$, it is evident that a value of x equal to $\frac{1}{5}$ will produce an error of $\frac{1}{50}$, or roughly 2 percent, if $\sqrt{1 + x^2}$ is approximated by 1. The regions are chosen accordingly, i.e.:

$$R1: \quad \left|\sin \frac{\Theta'}{2}\right| < \frac{\eta}{5}$$

$$R2: \quad \frac{\eta}{5} \leq \left|\sin \frac{\Theta'}{2}\right| \leq 5\eta$$

$$R3: \quad \left|\sin \frac{\Theta'}{2}\right| > 5\eta$$

The tabulation below indicates, for different values of Δ, the maximum angle Θ' for the region R1 and the minimum angle Θ' for the region R3. These angles are indicated by Θ'_1, and Θ'_2 respectively.

Δ	(θ_1') radians	(θ_1') degrees	(θ_2') radians	(θ_2') degrees
-6	.0452	2.590	1.20	68.8
-4	.0315	2.127	.812	46.5
-2	.0190	1.031	.454	26.0
-1	.0012	0.642	.280	16.0
0	.0080	0.458	.200	11.5
1	.0120	0.688	.300	17.2
2	.0196	1.123	.490	28.0
4	.0376	2.154	.820	47.0
6	.0584	3.346	1.46	83.7

The purpose of the above discussion is to define regions along the cable where the integration over that portion of the cable can be easily approximated. The approximate integral over P1, from (2.17-a), (2.18) and (I-17-a), is

$$(I_n)_{p1} = \int_0^{\theta_1'} \text{---} + \int_{2\pi - \theta_1'}^{2\pi} \text{---} =$$

$$\frac{e^{jkr}\left[1 - e^{-(\alpha + jk\hat{R}_{ca})\ell\theta_1'} + e^{(\alpha + jk\hat{R}_{ca})\ell(\theta_1' - 2\pi)} - e^{-(\alpha + jk\hat{R}_{ce})\ell 2\pi}\right]}{r^n (jk\hat{R}_{ca} + \alpha)\ell} \qquad \text{(I-17)}$$

where

$$r = \sqrt{A^2 + (z - b')^2}$$

The approximate integral over P2, from (2.17-a), (2.18) and (I-17-c), is

$$(I_n)_{P3} = \frac{1}{\left[2\ell\sqrt{1-\frac{\Delta}{\ell}}\right]^n}\int_{\theta_2'}^{2\pi-\theta_2'} d\theta' \frac{e^{jk2\ell\sqrt{1-\frac{\Delta}{\ell}}\left|\sin\frac{\theta'}{2}\right| - (jk\hat{k}_{ca}+\alpha)\ell\theta'}}{\left|\sin\frac{\theta'}{2}\right|^n} \tag{I-19}$$

Unfortunately, the integrals in (I-19) cannot be evaluated exactly, nor can the integral that would arise for region R2, where no approximations like those used in (I-18) or (I-19) can be used. Hence, unless we can validly assume that the integral given in (I-18) is the overwhelming contributor to the integral over the entire cable, the approximations due to the close proximity of the observation point to the cable do not help to evaluate the integral. The assumption that the integral in (I-18) is a good approximation to the integral over the entire cable is given credence by some of the approximate results in Section 3 (i.e., those based on Table 3.1 and Eqs. (3.3-a, ..., e)) which seem to indicate that the overwhelming contribution to the illuminating fields comes from the slots nearest the observation point and that for each component the field amplitudes seem to vary roughly as a particular power of $\frac{1}{\delta}$, where $\delta = \sqrt{\Delta^2 + (z - b')^2}$.

I-C The General Case

The actual evaluation of the integrals I_n implemented for machine computation was accomplished through a highly accurate numerical integration technique. A twelfth order Gaussian rule (Conte and deBoor, "Elementary numerical analysis - an algorithmic approach," McGraw-Hill, 1980; Pages 311-313, 325-326) was used. The first 12 coefficients in a series are determined in order to evaluate the zeros of a set of 12^{th} order orthogonal polynomials. Using 1200 to 2400 points, the method provides accuracy within 0.1 percent. These computations were carried out without significant expenditure of running time and tables of the values of I_n for required values

of ρ and z were generated. This task was simplified by the fact that the integrands of I_n depend only on $\theta' = \phi' - \phi$ and are independent of ϕ, the azimuthal angle of the observation point.

I-D General Approximations for the Integral I_n

The integrals given by (2.17-a), (2.17-b) or (2.17-c) (approximately equivalent by virtue of (2.18)) are all of the generic form

$$I = \int_{x_1}^{x_2} dx\, e^{j\Psi(x)}\, g(x) \qquad \text{(I-20-a)}$$

or

$$I = \int_{x_1}^{x_2} dx\, e^{\Phi(x)}\, f(x) \qquad \text{(I-20-b)}$$

where

$$x = \theta'$$

$$R(x) = \sqrt{a^2 + \rho^2 - 2\rho\cos x + (z - b')^2}$$

$$f(x) = \frac{1}{[R(x)]^n} \; ; \; n = 1, 2 \text{ or } 3$$

$$\Psi(x) = k(R(x) - \hat{k}_{ca}\, a\, x)$$

$$g(x) = e^{-\alpha x} f(x)$$

$$\Phi(x) = j\Psi(x) - \alpha x$$

The form (I-20-a) will be used in the discussion of the stationary phase method. The form (I-20-b) will be used in discussion of a technique that is an alternative to stationary phase in cases where no stationary phase points exist or the latter method is not easily applicable for other reasons.

First using the form (I-20-a), consider the possibility of applying stationary phase. In order to do so, we must have one or more stationary phase points, i.e., points x_0 where $\Psi'(x_0) = 0$. To investigate that, we differentiate $\Psi(x)$, with the result

$$\frac{d\Psi(x)}{dx} = \Psi'(x) = \frac{2\ell}{\rho}\sin x - \hat{k}_{ca}\,\alpha' = 0 \qquad \text{(I-21)}$$

From (I-21), a stationary phase point x_0 would exist wherever

$$\sin x_0 = \frac{\hat{k}_{ca} R}{\rho} = \frac{\hat{k}_{ca}}{\rho}\sqrt{\rho^2 + \alpha^2 - 2\rho\alpha\cos x_0 + (z - b')^2} \qquad \text{(I-22)}$$

Squaring both sides of (I-22)

$$1 - \cos^2 x_0 = \frac{\hat{k}_{ca}^2}{\rho}\left[\rho^2 + \alpha^2 - 2\rho\alpha\cos x_0 + (z - b')^2\right] \qquad \text{(I-23)}$$

Expressing (I-23) as a quadratic equation in $\cos x_0$, we have

$$\cos^2 x_0 - \frac{2\alpha\hat{k}_{ca}^2}{\rho}\cos x_0 + \left[(\hat{k}_{ca}^2 - 1) + \hat{k}_{ca}^2\left[\frac{\alpha^2 + (z - b')^2}{2}\right]\right] = 0 \qquad \text{(I-23)'}$$

whose solution is

$$\cos x_0 = \frac{\alpha\hat{k}_{ca}^2}{\rho} \pm \sqrt{\left[\frac{\alpha^2\hat{k}_{ca}^2}{\rho^2} - 1\right](\hat{k}_{ca}^2 - 1) - \frac{\hat{k}_{ca}^2(z - b')^2}{\rho^2}} \qquad \text{(I-24)}$$

In all cases of interest in this study

$$\left|\frac{z - b'}{\alpha}\right| \ll 1 \qquad \text{(I-25)}$$

Using (I-25) in (I-24), we can approximate $\cos x_0$ as follows:

$$\cos x_0 = -\frac{\alpha^2 \hat{k}_{ca}^2}{\rho} \pm \sqrt{\left(\frac{\alpha^2 \hat{k}_{ca}^2}{\rho^2} - 1\right)(\hat{k}_{ca}^2 - 1)} \qquad \text{(I-26)}$$

The value of k_{ca}^2 always exceeds unity; hence in order that $\cos x_0$ be a real number, the only requirement is that

$$\frac{\alpha^2 \hat{k}_{ca}^2}{\rho^2} - 1 \geq 0 \qquad \text{(I-27)}$$

or equivalently

$$\frac{\alpha^2}{\rho} \geq \frac{1}{\hat{k}_{ca}} \qquad \text{(I-27)'}$$

If we choose the plus sign in (I-26) then $\cos x_0$ as given by (I-26) is positive and the condition required is that $\cos x_0 \leq 1$. That condition is

$$\frac{\alpha^2 \hat{k}_{ca}^2}{\rho} + \sqrt{\hat{k}_{ca}^2 - 1}\sqrt{\frac{\alpha^2 \hat{k}_{ca}^2}{\rho^2} - 1} \leq 1 \qquad \text{(I-28)}$$

or equivalently

$$\left(\frac{\alpha^2 \hat{k}_{ca}^2}{\rho} - 1\right) + \sqrt{\hat{k}_{ca}^2 - 1}\sqrt{\frac{\alpha^2 \hat{k}_{ca}^2}{\rho^2} - 1} \leq 0 \qquad \text{(I-28)'}$$

Since the second term on the LHS of (I-28)' is positive, it is required that the first term be negative and greater in magnitude than the second term. The first of these conditions is

$$\frac{\alpha^2}{\rho} \leq \frac{1}{\hat{k}_{ca}^2} \qquad \text{(I-29)}$$

Combining (I-27)' and (I-29)

$$\frac{1}{\hat{k}_{ca}} \leq \frac{\alpha^2}{\rho} \leq \frac{1}{\hat{k}_{ca}^2} \qquad \text{(I-30)}$$

which implies that

$$\hat{k}_{ca} \leq 1 \qquad \text{(I-30)'}$$

But we know that $\hat{k}_{ca} \geq 1$, which is a contradiction of (I-30) or (I-30)'; therefore the positive sign in (I-26) is outlawed by the requirement that $\cos x_0 \leq 1$, which we have shown to be incompatible with that case.

Now consider the negative sign in (I-26), which allows $\cos x_0$ to be negative or positive. The required condition is

$$|\cos x_0| \leq 1 \qquad \text{(I-33)}$$

or equivalently

$$\cos^2 x_0 \leq 1 \qquad \text{(I-33)'}$$

which, based on (I-26), has the form

$$\left[\frac{\hat{k}_{ca}^2}{\rho}\right]^2 + \left[\frac{\beta^2 \hat{k}_{ca}^2}{\rho^2} - 1\right](\hat{k}_{ca}^2 - 1) - \frac{2\beta^2 \hat{k}_{ca}^2}{\rho}\sqrt{\frac{\beta^2 \hat{k}_{ca}^2}{\rho^2} - 1}\sqrt{\hat{k}_{ca}^2 - 1} \leq 1 \qquad \text{(I-33)"}$$

From (I-27)', we can write

$$\frac{\beta}{\rho} = \frac{\beta}{\hat{k}_{ca}} \text{, where } \beta \geq 1 \qquad \text{(I-34)}$$

Using (I-34) in (I-33)", we have the condition

$$\beta^2\hat{k}_{ca}^2 + (\beta^2 - 1)(\hat{k}_{ca}^2 - 1) - 2\beta\hat{k}_{ca}\sqrt{\beta^2 - 1}\sqrt{\hat{k}_{ca}^2 - 1} =$$

$$\beta^2(2\hat{k}_{ca}^2 - 1) - 2\beta\hat{k}_{ca}\sqrt{\hat{k}_{ca}^2 - 1}\sqrt{\beta^2 - 1} - \hat{k}_{ca}^2 \leq 0 \qquad \text{(I-35)}$$

Using the assigned value of $\hat{k}_{ca} = \sqrt{1.7}$, we can re-write (I-35) in the form

$$A = 2.4\beta^2 - 2.196\sqrt{\beta^2 - 1} - 1.7 \leq 0 \qquad \text{(I-36)}$$

A study of the inequality (I-35)' shows that there is a limited range of values of β (and hence of ρ) where stationary phase methods can be used. Since stationary phase points do not exist for all values of ρ, it was decided not to use that method to evaluate the integrals I_n. An alternative approximation method for integrals of the type (I-20-a) or (I-20-b) will be discussed in what follows.

Now we consider an asymptotic method, which was used in the original project and is given to first order in Reference 1, Section 4, Page 4-38. This method applies to cases not easily amenable to stationary phase methods and is based on partial integration. To derive the method, we use the form (I-20-b) and integrate successively by parts, i.e.,

$$I = \int_{x_1}^{x_2} dx\, e^{\phi(x)} f(x) = \int_{x_1}^{x_2} \left(\frac{e^{\phi(x)}}{\phi'(x)}\right)' f(x) =$$

$$\left[\frac{e^{\phi(x)}}{\phi'(x)} f(x)\right]_{x_1}^{x_2} - \int dx \frac{f'(x)\, e^{\phi(x)}}{\phi'(x)} \qquad \text{(I-37)}$$

After two more steps of integration by parts, we obtain

$$I_n = \left[\frac{e^{\phi(x)}}{\phi'(x)}\right]_{x_1}^{x_2} \left\{f(x) + f'(x)\left[\frac{-1}{[\phi'(x)]} - \frac{\phi''(x)}{[\phi'(x)]^3} - \frac{3[\phi''(x)]^2}{[\phi'(x)]^5}\right.\right.$$

$$\left. + \frac{\phi'''(x)}{[\phi'(x)]^4} + \ldots\right] + f''(x)\left[\frac{1}{[\phi'(x)]^2} + \frac{3\phi''(x)}{[\phi'(x)]^4} + \ldots\right]$$

$$\left. + f'''(x)\left[\frac{1}{[\phi'(x)]^3} + \ldots\right]\right] \qquad \text{(I-37)'}$$

This method can be applied to the integrals I_n as long as $\phi'(x)$ does not vanish at the end-points. Note that

$$\phi(x) = j\Psi(x) - \alpha\ell x = jk[R(x) - \hat{k}_{ca}\ell x] - \alpha\ell x \qquad \text{(I-38)}$$

and hence from (I-21)

$$\phi'(x) = \ell[jk(\frac{\rho}{\eta}\sin x - \hat{k}_{ca}) - \alpha] \qquad \text{(I-39)}$$

If the end-points are: $x_1 = 0$, $x_2 = 2\pi$, then

$$\phi'(0) = \phi'(x_1) = \phi'(x_2) = \phi'(2\pi) = -(\alpha + jk\hat{k}_{ca})\ell \qquad \text{(I-40)}$$

Since

$$R(x_1) = R(x_2) = R(0) = R(2\pi) = \sqrt{(\rho - \ell)^2 + (z - b')^2} = \eta \qquad \text{(I-41-a)}$$

$$f(x) = \frac{1}{[R(x)]^n} \qquad \text{(I-41-b)}$$

$$f(x_1) = f(x_2) = \frac{1}{\eta^n} \qquad \text{(I-41-c)}$$

$$\phi(x_1) = jk\eta \qquad \text{(I-41-d)}$$

$$\phi(x_2) = jk\eta - (\alpha + jk\hat{k}_{ca})\ell 2\pi \qquad \text{(I-41-e)}$$

The first order solution to the integral is given by (I-37)' with the aid of (I-40) and (I-41-a, ..., e) as follows

$$(I_n)_{\substack{\text{first}\\ \text{order}}} = \frac{e^{jk\eta}(1 - e^{-(\alpha + jk\hat{k}_{ca})\ell 2\pi})}{\eta^n(\alpha + jk\hat{k}_{ca})\ell} \qquad \text{(I-42)}$$

To obtain the second order term (i.e., that involving $f'(x)$), we calculate the following quantities

$$f'(x) = \frac{-n}{[R(x)]^{n+1}} \qquad \text{(I-43-a)}$$

$$\phi''(x) = \frac{jk\rho\ell}{\eta}\left[\cos x - \frac{2\ell}{\eta^2}\sin^2 x\right] \qquad \text{(I-43-b)}$$

$$\phi'''(x) = -\frac{jk\rho\ell}{R}\sin x\left(1 + \frac{3\rho\ell}{R^2}\cos x - \frac{3(\rho\ell)^2}{R^2}\sin^2 x\right) \qquad \text{(I-43-c)}$$

$$f'(x_1) = f'(x_2) = -\frac{n}{\ell^{n+1}} \qquad \text{(I-43-d)}$$

$$\phi''(x_1) = \phi''(x_2) = \frac{jk\rho\ell^2}{R} \qquad \text{(I-43-e)}$$

$$\phi'''(x_1) = \phi'''(x_2) = 0 \qquad \text{(I-43-f)}$$

Substituting (I-40) and (I-43-a, ..., f) into (I-37)' and adding the first order solution (I-42) the integral to second order is given approximately by

$$(I_n)_{\substack{\text{first and}\\ \text{second}\\ \text{order terms}}} \simeq \frac{e^{jkR}}{R^n}\frac{(1 - e^{-(\alpha + jk\hat{k}_{ca})\ell 2\pi})}{(\alpha + jk\hat{\rho}_{ca})\ell} \text{ ----- }$$

$$\left[1 - \frac{n}{R}\left[1 + \frac{jk\rho}{R(\alpha + jk\hat{k}_{ca})^2\ell} - \frac{3(jk\rho)^2}{R^2(\alpha + jk\hat{k}_{ca})^4\ell^2}\right]\right] \qquad \text{(I-44)}$$

More partial integration steps would lead to terms with increasingly higher order variation with $\frac{1}{R}$ and the ratio $(\frac{\rho}{\ell})$. The latter ratio approaches unity and R approaches $\frac{1}{(z - b')}$ as distance from the cable decreases. Hence close to the cable, we would obtain a series in increasing powers of the reciprocal height of the observation point.

We note that the factor $\frac{e^{jkR}}{R^n}$ is present in this solution. This is important in supporting the argument that the fields near the cable are very close to those that would be obtained from only those slots nearest to the observation point.

Appendix II

Details on Approaches Using Plane-Wave Spectral Representation of Fields

In the original project, the plane-wave spectral representation of each field component (See Ref. 1, Sections 3 and 4 and Appendices II and III) or a valid approximation to it, was needed for two purposes:

(a) To determine the ground reflected fields, based on the assumption of a plane wave incident on the ground surface

(b) in order to validly use the Barber scattering program (Ref. 1, Section 7) which assumes plane waves incident on the scatterer.

The theory behind the transformation between position space (x, y, z or ρ, φ, z coordinates) and "plane-wave spectrum" space (the space of the wave vector $\underset{\sim}{\beta}$, whose x, y and z coordinates are β_x, β_y, β_z, where $\beta_z = \pm\sqrt{1 - \beta_x^2 - \beta_y^2}$ is given in Reference 1, Appendix II. If $\underset{\sim}{V}(x, y, z)$ is a vector function of rectangular coordinates (x, y, z), then from Eq. (II-3) in Appendix II of Ref. 1, with some notational changes, we have the inverse Fourier transform of $\underset{\sim}{V}(x, y, z)$ in terms of the plane-wave spectrum for upward and downward propagating waves $\underset{\sim}{\tilde{V}}_+(\underset{\sim}{\beta}_h)$ and $\underset{\sim}{\tilde{V}}_-(\underset{\sim}{\beta}_h)$ respectively, where $\underset{\sim}{\beta}_h = \beta_x \hat{\underset{\sim}{x}} + \beta_y \hat{\underset{\sim}{y}}$, as follows:

$$\underset{\sim}{V}(x, y, z) = \int_{-1}^{1} d\beta_x \int_{-1}^{1} d\beta_y \, e^{jk(\beta_x x + \beta_y y)} \left(e^{-jk|\beta_z|z} \underset{\sim}{\tilde{V}}_-(\underset{\sim}{\beta}_h) + e^{jk|\beta_z|z} \underset{\sim}{\tilde{V}}_+(\underset{\sim}{\beta}_h) \right) \qquad \text{(II-1)}$$

where $|\beta_z| = \sqrt{1 - \beta_h^2}$

$\beta_h = \sqrt{\beta_x^2 + \beta_y^2}$

The inversion of (II-1) to determine $\tilde{\underline{V}}_{\pm}(\underline{\beta}_h)$ in terms of $\underline{V}(x, y, z)$ results in Eqs. (II-5-a, b) of Ref. 1, again with notational changes

$$\tilde{\underline{V}}_{\pm}(\underline{\beta}_h) = \frac{\left(\frac{k}{2\pi}\right)^2}{1 + |\beta_z|} \int_{-\infty}^{\infty} \int dx\, dy\, e^{-j\underline{\beta}_h \cdot \underline{\rho}} \left(|\beta_z|\, \underline{V}(x, y, 0) \mp \frac{1}{jk} \underline{V}'(x, y, 0) \right) \tag{II-2}$$

where $$\underline{V}'(x, y, 0) = \left[\frac{\partial \underline{V}(x, y, z)}{\partial z}\right]_{z=0}$$

$$\underline{\rho} = \hat{x}\, x + \hat{y}\, y$$

We will use (II-2) where $\underline{V}(x, y, z)$ is the electric field vector $\underline{E}(x, y, z)$ whose x, y, z components for a single slot are given by (2.8-a, b, c) or (2.10-a, b, c). The differentiation with respect to z gives nonzero values only for z-dependent factors in the terms of these equations. In the x and y components, the factors that are z-dependent are all of the form $\frac{e^{jkR}}{R^n}$, where n = 1, 2 or 3.

The z-component of the electric field can be obtained from the x and y components through the divergence equation

$$\nabla \cdot \underline{E} = 0 \tag{II-3}$$

which, for each point in the plane wave spectral space (i.e., the space of $\underline{\beta}$), takes the form

$$j(\beta_x [\tilde{E}_x(\underline{\beta}_h)]_{\pm} + \beta_y [\tilde{E}_y(\underline{\beta}_h)]_{\pm} \mp |\beta_z| [\tilde{E}_z(\underline{\beta}_h)]_{\pm} = 0 \tag{II-4}$$

Eq. (II-4) can be solved for $\tilde{E}_z$ if $|\beta_z| \neq 0$, i.e.,

$$[\tilde{E}_z(\underline{\beta}_h)]_{\pm} = \mp \frac{\beta_h}{|\beta_z|} \left([\tilde{E}_x(\underline{\beta}_h)]_{\pm} \cos \phi_\beta + [\tilde{E}_y(\underline{\beta}_h)]_{\pm} \sin \phi_\beta \right) \tag{II-5}$$

valid if $\beta_z \neq 0$

where $\beta_x = \beta_h \cos \phi_\beta$, $\beta_y = \beta_h \sin \phi_\beta$

Deferring the question of what happens if $\hat{\rho}_z = 0$, we will proceed to formulate expressions for $\tilde{E}_x$ and $\tilde{E}_y$.

To accomplish this, we must find the z-derivatives of $\frac{e^{jkR}}{R^n}$, easily determined as

$$\frac{\partial}{\partial z}\left(\frac{e^{jkR}}{R^n}\right) = (jk)^{n+2}\frac{e^{jkR}}{(jkR)^n}\left(1 - \frac{n}{jkR}\right)\frac{jk(z - b')}{jkR} \qquad \text{(II-6)}$$

at $z = 0$, (II-6) becomes

$$\left[\frac{\partial}{\partial z}\left(\frac{e^{jkR}}{R^n}\right)\right]_{z=0} = (jk)^{n+2}(-jkb')e^{jkR_o}\left[\frac{1}{(jkR_o)^{n+1}} - \frac{n}{(jkR_o)^{n+2}}\right] \qquad \text{(II-6)'}$$

where $R_o = \sqrt{\rho^2 + \rho'^2 - 2\rho\rho' \cos\phi'}$

Using (II-6)' in the differentiation of (2.3-a, b) with respect to z at $z = 0$ results in the following expressions for $\tilde{E}_x$ and $\tilde{E}_y$ for upward or downward propagating plane waves:

$$\left.\frac{\partial \tilde{E}_x}{\partial z}\right|_{z=0} = (jk)^3(-jkb')C\,e^{-(\alpha + jk\hat{\rho}_{ca})\cdot(\rho + \rho')}e^{jkR_o} \quad ---$$

$$--- \left\{(jk\rho\cos\phi - jk\rho'\cos\phi')\left[\frac{1}{(jkR_o)^3} - \frac{3}{(jkR_o)^4} + \frac{3}{(jkR_o)^5}\right]\right.$$

$$\left. + \hat{\rho}'_{ca}\sin\phi'\left[\frac{1}{(jkR_o)^2} - \frac{1}{(jkR_o)^3}\right]\right\} \qquad \text{(II-7-a)}$$

$$\left.\frac{\partial \tilde{E}_y}{\partial z}\right|_{z=0} = (jk)^3(-jkb')C\,e^{-(\alpha + jk\hat{\rho}_{ca})\cdot(\rho + \rho')}e^{jkR_o} \quad ---$$

$$--- \left\{(jk\rho\sin\phi - jk\rho'\sin\phi')\left[\frac{1}{(jkR_o)^3} - \frac{3}{(jkR_o)^4} + \frac{3}{(jkR_o)^5}\right]\right.$$

$$\left. - \hat{\rho}'_{ca}\cos\phi'\left[\frac{1}{(jkR_o)^2} - \frac{1}{(jkR_o)^3}\right]\right\} \qquad \text{(II-7-b)}$$

We will now combine (II-7-a, b) with (2.8-a, b) or (2.10-a, b) to form the integrands of the expressions (II-2) where the vectors $\underline{V}$ and $\underline{\mathcal{V}}$ in (II-2) are the electric field vector $\underline{E}$ due to the slot at $\phi' = \phi + \theta'$ and its plane wave spectrum $\underline{\mathcal{E}}$ respectively.

$$([\mathcal{E}_x(\beta_h)]_{\pm})_{\phi'} = \frac{-k^4}{4\pi^2} C \int_0^{\infty} d\rho\rho \int_0^{2\pi} d\phi\, e^{jk[R_o - \beta_h \rho \cos(\phi - \phi_\beta)]}$$

$$e^{-(\alpha + jk\hat{R}_{ca})\ell(\phi + \theta')} \left\{ \frac{1}{(jkR_o)} [|\beta_z| \hat{R}'_{ca} \sin\phi'] \right.$$

$$+ \frac{1}{(jkR_o)^2} [(jk\rho \cos\phi - jk\ell \cos\phi')|\beta_z| \mp jk\rho' \hat{R}'_{ca} \sin\phi']$$

$$+ \frac{1}{(jkR_o)^3} [(jk\rho \cos\phi - jk\ell \cos\phi')(-|\beta_z| \pm jk\rho' \hat{R}'_{ca} \sin\phi']$$

$$+ \frac{1}{(jkR_o)^4} [(jk\rho \cos\phi - jk\ell \cos\phi')(\pm 3\, jk\rho')]$$

$$\left. + \frac{1}{(jkR_o)^5} [(jk\rho \cos\phi - jk\ell \cos\phi')(\mp 3\, jk\rho')] \right\} \qquad \text{(II-3-a)}$$

$$([\mathcal{E}_y(\beta_h)]_{\pm})_{\phi'} = \frac{-k^4}{4\pi^2} C \int_0^{\infty} d\rho\rho \int_0^{2\pi} d\phi\, e^{jk[R_o - \beta_h \rho \cos(\phi - \phi_\beta)]}$$

$$e^{-(\alpha + jk\hat{R}_{ca})\ell(\phi + \theta')} \left\{ \frac{1}{(jkR_o)} [-|\beta_z| \hat{R}'_{ca} \cos\phi'] \right.$$

$$+ \frac{1}{(jkR_o)^2} [(jk\rho \sin\phi - jk\ell \sin\phi')|\beta_z| \pm jk\rho' \hat{R}'_{ca} \cos\phi']$$

$$+ \frac{1}{(jkR_o)^3} [(jk\rho \sin\phi - jk\ell \sin\phi')(-|\beta_z| \mp jk\rho' \hat{R}'_{ca} \cos\phi']$$

$$+ \frac{1}{(jkR_o)^4} [(jk\rho \sin\phi - jk\ell \sin\phi')(\pm 3\, jk\rho')]$$

$$+ \frac{1}{(jk\rho_o)^3}\left[(jk\rho \sin\phi - jk\alpha \sin\phi')(\mp 3\, jkb')\right]\Big\} \qquad \text{(II-8-b)}$$

To ensure the validity of (II-8-a, b), it is necessary that it be consistent with (II-5) and (2.8-c) or (2.10-c). If we were to calculate the plane-wave spectrum of E_z through (2.8-c) or (2.10-c) and the z-component of Eq. (II-2), the result must be the same as that obtained by applying (II-5) to the results (II-8-a, b). The latter operation yields

$$(\tilde{E}_z(\beta_h))_{\pm})_{cyl} = \frac{-k^4}{4\pi^2}\frac{C}{1+|\beta_z|}\int_0^\infty d\rho\rho \int_0^{2\pi} d\phi\, e^{jk[\beta_o - \beta_h \rho \cos(\phi - \phi_\beta)]}$$

$$e^{-(\alpha + jk\hat{\rho}_{ca})\rho\cos(\phi+\phi')}\Big\{\frac{1}{(jk\rho_o)}\left[\mp \hat{\rho}'_{ca}\beta_h \sin(\phi' - \phi_\beta)\right]$$

$$+ \frac{1}{(jk\rho_o)^2}\left[\mp (jk\rho \beta_h \cos(\phi - \phi_\beta) - jk\alpha \beta_h \cos(\phi' - \phi_\beta)) + \right.$$

$$\left. jk\frac{b'\beta_h}{|\beta_z|}\hat{k}'_{ca}\sin(\phi' - \phi_\beta)\right]$$

$$+ \frac{1}{(jk\rho_o)^3}\left[(jk\rho \beta_h \cos(\phi - \phi_\beta) - jk\alpha \beta_h \cos(\phi' - \phi_\beta))(\pm 1 + \frac{jkb'}{|\beta_z|})\right.$$

$$\left. - jk\frac{b'\beta_h}{|\beta_z|}\hat{k}'_{ca}\sin(\phi' - \phi_\beta)\right]$$

$$+ \frac{1}{(jk\rho_o)^4}\left[\mp (3\, jk\frac{b'\beta_h}{|\beta_z|})(jk\rho\cos(\phi - \phi_\beta) - jk\alpha\cos(\phi' - \phi_\beta))\right]$$

$$+ \frac{1}{(jk\rho_o)^5}\left[+ (3\, jk\frac{b'\beta_h}{|\beta_z|})(jk\rho\cos(\phi - \phi_\beta) - jk\alpha\cos(\phi' - \phi_\beta))^2\right]\Big\}$$

(II-8-c)

The direct route to the vertical component of the plane-wave spectrum of the field, through (II-5), from (2.8-c) with the aid of (II-6)', yields

$$([\tilde{\Gamma}_z(\beta_h)]_\pm)_{\theta'} = \frac{-k^4 C}{\frac{4\pi^2}{1+|\beta_z|}} \int_0^\infty d\rho\rho \int_0^{2\pi} d\phi\, e^{jk[\beta_o - \beta_h \cos(\phi - \phi_2)]}$$

$$e^{-(\alpha + jk\hat{\beta}_{ca})\ell(\phi + \theta')} \frac{1}{jk\beta_o}[0] + \frac{1}{(jk\beta_o)^2}[|\beta_z| b' \mp \frac{1}{jk}]$$

$$+ \frac{1}{(jk\beta_o)^3}[-|\beta_z| b' \mp \frac{1}{jk} \mp jk (b')^2] + \frac{1}{(jk\beta_o)^4}[\mp 3 (jk)^2 (b')^2]$$

$$+ \frac{1}{(jk\beta_o)^5}[\pm 3 (jk)^3 (b')^2]\Big\} \qquad \text{(II-9)}$$

The quantities $[\tilde{\Gamma}_z(\beta_h)]_\pm$, whether calculated from (II-8-c) or (II-9) must be exactly **equivalent.** Of course, from a practical viewpoint, the most efficient way to obtain $\tilde{\Gamma}_z$ is to compute $\tilde{\Gamma}_x$ and $\tilde{\Gamma}_y$ from (II-8-a, b) and then compute $\tilde{\Gamma}_z$ from (II-5). The only reason one might compute $\tilde{\Gamma}_z$ from (II-9) is for checking purposes.

Carrying out the integrations around the cable slots in (II-8-a, b, c) and invoking (2.17-a, b, c) and the approximation(2.18), we obtain

$$[\tilde{\underset{\sim}{\Gamma}}_z(\beta_h)]_\pm = \frac{-k^4 C}{\frac{4\pi^2}{1+|\beta_z|}} \int_0^\infty d\rho\rho \int_0^{2\pi} d\phi\, e^{-jk[\beta_h \rho \cos(\phi - \phi_2) - \hat{\beta}_{ca}\ell\phi]} \cdot$$

$$e^{-\alpha\ell(\phi)} \left[a_{\underset{\sim}{z}} \hat{I}_1 + b_{\underset{\sim}{z}} \hat{I}_2 + c_{\underset{\sim}{z}} \hat{I}_3 + d_{\underset{\sim}{z}} \hat{I}_4 + e_{\underset{\sim}{z}} \hat{I}_5\right] \qquad \text{(II-10)}$$

where

$$a_x = \frac{|\beta_z|}{jk} \hat{\beta}'_{ca} \sin\phi$$

$$b_x = \frac{1}{(jk)} [(\phi - \phi_2)\{|\beta_z| \cos\phi \mp b' \hat{\beta}'_{ca} \sin\phi\}$$

$$c_x = \frac{1}{(jk)^2} [(\phi - \phi_2) \cos\phi (-|\beta_z| \mp jkb') \pm b' \hat{\beta}'_{ca} \sin\phi]$$

$$d_x = \pm \frac{1}{(jk)^2} [3b' (\rho - \ell) \cos \phi]$$

$$e_x = \mp \frac{1}{(jk)^3} [3b' (\rho - \ell) \cos \phi]$$

$$a_y = - \frac{|\beta_z|}{(jk)} \hat{R}'_{ca} \cos \phi$$

$$b_y = \frac{1}{(jk)} [(\rho - \ell) |\beta_z| \sin \phi \pm b' \hat{R}'_{ca} \cos \phi]$$

$$c_y = \frac{1}{(jk)^2} [(\rho - \ell) \sin \phi (- |\beta_z| \mp jkb') \mp b' \hat{R}'_{ca} \cos \phi]$$

$$d_y = \pm \frac{1}{(jk)^2} [3b' (\rho - \ell) \sin \phi]$$

$$e_y = \mp \frac{1}{(jk)^3} [3b' (\rho - \ell) \sin \phi]$$

$$a_z = \mp \frac{\hat{R}'_{ca}}{(jk)} \beta_h \sin (\phi - \phi_\beta)$$

$$b_z = \frac{\beta_h}{(jk)|\beta_z|} [\mp |\beta_z| (\rho - \ell) \cos (\phi - \phi_\beta) + b' \hat{R}'_{ca} \sin (\phi - \phi_\beta)]$$

$$c_z = \frac{\beta_h}{(jk)^2 |\beta_z|} [(\rho - \ell) \cos (\phi - \phi_\beta)(\pm |\beta_z| + jkb') - b' \hat{R}'_{ca} \sin (\phi - \phi_\beta)]$$

$$d_z = \frac{-\beta_h}{(jk)^2 |\beta_z|} [3b' (\rho - \ell) \cos (\phi - \phi_\beta)]$$

$$e_z = \frac{+\beta_h}{(jk)^3 |\beta_z|} [3b' (\rho - \ell) \cos (\phi - \phi_\beta)]$$

and where

$$\hat{I}_n = \int_0^{2\pi} d\theta' \frac{1}{\rho_o^n} e^{jk\rho_o - (jk\hat{R}_{ca} + \alpha)\ell\cos\theta'}$$

where

$$\rho_o = \sqrt{\rho^2 + \ell^2 - 2\rho\ell \cos\theta'}$$

A serious attempt was made to carry out the double integrations indicated in (II-2-a, b, c), both by approximate analytical methods and numerical methods (such as the method used for integration around the cable, discussed in Appendix I, Section I-C).

Since the $\hat{I}_n$'s are independent of ϕ, and the remainder of the amplitude of the integrand varies slowly with ϕ, the integration on ϕ appears to be very easy. Stationary phase methods were considered, but it was found that the stationary phase points, given by

$$\sin(\phi - \phi_0) = -\frac{\hat{k}_{ca}\rho}{\hat{k}_h \rho} \qquad \text{(II-11)}$$

do not exist because the RHS of (II-11) exceeds unity over a significant portion of the integration region.* The other approximation method discussed in Appendix I, Section D, applicable in cases where stationary phase points don't exist, was also considered. Finally, the ϕ integrations were actually carried out using the very accurate numerical method discussed in Appendix I, Section C. However, when the integration on ρ was attempted by numerical methods, it was found that coverage of the region near the cable (the most important contribution to the integral) required a prohibitive amount of computer time and that approach was abandoned. At that point, an approximate approach was considered wherein the field components are given by (2.7-a, b, c) only within a region that contains the scatterer volume and vanish outside that region. This might be a satisfactory approach because the scatterer in free space only responds to the fields impinging upon it and the scattering is independent of the fields in the surrounding regions. Of course, the plane wave spectrum obtained by this technique would be different from that obtained by integrating (II-10) over all space (e.g., there would be significant

* In order for a stationary phase point to exist, ρ would have to exceed $\frac{\hat{k}_{ca}\rho}{\hat{k}_h} = \frac{31.2}{\hat{k}_h}$. Since the largest possible value of $\hat{k}_h$ is 1, that would only apply for points far outside the cable.

contributions from a larger portion of $\underline{\beta}$-space). However, when the inverse Fourier transformation is performed, the recovered field components should be approximately the same as those obtained through integration of (II-10) over all position space.

The numerical implementation of this method is very simple. It amounts to replacing the double integration $\int_0^{\infty} d\rho\rho \int_0^{2\pi} d\phi$ in (II-10) by $\int_{\rho_o - \frac{\Delta\rho}{2}}^{\rho_o + \frac{\Delta\rho}{2}} d\rho\rho$ $\int_{\phi_o - \frac{\Delta\phi}{2}}^{\phi_o + \frac{\Delta\phi}{2}} d\phi$, where (ρ_o, ϕ_o) is the center of the integration volume, $\Delta\rho$ the width of that integration volume in ρ-space and $\Delta\phi$ the width in ϕ-space.

The above approach was not actually implemented. Although it would have been ideal to attain the plane-wave spectral field components by actually carrying out the integrations in (II-8-a, b, c) there was insufficient time and resources to do justice to that approach. It was then decided to adopt an approach that was also used in the original project and which circumvents the need for the double integration in (II-10). That approach is based on the relationship (III-1) in Reference 1 derived in Appendix IIIof Ref. 1 and repeated below with small notational modifications.

$$e^{jk\underline{\beta}\cdot\underline{R}} = \frac{jkR}{4\pi} \int_0^{2\pi} d\phi_\beta \int_0^{\pi} d\theta_\beta \sin\theta_\beta \left[1 + \cos\theta_\beta + \frac{1}{jkR}\right] e^{jkR\cos\theta_\beta} \qquad \text{(II-12)}$$

where the integration over the spherical angles $(\theta_\beta, \phi_\beta)$ covers all possible directions of the $\underline{\beta}$-vector.

Eq. (II-12) is adapted to the analysis in this study by first noting that

$$\cos\theta_\beta = \frac{\underline{\beta}\cdot\underline{R}}{\beta R} \qquad \text{(II-13-a)}$$

and

$$\int_0^{2\pi} d\phi_\beta \int_0^{\pi} d\theta_\beta \sin\theta_\beta = \int_0^{2\pi} d\phi_\beta \int_0^{1} d\beta_h \, \beta_h \qquad \text{(II-13-b)}$$

Using (II-13-a, b) in (II-12), we obtain the latter in the form

$$e^{jkR} = \frac{1}{4\pi} \int_0^{2\pi} d\phi_\beta \int_0^{1} d\beta_h \, \beta_h \left[1 + jk(R + \underline{\hat{\rho}} \cdot \underline{\rho})\right] e^{jk\underline{\beta}^{\pm} \cdot \underline{r}} \qquad \text{(II-14)}$$

or equivalently, in order to separate out "upward" and "downward" propagating waves

$$e^{jkR} = \frac{1}{4\pi} \int_0^{2\pi} d\phi_\beta \int_0^{1} d\beta_h \, \beta_h \, e^{jk\beta_h(\rho - \rho') \cos(\phi - \phi_\beta)} \cdot$$

$$\left(e^{jk|\beta_z|(z - z')} \left[1 + jk(R + \underline{\beta}^{+} \cdot \underline{\rho})\right] \right.$$

$$\left. + e^{-jk|\beta_z|(z - z')} \left[1 + jk(R + \underline{\beta}^{-} \cdot \underline{\rho})\right] \right)$$

where

$$\underline{\beta}^{+} = \hat{x} \beta_x + \hat{y} \beta_y + \hat{z} |\beta_z| = \beta_h (\hat{x} \cos\phi_\beta + \hat{y} \sin\phi_\beta) + \hat{z} |\beta_z|$$

$$\underline{\beta}^{-} = \hat{x} \beta_x + \hat{y} \beta_y - \hat{z} |\beta_z| = \beta_h (\hat{x} \cos\phi_\beta + \hat{y} \sin\phi_\beta) - \hat{z} |\beta_z|$$

The procedure based on the use of (II-14) begins by assuming a "local plane wave spectrum." By "local," we mean that the plane-wave spectral field components, which are independent of position coordinates, are approximated at a point in position space by the actual field components (2.13-a, b, c) multiplied by a particular factor. That factor is

$$f^{\pm}(\underline{\rho}) = \frac{1}{4\pi} \left[1 + jk(R(0) + \underline{\hat{\rho}}^{\pm} \cdot \underline{\rho}(0))\right] e^{-jkR(0)} e^{-jk\underline{\beta}^{\pm} \cdot \underline{r}'(0)} \qquad \text{(II-15)}$$

where $R(0)$ = distance between observation point and the nearest cable slot = $\sqrt{(\rho - a)^2 + (z - b')^2}$ and $\underline{r}'(0)$ = position of nearest cable slot = $\hat{x}(a \cos\phi) + \underline{y}(\ \sin\phi) + \underline{z}b'$.

The logic behind this approach is explained below. The field components from an individual slot, as given by (2.8-a, b, c), all contain the factor e^{jkR}, where R is the distance between that slot and the observation point. The quantity e^{jkR} is then expressed as a superposition of plane-wave spectra through Eq. (II-14). In the original project, this was done for each slot and then the integration over the slots was carried out for the "local" spectral field, where the factor e^{jkR} was replaced by

$$\frac{1}{4\pi}\left(1 + jk\,(R + \hat{\beta}\cdot\underline{\beta})\right) e^{jk\hat{\beta}\cdot\underline{\beta}}$$

The integration was then accomplished by approximate methods (Ref. 1, Sections 3 and 4 in Appendix III).

In the present project, the integration over the cable was done for the actual fields as functions of position coordinates, not for their plane-wave spectra. Therefore, having accomplished that integration and obtained the field components from the entire cable at a point in space, we would like to implement the "local plane wave spectrum" model based on these results (i.e., based on Eqs. (2.19-a, b, c) rather than (2.8-a, b, c)). However, the deterrent to that is the fact that the factors e^{-jkR} have disappeared in the process of integrating around the cable. The factors $\frac{e^{jkR}}{R^n}$ in (2.8-a, b, c) or (2.10-a, b, c) have been replaced by I_n in (2.19-a, b, c)).

If I_n is evaluated by the partial integration method indicated in Section I-B of Appendix I, the factor $e^{jkR(0)}$ appears in I_n. However, since the more accurate numerical integration technique discussed in Section I-C of Appendix I was actually used to obtain I_n, the factor $e^{jkR(0)}$ is not explicitly indicated but we know* that I_n could be written in the form

---

* The results using the partial integration method were compared with those from the numerical technique and the agreement was nearly perfect.

$$I_n = \hat{I}_n e^{jkR(0)} \tag{II-16}$$

A field component as given by (2.19-a), (2.19-b) or (2.19-c) could be written (through (II-16) and (II-14) in the form

$$E(\underline{r}) = \sum_{n=1}^{3} E_n I_n = \left(\sum_{n=1}^{3} E_n \hat{I}_n \right) e^{jkR(0)} =$$

$$\int_0^{2\pi} d\phi_s \int_0^1 d\theta_h \, s_h \, e^{jk\underline{\hat{s}}\cdot\underline{r}} \, \tilde{E}(\underline{\hat{s}}, \underline{r}) \tag{II-17}$$

where

$$\tilde{E}(\underline{\hat{s}}, \underline{r}) = \frac{1}{4\pi} \sum_{n=1}^{3} E_n \hat{I}_n e^{-jk\underline{\hat{s}}\cdot\underline{r}'(0)} \left[1 + jk(R(0) + \underline{\hat{s}}\cdot\underline{R}(0)) \right]$$

$$= \left(\frac{1}{4\pi} E(\underline{r}) e^{-jk\underline{\hat{s}}\cdot\underline{r}'(0)} \left[1 + jk(R(0) + \underline{\hat{s}}\cdot\underline{R}(0)) \right] \right) e^{-jkR(0)}$$

The field component $\tilde{E}(\underline{\hat{s}}, \underline{r})$, a function of both $\underline{\hat{s}}$ and the observation point vector $\underline{r} = (\rho, \phi, z)$, is interpreted as the "local plane wave spectrum" of $E(\underline{r})$ and is obtained by multiplying the actual $E(\underline{r})$ by the factor $\frac{1}{4\pi}[1 + jk(R(0) + \underline{\hat{s}}\cdot\underline{R}(0))]e^{-jkR(0)} e^{-jk\underline{\hat{s}}\cdot\underline{r}'(0)}$ as indicated in (II-15).

This method was used and a number of computations were performed with it including production runs for scattered fields. The results were judged to be unsatisfactory and eventually it was abandoned and replaced bythe method described in Section 4 in the main body of this report.

One of the major deficiencies of the method is as follows. While it produces a spectrum of "plane waves," i.e., waves with the plane wave propagation factor $e^{jk\underline{\hat{s}}\cdot\underline{r}}$, there waves are not necessarily transverse. The method described in Section 4, on which our numerical results are based, does produce an approximation to the true field at the scatterer that res[illegible] a TEM wave.

Appendix III

System Parameters

In the table below, the parameters inputted into the computer program are listed, with the algebraic symbol used for each variable in analysis, the Fortran name of the variable, its definition and the values assigned to it in the program. This material is taken from Ref. 1, Section 11, Pages 11-2 through 11-6. The original material has been changed to reflect the modifications made in the new program.

Parameters associated with the cable

Fortran Name	Algebraic Symbol	Definition	Value
R	R	Radius of cable configuration in meters	24 (approximation based on circumference of 151 meters)
A	a	Inner radius of coaxial cable meters	.00476
B	b	Outer radius of coaxial cable-meters	.0127
LENGTH	l_s	Slot length (along cable); same for all slots-meters	.003
WIDTH	w_s	Slot width (around cable); same for all slots-meters	.0155
EPSILON	ε_{cn}	Permittivity of cable material - farads/meter	$1.7\ \varepsilon_0$ = $15.05\ (10^{-12})$

Fortran Name	Algebraic Symbol	Definition	Value
SIGMACA	σ_{ca}	Conductivity of cable material - mhos/meter	0
PHIRAD	ϕ_{10}	Azimuthal angle along the cable of Slot #1. (The slot nearest the power source) in ground frame	0
PHI	$\phi''_{50} = \phi''_{0}$	Angle of slot center around periphery of cable	$\frac{\pi}{4} = 45°$
ALPHA	α	Attenuation of TEM mode-nepers/ meter	.002
F	f	Radio frequency in Hertz	$57(10^{6}) = 57$ MHz
VO	V_o	Voltage between inner and outer conductors of coaxial cable-used in amplitude of TEM mode-volts. Parameters associated with the ground	1
E	ε	Permittivity of ground-farads/ meter	$15.413(10^{-12}) = 4\varepsilon_0$
SIGMA	σ	Ground conductivity-mhos/meter Parameters associated with the geometry	0.002
XAP	x_a	x-coordinate of antenna-meters	(antenna at center of circular configuration)

Fortran Name	Algebraic Symbol	Definition	Value
YAP	y_A	y-coordinate of antenna-meters	0 (same remarks as above)
ZAP	z_A	z-coordinate of antenna-meters	0.5
RI	β_n	Magnitude of (x-y) plane projection of $\hat{\beta}$, i.e. $\sqrt{\beta_x^2 + \beta_y^2}$	Varied from 0 to 1
PHI	ϕ_β	Azimuthal angle of (z-y) plane projection of $\hat{\beta}$, $\tan^{-1}\left(\frac{\beta_y}{\beta_x}\right)$	Varied from 0° to 360°

Parameters Associated with the Scatterer

Fortran Name	Algebraic Symbol	Definition	Values
XSP	x_S	x-coordinate of scatterer center-meters	Varied from case to case
YSP	y_S	y-coordinate of scatterer center-meters	Varied
ZSP	z_S	z-coordinate of scatterer center-meters	Varied

Fortran Name	Algebraic Symbol	Definition	Value
THB	θ_b	Spherical polar angle of long axis of prolate spheroidal scatterer (in ground-frame)	Varied: 0 for "upright man" cases; $\frac{\pi}{2}$ for "crawling man" cases
PHB	ϕ_b	Azimuthal angle of long axis of scatterer (in ground-frame)	Varied
ES	ϵ_s	Permittivity of scatterer material-farads/meter	$408.282(10^{-11}) = 46.2\epsilon_0$ based on Reference 9.19
SIGMAS	σ_s	Conductivity of scatterer material-mhos/meter	0.502 based on Reference 47
RS (computed variable	r_s	$\sqrt{x_s^2 + y_s^2}$ = radial coordinate of scatterer center in ground frame	Varied
PHIS (computed variable)	ϕ_s	$\tan^{-1}\left(\frac{y_s}{x_s}\right)$ = azimuth angle of scatterer center in ground frame	Varied
RS	R_s	Radius of prolate spheroidal scatterer-meters	0.25
LS	l_s	Length of prolate spheroidal scatterer-meters	2.0

MISSION
of
Rome Air Development Center

RADC plans and executes research, development, test and selected acquisition programs in support of Command, Control Communications and Intelligence (C^3I) activities. Technical and engineering support within areas of technical competence is provided to ESD Program Offices (POs) and other ESD elements. The principal technical mission areas are communications, electromagnetic guidance and control, surveillance of ground and aerospace objects, intelligence data collection and handling, information system technology, solid state sciences, electromagnetics and electronic reliability, maintainability and compatibility.

Printed by
United States Air Force
Hanscom AFB, Mass. 01731

END

FILMED

4-86

DTIC